ISSN 1881-7831 Online ISSN 1881-784X

DD&T

Drug Discoveries & Therapeutics

Volume 19, Number 6
December 2025

IRCA BSSA
IACMHR

www.ddtjournal.com

DD&T
Drug Discoveries & Therapeutics

ISSN: 1881-7831
Online ISSN: 1881-784X
CODEN: DDTRBX
Issues/Year: 6
Language: English
Publisher: IACMHR Co., Ltd.

Drug Discoveries & Therapeutics is one of a series of peer-reviewed journals of the International Research and Cooperation Association for Bio & Socio-Sciences Advancement (IRCA-BSSA) Group. It is published bimonthly by the International Advancement Center for Medicine & Health Research Co., Ltd. (IACMHR Co., Ltd.) and supported by the IRCA-BSSA.

Drug Discoveries & Therapeutics publishes contributions in all fields of pharmaceutical and therapeutic research such as medicinal chemistry, pharmacology, pharmaceutical analysis, pharmaceutics, pharmaceutical administration, and experimental and clinical studies of effects, mechanisms, or uses of various treatments. Studies in drug-related fields such as biology, biochemistry, physiology, microbiology, and immunology are also within the scope of this journal.

Drug Discoveries & Therapeutics publishes Original Articles, Brief Reports, Reviews, Policy Forum articles, Case Reports, Communications, Editorials, News, and Letters on all aspects of the field of pharmaceutical research. All contributions should seek to promote international collaboration in pharmaceutical science.

Editorial Board

International Field Chief Editors:

Nobuyoshi AKIMITSU
The University of Tokyo, Tokyo, Japan

Fen-Er CHEN
Fudan University, Shanghai, China

Hiroshi HAMAMOTO
Yamagata University, Yamagata, Japan

Takashi KARAKO
Japan Institute for Health Security, Tokyo, Japan

Hongzhou LU
National Clinical Research Centre for Infectious Diseases, Shenzhen, Guangdong, China

Sven SCHRÖDER
University Medical Center Hamburg Eppendorf (UKE), Hamburg, Germany

Kazuhisa SEKIMIZU
Teikyo University, Tokyo, Japan

Corklin R. STEINHART
CAN Community Health, FL, USA

Associate Editors:

Feihu CHEN
Anhui Medical University, Hefei, Anhui, China

Jianjun GAO
Qingdao University, Qingdao, Shandong, China

Chikara KAITO
Okayama University, Okayama, Japan

Gagan KAUSHAL
Jefferson College of Pharmacy, Philadelphia, PA, USA

Hironori KAWAKAMI
Sanyo-Onoda City University, Yamaguchi, Japan

Xiao-Kang LI
National Research Institute for Child Health and Development, Tokyo, Japan

Yasuhiko MATSUMOTO
Meiji Pharmaceutical University, Tokyo, Japan

Atsushi MIYASHITA
Teikyo University, Tokyo, Japan

Tomofumi SANTA
The University of Tokyo, Tokyo, Japan

Tianqiang SONG
Tianjin Medical University, Tianjin, China

Sanjay K. SRIVASTAVA
Texas Tech University Health Sciences Center, Abilene, TX, USA

Hongbin SUN
China Pharmaceutical University, Nanjing, Jiangsu, China

Fengshan WANG
Shandong University, Jinan, Shandong, China.

Proofreaders:

Curtis BENTLEY
Roswell, GA, USA
Thomas R. LEBON
Los Angeles, CA, USA

Editorial and Head Office:

Pearl City Koishikawa 603,
2-4-5 Kasuga, Bunkyo-ku,
Tokyo 112-0003, Japan
E-mail: office@ddtjournal.com

Drug Discoveries & Therapeutics

Editorial and Head Office

Pearl City Koishikawa 603, 2-4-5 Kasuga, Bunkyo-ku,
Tokyo 112-0003, Japan

E-mail: office@ddtjournal.com
URL: www.ddtjournal.com

Editorial Board Members

Alex ALMASAN
(Cleveland, OH)
John K. BUOLAMWINI
(Memphis, TN)
Jianping CAO
(Shanghai)
Shousong CAO
(Buffalo, NY)
Jang-Yang CHANG
(Tainan)
Zhe-Sheng CHEN
(Queens, NY)
Zilin CHEN
(Wuhan, Hubei)
Xiaolan CUI
(Beijing)
Saphala DHITAL
(Clemson, SC)
Shaofeng DUAN
(Lawrence, KS)
Hao FANG
(Ji'nan, Shandong)
Marcus L. FORREST
(Lawrence, KS)
Tomoko FUJIYUKI
(Tokyo)
Takeshi FUKUSHIMA
(Funabashi, Chiba)
Harald HAMACHER
(Tübingen, Baden-Württemberg)
Kenji HAMASE
(Fukuoka, Fukuoka)
Junqing HAN
(Ji'nan, Shandong)
Xiaojiang HAO
(Kunming, Yunnan)
Kiyoshi HASEGAWA
(Tokyo)
Waseem HASSAN
(Rio de Janeiro)
Langchong HE
(Xi'an, Shaanxi)
Rodney J. Y. HO
(Seattle, WA)
Hsing-Pang HSIEH
(Zhunan, Miaoli)
Yongzhou HU
(Hangzhou, Zhejiang)
Youcai HU
(Beijing)
Yu HUANG
(Hong Kong)
Zhangjian HUANG
(Nanjing Jiangsu)
Amrit B. KARMARKAR
(Karad, Maharashra)
Toshiaki KATADA
(Tokyo)
Ibrahim S. KHATTAB
(Kuwait)
Shiroh KISHIOKA
(Wakayama, Wakayama)
Robert Kam-Ming KO
(Hong Kong)
Nobuyuki KOBAYASHI
(Nagasaki, Nagasaki)
Toshiro KONISHI
(Tokyo)
Peixiang LAN
(Wuhan, Hubei)
Chun-Guang LI
(Melbourne)
Minyong LI
(Ji'nan, Shandong)
Xun LI
(Ji'nan, Shandong)
Dongfei LIU
(Nanjing, Jiangsu)
Jian LIU
(Hefei, Anhui)
Jikai LIU
(Wuhan, Hubei)
Jing LIU
(Beijing)
Xinyong LIU
(Ji'nan, Shandong)
Yuxiu LIU
(Nanjing, Jiangsu)
Hongxiang LOU
(Jinan, Shandong)
Hai-Bin LUO
(Haikou, Hainan)
Xingyuan MA
(Shanghai)
Ken-ichi MAFUNE
(Tokyo)
Sridhar MANI
(Bronx, NY)
Tohru MIZUSHIMA
(Tokyo)
Jasmin MONPARA
(Philadelphia, PA)
Masahiro MURAKAMI
(Osaka)
Yoshinobu NAKANISHI
(Kanazawa, Ishikawa)
Munehiro NAKATA
(Hiratsuka)
Siriporn OKONOGI
(Chiang Mai)
Weisan PAN
(Shenyang, Liaoning)
Chan Hum PARK
(Eumseong)
Rakesh P. PATEL
(Mehsana, Gujarat)
Shivanand P. PUTHLI
(Mumbai, Maharashtra)
Shafiqur RAHMAN
(Brookings, SD)
Gary K. SCHWARTZ
(New York, NY)
Luqing SHANG
(Tianjin)
Yuemao SHEN
(Ji'nan, Shandong)
Rong SHI
(Shanghai)
Yoshitaka SHIMOTAI
(Yamagata)
Chandan M. THOMAS
(Bradenton, FL)
Michihisa TOHDA
(Sugitani, Toyama)
Li TONG
(Xining, Qinghai)
Murat TURKOGLU
(Istanbul)
Hui WANG
(Shanghai)
Quanxing WANG
(Shanghai)
Stephen G. WARD
(Bath)
Zhun WEI
(Qingdao, Shandong)
Tao XU
(Qingdao, Shandong)
Yuhong XU
(Shanghai)
Yong XU
(Guangzhou, Guangdong)
Akiho YAGI
(Sendai, Miyagi)
Bing YAN
(Ji'nan, Shandong)
Chunyan YAN
(Guangzhou, Guangdong)
Xiao-Long YANG
(Chongqing)
Yun YEN
(Duarte, CA)
Yongmei YIN
(Tianjin)
Yasuko YOKOTA
(Tokyo)
Yun YOU
(Beijing)
Rongmin YU
(Guangzhou, Guangdong)
Tao YU
(Qingdao, Shandong)
Guangxi ZHAI
(Ji'nan, Shandong)
Liangren ZHANG
(Beijing)
Lining ZHANG
(Ji'nan, Shandong)
Na ZHANG
(Ji'nan, Shandong)
Ruiwen ZHANG
(Houston, TX)
Xiu-Mei ZHANG
(Ji'nan, Shandong)
Xuebo ZHANG
(Baltimore, MD)
Yingjie ZHANG
(Ji'nan, Shandong)
Yongxiang ZHANG
(Beijing)
Haibing ZHOU
(Wuhan, Hubei)
Jian-hua ZHU
(Guangzhou, Guangdong)

(*As of June 2025*)

Original Article

360-377 **Zhimu-Huangbo ameliorates AQP4 depolarization in diabetic cognitive impairment rats by targeting the serum-derived exosomal TIMP3-mediated MMP9/β-DG pathway.**
Ying Li, Xueling Lin, Jie Bu, Genhui Yang, Lin Niu, Lin Zhang, Dingbin Liu, Yanjun Zhang, Qingsheng Yin, Pengwei Zhuang

378-388 **Real-world use of non-oral administration of oral anticancer agents via the simple suspension method in Japanese patients with cancer: A nationwide claims-based analysis.**
Hiroaki Ohta, Takeo Yasu

389-394 **Disproportionality and time-to-onset analyses of drug-induced weight gain using the Japanese Adverse Drug Event Report database.**
Naohito Ide, Rika Shibata, Ken-ichi Sako, Tomoji Maeda

395-403 **Verification of the protective effect of transfecting brain-derived neurotrophic factor and B-cell lymphoma 2 genes on retina ganglion cells in a rat model of optic nerve injury.**
Zijia Zhao, Yuan Fang, Gezhi Xu, Jiawei Xiong, Xiaofen Mo, Jiawen Fan

404-413 **A phase II investigator-initiated, continuation trial of 5-aminolevulinic acid hydrochloride/sodium ferrous citrate (5-ALA-HCl/SFC) for patients with adult-onset Still's disease (AOSD) refractory to glucocorticoids.**
Remi Sumiyoshi, Tomohiro Koga, Osamu Kamisawa, Shimpei Morimoto, Naoki Hosogaya, Hiroshi Yamamoto, Makoto Hori, Yosuke Inaba, Yoko Hattori, Tamiki Hikake, Tomoya Kurokawa, Hideki Hanaoka, Shuzo Sato, Kiyoshi Migita, Noriyoshi Ogawa, Motomu Hashimoto, Atsushi Kawakami

414-424 **Comparative study of contrast-enhanced ultrasound and contrastenhanced computed tomography in the diagnosis of benign and malignant lesions of the gallbladder.**
Liang Fang, Zhiying Qiu, Lingwen Xu, Fei Hu, Yuchen Tao, Shengnan Ding, Jing Zhou, Ling Wang, Lin Chen

Brief Report

425-430 **Modulatory effects of ingesting dietary fiber and protein before carbohydrates on postprandial interstitial glucose responses.**
Yuko Wada Imanaka, Sanae Tanaka, Chisato Watanabe, Ken-ichi Shimokawa, Fumiyoshi Ishii

Correspondence

431-434 **Clinical significance of imeglimin in older patients with type 2 diabetes: Analysis of a national database and a long-term case suggesting the potential for sarcopenia prevention.**
Atsushi Ishimura, Kaori Hashimoto, Hirofumi Ogino

435-436 **Elamipretide: The first cardiolipin-directed mitochondrial therapeutic for Barth syndrome approved under accelerated approval.**
Chenru Zhao, Xuemei Zhuang, Jianjun Gao

News

437-439 **New diagnostic code "5B72 Undernutrition in Adults" approved for inclusion in the 11th Revision of the International Classification of Diseases (ICD-11).**
Machiko Uenishi, Peipei Song

Original Article

DOI: 10.5582/ddt.2025.01102

Zhimu-Huangbo ameliorates AQP4 depolarization in diabetic cognitive impairment rats by targeting the serum-derived exosomal TIMP3-mediated MMP9/β-DG pathway

Ying Li[1,2,§], Xueling Lin[1,2,§], Jie Bu[1,2], Genhui Yang[1,2], Lin Niu[1,2], Lin Zhang[1], Dingbin Liu[5], Yanjun Zhang[1,2,3,4,*], Qingsheng Yin[1,2,*], Pengwei Zhuang[1,2,3,4,*]

[1] State Key Laboratory of Chinese Medicine Modernization, Tianjin University of Traditional Chinese Medicine, Tianjin, China;
[2] Haihe Laboratory of Modern Chinese Medicine, Tianjin University of Traditional Chinese Medicine, Tianjin, China;
[3] First Teaching Hospital of Tianjin University of Traditional Chinese Medicine, Tianjin, China;
[4] National Clinical Research Center for Chinese Medicine Acupuncture and Moxibustion, Tianjin, China;
[5] Nankai University, Tianjin, China.

SUMMARY: Aquaporin-4 (AQP4) depolarization-mediated glymphatic system (GS) dysfunction is a critical pathological mechanism in diabetic cognitive impairment (DCI). However, its underlying mechanism has not been clarified. The Zhimu-Huangbo (ZMHB) herb pair, a classic formulation historically employed in traditional Chinese medicine, demonstrates neuroprotective effects, including the amelioration of cognitive dysfunction. Emerging evidence suggests that the exosomal pathway may regulate abnormalities in diabetes-induced AQP4 polarization. Nevertheless, whether the neuroprotective effects of ZMHB mediate the restoration of AQP4 polarity through the exosomal pathway remains to be elucidated. This study takes the exosomal pathway as the entry point to elucidate the mechanism of AQP4 depolarization in DCI and determine how ZMHB restores AQP4 polarization and improves cognitive function. ZMHB significantly improved cognitive function, effectively restored GS function and maintained AQP4 polarization. Pharmacological blockade of exosomal pathways partially reduced the therapeutic effects of ZMHB, demonstrating that its efficacy depends on exosome-mediated signaling; proteomics combined with western blotting validation revealed tissue inhibitor of metalloproteinase 3 (TIMP3) as a pivotal protein modulated by ZMHB, which restored AQP4 polarization by inhibiting matrix metalloproteinase-9 (MMP9) activity and blocking β-dystroglycan (β-DG) cleavage in astrocytes. *In vitro* studies further demonstrated that both ZMHB-treated serum exosomes (ZMHB-sExos) and the TIMP3 agonist MPT0B390 restored astrocytic AQP4 polarization by modulating the MMP9/β-DG pathway. We demonstrated that ZMHB restored AQP4 depolarization in DCI rats by modulating the exosomal TIMP3-MMP9/β-DG pathway.

Keywords: Zhimu-Huangbo, diabetic cognitive impairment, glymphatic system, exosomes, AQP4, TIMP3

1. Introduction

Diabetes is a chronic metabolic disease that is characterized by persistent hyperglycemia and insulin resistance. Cognitive impairment is a common complication of diabetes (*1-3*), affecting 25–35% of diabetic patients and increasing their risk of cognitive decline by 1.5–2.5 times compared with nondiabetic individuals (*4,5*). Unfortunately, the incomplete understanding of diabetic cognitive impairment (DCI) pathogenesis has resulted in the absence of U.S. Food and Drug Administration (FDA)-approved drugs to clinically treat this condition.

Impaired glymphatic system (GS) function, characterized by diminished clearance of neurotoxic metabolites, underlies the pathogenesis of DCI (*6-8*). The clearance capacity of the GS critically depends on the polarized distribution of aquaporin-4 (AQP4) at perivascular astrocytic endfeet (*9,10*), and AQP4 depolarization may represent a pivotal factor in DCI pathogenesis. Previous studies have indicated that exosomes restore GS function by modulating AQP4 polarization, but the detailed mechanism remains unknown. Under pathological diabetic conditions, aberrant protein expressions in exosomes may exacerbate cognitive deficits (*11*). Notably, whether circulating serum-derived exosomes, as essential protein-delivery vehicles (*12*), mediate DCI progression by regulating

cerebral AQP4 polarization and GS functional integrity has not been fully investigated.

The distribution of AQP4 polarization is partially dependent on β-dystroglycan (β-DG), while matrix metalloproteinase-9 (MMP9) acts on specific polysaccharide structures within β-DG through its active enzymatic sites, leading to β-DG cleavage or defects and affecting the localization and function of AQP4 (*13*). Importantly, the tissue inhibitor of metalloproteinase 3 (TIMP3) is a natural inhibitor of MMP9 that inhibits the activity of MMP9 and protects β-DG from degradation, thus supporting the polarization and function of AQP4 (*14,15*). Research has shown that the absence of β-DG after DCI leads to the loss of AQP4 polarization, thereby exacerbating cognitive impairment (*16*). Therefore, investigating whether TIMP3 improves cognitive function by regulating the MMP9/β-DG pathway and affecting AQP4 polarization in DCI models is necessary.

According to traditional Chinese medicine (TCM), DCI is recognized as a chronic disorder that is primarily attributed to the pathogenic mechanism of "toxin damaging brain collaterals", with "heat clearing and detoxification" serving as its fundamental therapeutic strategy. Leveraging the unique advantages of TCM in the multipathway and multitarget regulation of complex diseases, Tong Guan Wan, a classic formula composed of Anemarrhenae Rhizoma (Zhimu, dried rhizome of *Anemarrhena asphodeloides* Bunge) and Phellodendri Chinensis Cortex (Huangbo, dried bark of *Phellodendron chinense* C.K.Schneid.); this formula is described in the Yuan Dynasty text Secret Record of the Chamber of Orchids (*17,18*). Zhimu, characterized by its cold nature and moistening properties, excels in nourishing Yin, moistening dryness, clearing heat, and purging fire. Huangbo is bitter and cold in nature, excelling at purging fire and detoxifying. Both herbs act on the kidney meridian, exhibiting synergistic interactions: they mutually increase heat-clearing and fire-purging effects while maintaining a dynamic equilibrium between Yin-nourishing and damp-drying, thereby preventing Yin impairment caused by bitter-cold properties. This collaboration achieves Yin-nourishing, heat-clearing, and detoxification effects. Recent studies have shown that "bitter-cold" herbs exhibit heat-clearing and detoxification functions that significantly enhance neural protection by increasing neuronal vitality and promoting neural repair (*19*). Importantly, previous research has shown that the herb pair ZMHB, a commonly used heat-clearing and detoxifying formulation, can significantly increase the learning and memory abilities of DCI mice (*20,21*). However, whether ZMHB improves cognitive function by regulating AQP4 polarization remains unclear.

Therefore, in this study, the exosome release inhibitor GW4869 was used to confirm the essential role of the exosomal pathway in the ZMHB-mediated improvement in AQP4 polarization. Serum exosomal proteomics was performed to identify differentially expressed proteins and pinpoint key regulatory proteins, and western blotting and immunofluorescence staining were used to evaluate the effects of ZMHB on the TIMP3-MMP9/β-DG pathway. Furthermore, ZMHB-treated serum exosomes (ZMHB-sExos) and the TIMP3-specific agonist MPT0B390 were applied to astrocytes, revealing the targeted regulatory role of the TIMP3-MMP9/β-DG pathway in the distribution of polarized AQP4 at the molecular mechanism level. Overall, these studies revealed the underlying mechanism by which ZMHB restores AQP4 polarization in DCI rats through modulating the exosomal TIMP3-mediated MMP9/β-DG pathway, thereby providing a novel therapeutic strategy for clinical intervention in DCI. The graphical abstract below visually illustrates the overall framework of the DCI pathological mechanisms and the protective effects of ZMHB (Figure S1).

2. Materials and Methods

2.1. Preparation of ZMHB

Zhimu (dried rhizome of *Anemarrhena asphodeloides* Bunge) was purchased from Beijing Bencao Fangyuan Pharmaceutical Group Co., Ltd. (origin Hebei Province, China, Batch No.20150136). Huangbo (dried bark of *Phellodendron Chinense* C.K.Schneid.) was purchased from Beijing Bencao Fangyuan (BoZhou) Pharmaceutical Technology Co., Ltd. (origin Sichuan Province, China; batch no. 20160125). Herbs were extracted 3 times by reflux with 8× 80% ethanol at a ratio of 1:1, each time for 2 h, filtered, and the filtrate was removed. The drug extract was concentrated to 0.36 g/mL with a rotary evaporator and stored in a refrigerator at -20°C.

2.2. Chemical component analysis of ZMHB

For quality assurance, ultra-high performance liquid chromatography quadrupole-time-of-flight mass spectrometry (UPLC–Q–TOF–MS) was used to analyze the chemical profile of ZMHB. The ZMHB extract was diluted to 0.1 g/mL. A Waters ACQUITY UPLC BEH C18 (2.1 mm × 50 mm, 1.7 μm) was used for separation. The mobile phase consisted of water (A) and acetonitrile (B), with a column temperature of 45°C and an injection volume of 5 μL; the flow rate was set at 0.3 mL/min. The gradient profile was:0–0.5 min (A:95%; B:5%), 0.5–6 min (A:80%; B:20%), 6–8 min (A:78%; B:22%), 8–13 min (A:62%; B:38%), 13–18 min (A:50%; B:50%), 18–26 min (A:0%; B:100%), and 26–30 min (A:98%; B:2%). Positive ion and negative ion modes were used for data collection. The positive ion mode was as follows: source temperature (120°C), desolvation temperature (450°C), capillary voltage (3 kV), collision energy (30–50 V), desolvation (800 L/h), cone gas (50 L/h), and scan range

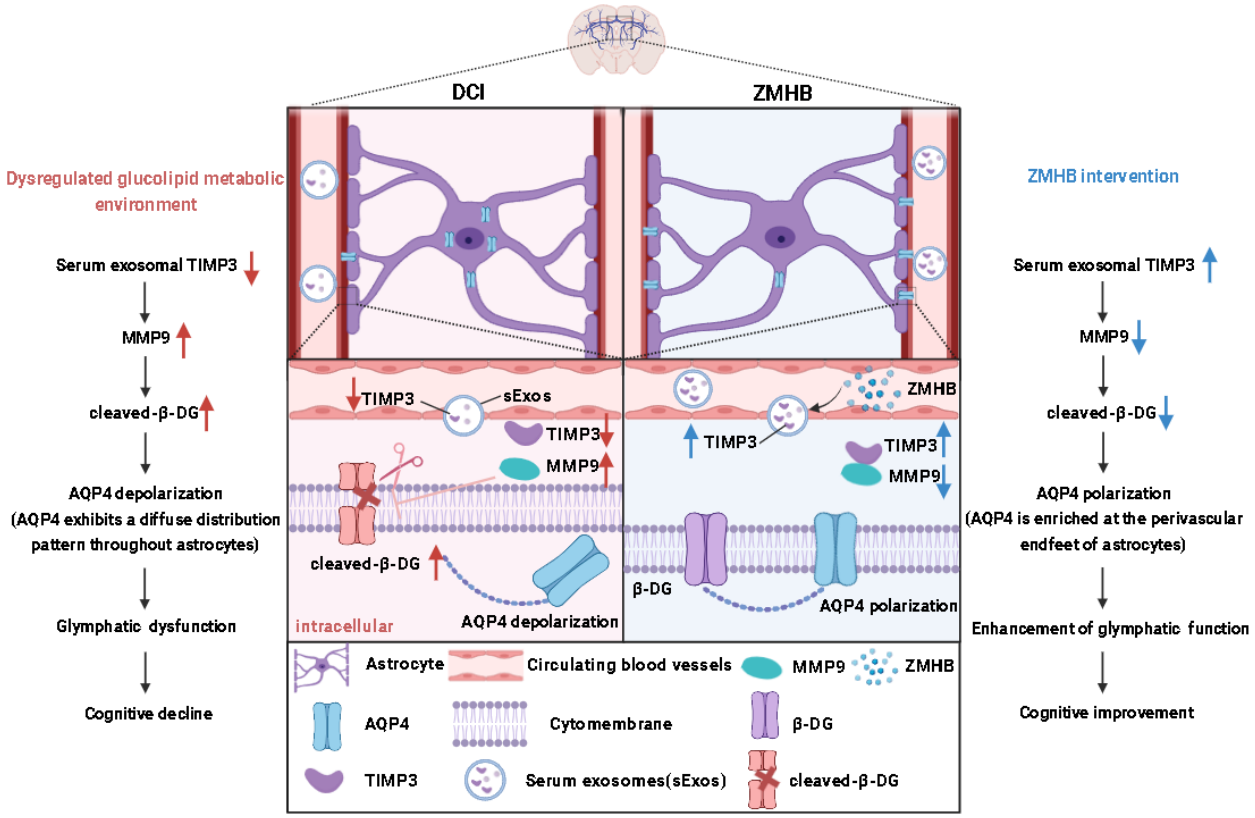

Figure S1. Schematic representation of DCI pathogenesis and the protective actions of ZMHB.

(50–1,200 m/z). The negative ion mode was as follows: source temperature (120°C), desolvation temperature (400°C), capillary voltage (2 kV), collision energy (30–50 V), desolvation (800 L/h), cone gas (50 L/h), and scan range (50–1,200 m/z). The data were processed using MassLynx™4.1 software.

2.3. Experimental animals

Wistar rats (n = 120, male, 4 weeks old) were purchased from Beijing Vital River Laboratory Animal Technology Co., Ltd. (SCXK (Jing) 2018-0006) and raised in the SPF-level barrier laboratory of the Animal Center of Tianjin University of Traditional Chinese Medicine. The temperature of the feeding room was 21 ± 2°C, the air pressure was constant, the animals were subjected to alternating day and night conditions of 12 h each, and food and water were freely available. This study passed the ethical review for animal experiments at Tianjin University of Traditional Chinese Medicine (TCM-LAEC2021152). The welfare of the laboratory animals was ensured by following the Laboratory Animal Guidelines for Ethical Review of Animal Welfare (GB/T 35892-2018).

2.4. Induction of the diabetic model and therapeutic intervention

The rats (n = 60) were acclimatized to laboratory conditions for one week prior to experimentation. Cognitive performance was evaluated using a Morris water maze (MWM; Anhui Zhenghua Biotechnology, Anhui, China), with 3 rats excluded because they demonstrated congenital frailty, locomotor impairments, or nonnavigational swimming patterns. The remaining experimental rats were randomly divided into a Control (Con) group (n = 12) and a model group (n = 45). The Con group was fed a normal diet, and the model group was fed a high-fat diet (HFD; Beijing Xiaoshu Youtai Biotechnology Co., Ltd., Beijing, China, D12492) for three weeks. After fasting for 12 h, the model group received 35 mg/kg intraperitoneal injections of streptozotocin (STZ, Sigma-Aldrich, St. Louis, MO, USA, S0130) three times, with an interval of 2 days between each injection. The Con group was injected with only an equal amount of citric acid sodium citrate buffer (pH 4.5, 0.1 mol/L, Solarbio, Beijing, China, C1013) under the same conditions. One week later, rats whose fasting blood glucose (FBG) concentrations exceeded 16.7 mmol/L, taken from their tail veins, were selected as diabetes model rats for subsequent experiments. The abovementioned screened rats (n = 36) were randomly divided into three groups: the DCI group, the ZMHB low-dose (ZMHB-L) group (2.16 g/kg, ig), and the ZMHB high-dose (ZMHB-H) group (4.32 g/kg, ig), with 12 rats in each group.

To determine whether ZMHB could prevent and treat cognitive impairment by regulating the exosomes,

an additional ZMHB + exosome release inhibitor GW4869 (MedChemExpress, NJ, USA, HY-19363) group (4.32 g/kg, ig + 1 mg/kg, ip) was added. The cognitive performance of the rats (n = 60) was initially assessed using the MWM test, and 2 rats were excluded because of congenital weakness, motor dysfunction, or nonnavigational swimming patterns. The remaining rats were randomly divided into a Con group (n = 12) and a model group (n = 46). A diabetic model was induced using STZ combined with a HFD, and 10 rats with FBG concentrations less than 16.7 mmol/L were excluded. The final selected rats (n = 36) were randomly divided into three groups: the DCI group, the ZMHB group (4.32 g/kg, ig), and the ZMHB + exosome release inhibitor GW4869 group (4.32 g/kg, ig + 1 mg/kg, ip), with 12 rats in each group. ZMHB was administered continuously for 8 weeks; the Con and DCI groups were given equal amounts of physiological saline orally once a day for a total of 8 weeks; in the combination group, GW4869 was injected intraperitoneally every other day. It has been reported in the literature that diabetic rats exhibit obvious symptoms of cognitive impairment symptoms after 8 weeks of modeling. Therefore, this experiment was conducted 8 weeks in advance before DCI was established (*22,23*).

The basis for calculating the 2-fold clinically equivalent dose of ZMHB (4.32 g/kg) was as follows: Based on the recommended human dosages of Zhimu and Huangbo that were provided in the Pharmacopoeia of the People's Republic of China (2020 edition) (total crude drug: 24 g; ratio: Zhimu 12 g; Huangbo 12 g), the clinically equivalent dose for rats was derived using the following human-to-rat dose conversion formula: Rat dose (g/kg) = Human dose (g)/70 kg (standard human body weight) × 6.3 (conversion factor). This yielded a rat-equivalent dose of 2.16 g/kg, and the 2-fold clinically equivalent dose was accordingly 4.32 g/kg.

2.5. Weight and fasting blood glucose

During the administration period, the body weights and FBG levels (after a fasting period from 8:00 PM on the previous day to 8:00 AM the next day) of the rats in each group were measured at four-week intervals, and the dynamic changes in their body weights and FBG levels were observed.

2.6. Morris water maze

The MWM test was used to evaluate the learning and memory abilities of the experimental animals. Within the time range of the learning and memory test on Days 1–5, the rats were allowed to swim in a dark pool, which was 150 cm in diameter and 50 cm in height, for 60 s to find the target platform (10 cm diameter) located in the center of one quadrant. If the platform was not found after 60 s of swimming, the rats were gently guided to the platform and allowed to redirect to the remote visual prompt for 20 s before being removed from the swimming pool. On the 6th day, the target platform was removed, and the rats were allowed to swim freely for 60 s while the time to reach the platform, frequency of crossing the platform, and duration in the zone were recorded.

2.7. Cresol violet staining

Brain tissue samples were fixed, embedded, and sectioned, and changes in the number of hippocampal neurons in each group were observed by cresyl violet staining. The details are as follows: the paraffin sections were dewaxed and dehydrated with xylene and gradient ethanol, rinsed with distilled water, stained with cresyl violet at 60℃ for 30 min, rinsed with running water for 30 s, differentiated with Nissl differentiation solution for 1 min, dehydrated with gradient ethanol and xylene, mounted with neutral resin, and finally observed under a digital slide scanner (3DHISTECH, Budapest, Hungary, Pannoramic MIDI).

2.8. Magnetic resonance imaging

Nest, 10 μL of gadolinium-diethylenetriaminepentaacetic acid (Gd-DTPA) at a concentration of 21 mmol/L was injected into the cerebellomedullary cistern of each experimental animal at a speed of 1.6 μL/min. After the Gd-DTPA injections were complete, the experimental animals were immediately fixed in a small animal magnetic resonance imaging (MRI) fixed slot with set parameters. Continuous scans were performed at 10 min, 20 min, 30 min, 40 min, and 50 min after injection, and the images were saved after scanning (Bruker Biospin, Ettlingen, Germany, Bruker Biospec 70/20 USR, Paravision 6.0). The dynamic exchange of cerebrospinal fluid and interstitial fluid was detected using three-dimensional T1-weighted images (3D T1WIs). 3D T1WIs were obtained with the following parameters: echo time of 2.4 ms, repetition time of 16.63 ms, field-of-view of 2.0 × 2.0 × 1.0 cm, flip angle of 20°, and scanning time of 8 min and 4 s, resulting in a 0.14 × 0.14 × 0.14 mm image. Finally, the MRI data were processed, including the extraction and calibration of the head signal, as well as the percentage of stereo pixels converted into baseline signals using SPM8 software.

2.9. Western blotting

RadioImmunoPrecipitation Assay (RIPA) protein lysis buffer and phenylmethylsulfonyl fluoride (PMSF) were used to extract total protein from the brain at a ratio of 100:1. A Bicinchoninic Acid Assay (BCA) protein concentration assay kit was used for protein quantification. Forty micrograms of protein was electrophoresed *via* 4-12% sodium dodecyl sulfate-polyacrylamide gel electrophoresis (SDS-PAGE),

transferred to a polyvinylidene difluoride (PVDF) membrane and blocked with blocking buffer at room temperature for 20 min. Subsequently, primary antibodies were added and incubated at 4℃ for 12 h. The primary antibodies used in the experiments included rabbit anti-CD81 (Abcam, Cambridge, UK, ab109201, 1:1,000); rabbit anti-TSG101 (CST, Boston, MA, USA, 72312S, 1:1,000); rabbit anti-AQP4 (Santa Cruz Biotechnology, Dallas, TX, USA, sc-390488, 1:1,000); rabbit anti-TIMP3 (Proteintech, Wuhan, Hubei, China, 10858-1-AP, 1:1,000); MS anti-β-DG (Santa Cruz Biotechnology, sc165998, 1:100); rabbit anti-MMP9 (Proteintech, 10375-2-AP, 1:500); MS anti-β-actin (Abcam, ab8226, 1:1,000); and rabbit anti-β-tubulin (Abcam, ab108342, 1:1,000). HRP-labeled secondary antibodies (goat-anti-rabbit IgG; CST, Cat#7074, 1:3,000, and goat anti-MS IgG; Abcam, ab6789, 1:1,000) were added and incubated for 2 h at room temperature, after which the blots were developed using a highly sensitive ECL kit. Image-Pro Plus 6.0 optical density analysis software was used to determine the gray values of the protein bands. β-actin or β-tubulin was used as a loading control. The relative expression level is the ratio of the gray value of the target protein and reference protein.

2.10. Immunofluorescence staining

After dehydration, dewaxing, and antigen repair, the brain tissue sections were incubated with primary antibodies (MS anti-AQP4: Servicebio, Wuhan, Hubei, China, GB12529, 1:500; rabbit anti-GFAP Servicebio, GB11096, 1:500; rabbit anti-CD31: Servicebio, GB113151, 1:200; rabbit anti-TIMP3: Thermo Fisher Scientific, Waltham, MA, USA, PA5-116049, 1:200; MS anti-GFAP: CST, 3970S, 1:400; MS anti-β-DG: Santa Cruz Biotechnology, sc-33702, 1:50; and rabbit anti-AQP4, CST, D1F8E, 1:50) at 4℃ overnight. On the next day, the slices were washed 3 times with PBS and incubated with secondary antibodies (goat-anti-MS IgG: Servicebio, GB21301, 1:300; goat-anti-rabbit IgG: Servicebio, GB25303, 1:400; goat-anti-rabbit IgG: Abcam, ab150077, 1:500; and goat-anti-MS IgG: Abcam, ab150113, 1:500) at room temperature for 2 h. Finally, the slices were washed 3 times with PBS and sealed with an anti-fluorescence quenching agent. Finally, ImageJ software was used to analyze the areas of protein-positive regions.

2.11. Exosome isolation and identification

First, blood was taken from the abdominal aorta of each rat, and the supernatant was collected by centrifugation. The supernatant was subsequently centrifuged at 2,000 × g for 30 min at 4℃. Afterward, the supernatant was transferred to a new centrifuge tube and centrifuged at 12,000 × g for 45 min at 4℃ to remove the largest vesicle, after which the supernatant was filtered through a 0.45 μm filter. The filtrate was subsequently subjected to ultracentrifugation (Beckman Coulter, Brea, CA, USA, Optima XP-CTZ19D16) at 110,000 × g for 2 h at 4℃, followed by resuspension in PBS. The exosomes that were obtained through ultracentrifugation were diluted at a 1:2 ratio and 10 μL of sample and 10 μL of phosphotungstic acid were dropped onto a copper mesh, precipitated for 1 min and dried. The imaging results were obtained through transmission electron microscopy (TEM) under 580 kV conditions. The samples were subsequently subjected to nanoparticle tracking analysis (NTA) and western blotting.

2.12. 4D-Label-free Proteomics

To explore the potential mechanism through which circulating serum exosomes (sExos) from the ZMHB group affect the repair of cognitive damage, 4D label-free quantitative proteomics technology were used to detect macroscopic changes in the expressions of circulating serum proteins in each group. The SDT lysate was added to the processed sExos from each group for protein extraction, and the BCA method was used for protein quantification. Twenty micrograms of protein from each sample were added to an appropriate amount of 5× loading buffer. After 5 min in a water bath, electrophoresis (180 V, 45 min) was performed. Coomassie blue R-250 staining was performed, followed by tryptic digestion using the filter aided sample preparation (FASP) method. The peptide segments were desalinated using a C18 cartridge. After freeze-drying, 40 μL of 0.1% formic acid solution was added for redissolution, and the peptide segments were quantified (OD280). Each group of samples was separated using a nanoElute HPLC system with a nanoliter flow rate. Buffer solution A was a 0.1% formic acid aqueous solution, and solution B was a 0.1% formic acid acetonitrile aqueous solution. The chromatographic column was equilibrated with 95% liquid A, and the samples were separated by C18 reversed-phase analysis at a flow rate of 300 nL/min. After chromatographic separation, a TOF Pro mass spectrometer was used for mass spectrometry analysis, with a positive ion detection method and a scanning range of 100–1,700 m/z. Data were collected in parallel accumulation serial fragmentation (PASEF) mode. Finally, in this study, the label-free algorithm in MaxQuant software (version 1.6.14) was used for nonlabel quantitative analysis of the proteomic data. This experiment was completed by APPLIED Protein Technology.

2.13. Cell line and cell culture

Mouse astrocytes were purchased from Pricella (C8-D1A; Wuhan, Hubei, China) and cultured in low-sugar Dulbecco's Modified Eagle's Medium (DMEM; Gibco,

New York, NY, USA, 11885084) supplemented with 10% fetal bovine serum at 37°C and 5% CO_2.

2.14. Induction of high-glucose-induced cellular injury model

After they reached 80%-90% confluence, 100 μL (5×10^5 cells) of astrocytes were cultured in 96-well plates for 24 h. Subsequently, the cells were cultured in basic medium for 24 h to maintain the same logarithmic growth period. The cultures were subsequently treated with different concentrations of glucose (5, 15, 25, 35, 45, and 55 mM) for 24 h to induce high-sugar damage. After treatment, 10 μL of Cell Counting Kit-8 (CCK-8; Beyotime, Shanghai, China, C0039) was added to each well and incubated at 37°C for 30 min, after which the absorbances were measured at 450 nm using a microplate reader (TECAN, Männedorf, Switzerland).

2.15. MPT0B390 administration concentration screening

To determine the optimal concentration of MPT0B390 (MedChemExpress, HY-145426) for C8-D1A cells, C8-D1A cells were pretreated with serum-free medium for 24 h to achieve cell cycle synchronization. The cells were then exposed to gradient concentrations of MPT0B390 (*e.g.*, 0.01, 0.1, 1, and 2 μM) or the solvent control (0.1% DMSO) for 24 h. Cell viability was subsequently assessed using the CCK-8 assay.

2.16. Exosome labeling and uptake

In accordance with the manufacturer's instructions, PKH26 Fluorescent Cell Linker Kits (Umibio, Shanghai, China, UR52302) were used to label the exosomes. Next, the exosomes (200 μg/mL) were incubated with 5×10^5 astrocytes for 24 h, fixed with 4% formaldehyde for 30 min, stained with DAPI for 15 min, and observed under a fluorescence microscope (KEYENCE, Osaka, Japan).

2.17. Cellular immunofluorescence staining

After cell fixation and goat serum blocking, the cells were incubated with primary antibodies (MS anti-AQP4: Bioss antibodies, Beijing, China, bsm-33068M, 1:100; rabbit anti-TIMP3: Thermo Fisher Scientific, PA5-116049, 1:100; MS anti-β-DG: Santa Cruz Biotechnology, sc-33702, 1:50) at 4°C overnight. On the next day, the 96-well plates were washed 3 times with PBS and incubated with secondary antibodies (goat-anti-rabbit IgG: Abcam, ab150077, 1:500 and goat-anti-MS IgG: Abcam, ab150113, 1:500) at room temperature for 2 h. Finally, the cells were washed 3 times with PBS and sealed with an anti-fluorescence quenching agent. Finally, ImageJ software was used to analyze the areas of TIMP3, AQP4 and β-DG expressions.

2.18. Statistical analysis

The experimental data are presented as the means ± SDs and were analyzed using SPSS 29.0 statistical software. Escape latency data were analyzed by repeated-measures analysis of variance. One-way ANOVA was used for normally distributed data, whereas the Kruskal-Wallis test was used for abnormally distributed data. A *P* value less than 0.05 was used to indicate statistical significance. All the data were plotted using GraphPad Prism 8 software and assembled using Adobe Photoshop CS6 software.

3. Results

3.1. Identification of chemical constituents in ZMHB extracts

For quality assurance, we used UPLC–Q–TOF–MS to analyze the chemical profile of ZMHB. The ion chromatograms and detailed information of the ZMHB component analysis are shown in Figure 1 and Table 1. By searching the literature, Traditional Chinese Medicine Database (TCMD) and Traditional Chinese Medicine Systems Pharmacology Database and Analysis Platform (TCMSP), the chemical constituents of ZMHB were summarized. The main components are as follows: mangiferin from Anemarrhenae Rhizoma, and berberine and phellodendrine from Phellodendri Chinensis Cortex.

3.2. ZMHB improved the cognitive function of DCI rats

The procedures for model induction and drug treatment are shown in Figure 2A. We first investigated the effects of ZMHB on body weight and FBG levels in DCI rats. At the endpoint of treatment, our results demonstrated that DCI rats exhibited significantly reduced body weights (Figure 2B) and markedly elevated FBG levels (Figure 2C), which are consistent with the clinical manifestations of patients with type 2 diabetes. Postintervention, the body weights of both ZMHB-L and ZMHB-H tended to increase in DCI rats (Figure 2B). However, neither ZMHB-L nor ZMHB-H reduced the elevated FBG levels in DCI rats (Figure 2C). To investigate the impact of ZMHB on cognitive function in DCI rats, we evaluated spatial learning and memory abilities using the MWM test. Compared with the Con group, the DCI group exhibited longer escape latencies, indicating impaired learning ability (Figure 2D). Notably, the ZMHB-L and ZMHB-H treatments significantly shortened the escape latencies (Figure 2D), suggesting that ZMHB ameliorates DCI-induced learning deficits. In the spatial probe trial (platform removed), DCI rats exhibited prolonged times to first reach the original platform location, whereas ZMHB-treated animals exhibited significantly shorter times

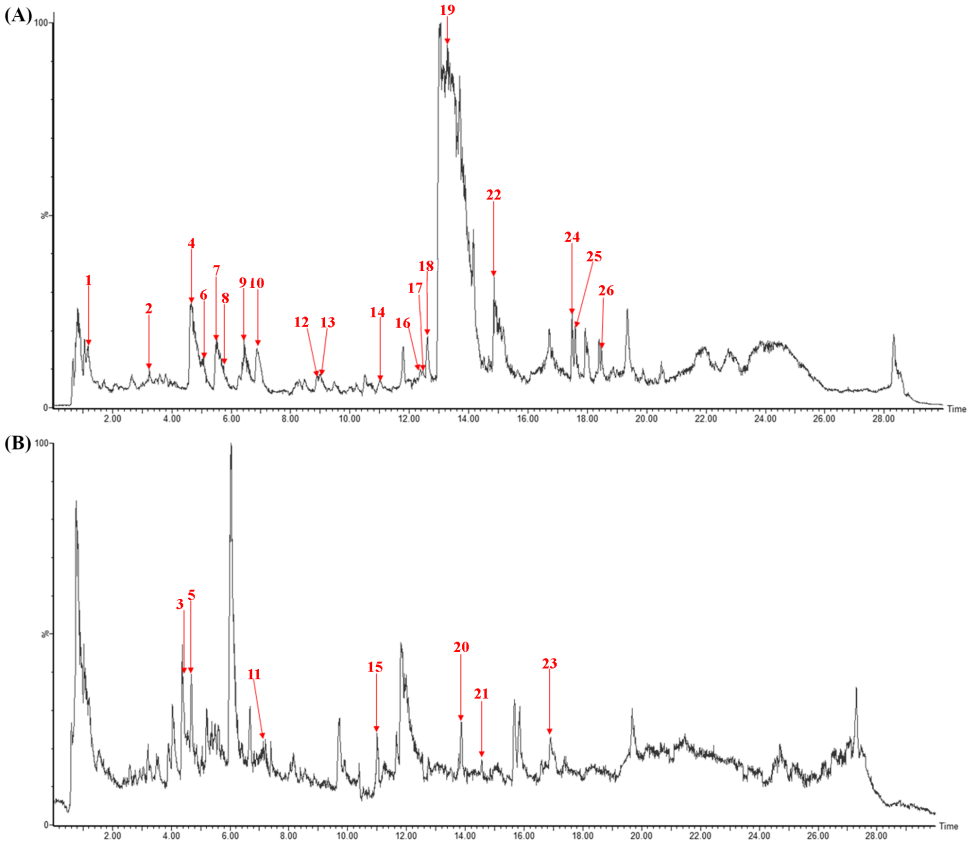

Figure 1. Identification of chemical constituents in ZMHB extracts. (**A**) shows the positive acquisition mode. (**B**) shows the negative acquisition mode.

Table 1. Identification of chemical constituents in ZMHB extracts

No	t/min	Mz	Exact mass	Error	Formula	Name	Plant material
1	1.17	180.1391	181.278	1.14	$C_{11}H_{18}NO$	N-Candicine	Huangbo
2	3.24	585.1458	585.4957	0.35	$C_{25}H_{28}O_{16}$	Neomangiferin	Zhimu
3	4.43	353.0870	353.3056	0.22	$C_{16}H_{18}O_9$	Chlorogenic acid	Huangbo
4	4.65	342.1711	343.4228	1.25	$C_{20}H_{24}NO_4$	Phellodendrine	Huangbo
5	4.69	367.1025	366.3245	-0.80	$C_{17}H_{19}O_9$	Amurenlactone A/B	Huangbo
6	5.07	448.1981	449.5011	1.30	$C_{23}H_{30}NO_8$	7-O_x005f_x005f_x005fglucopyranoside of 1-(p_x0002_hydroxybenzyl)- 6,7-dihydroxy-Nmethylisoquinoline	Huangbo
7	5.41	423.0928	423.3533	0.26	$C_{19}H_{18}O_{11}$	Mangiferin	Zhimu
8	5.63	342.1703	343.4228	1.25	$C_{20}H_{24}NO_4$+	Magnoflorine	Huangbo
9	6.43	369.1196	369.3483	0.23	$C_{17}H_{20}O_9$	3-Feruloylquinic acid	Huangbo
10	6.93	314.1752	314.4045	0.23	$C_{19}H_{23}NO_3$	Lotusine	Huangbo
11	7.21	567.2085	567.5671	0.36	$C_{27}H_{36}O_{13}$	(+/-) 8- (4-Hydroxy_x005f3-methoxyphenyl)- 6,7-bis(hydroxymethyl) -3-methoxy_x0002_5,6,7,8-tetrahydro_x0002_2-naphthalenyl-β-D-glucopyranoside	Huangbo
12	8.90	344.1854	345.4387	1.25	$C_{20}H_{26}NO_4$	Tembetarine	Huangbo
13	9.00	356.1856	356.4418	0.26	$C_{21}H_{25}NO_4$	Menisperine	Huangbo
14	10.99	356.1855	356.4418	0.26	$C_{21}H_{25}NO_4$	Tetrahydropalmati	Huangbo
15	11.03	259.0604	259.2383	0.18	$C_{14}H_{12}O_5$	2,6,4'-trihydroxy-4- methoxybenzophenoe	Zhimu
16	12.39	322.1076	323.3483	1.24	$C_{19}H_{16}NO_4$	Berberrubine	Huangbo
17	12.44	338.1392	339.3911	1.25	$C_{20}H_{20}NO_4$	Columbamine	Huangbo
18	12.61	338.1391	339.3911	1.25	$C_{20}H_{20}NO_4$+	Jatrorrhizine	Huangbo
19	13.27	336.1237	337.3752	1.25	$C_{20}H_{18}NO_4$	Berberine	Huangbo
20	13.86	947.4879	947.0816	-0.40	$C_{46}H_{75}O_{20}$	Timosaponin C	Zhimu
21	14.56	329.2313	329.4570	0.23	$C_{18}H_{34}O_5$	Sanleng acid	Huangbo
22	14.86	903.4950	904.0797	0.58	$C_{45}H_{74}O_{18}$	Timosaponin B	Zhimu
23	16.91	251.1075	251.3049	0.20	$C_{17}H_{16}O_2$	Nyasol	Zhimu
24	17.49	471.2027	471.5273	0.32	$C_{26}H_{30}O_8$	Obaculactone	Huangbo
25	17.60	741.4406	741.9373	0.50	$C_{39}H_{64}O_{13}$	Timosaponin A-III	Zhimu
26	18.38	455.2066	455.5279	0.32	$C_{26}H_{30}O_7$	Obacunone	Huangbo

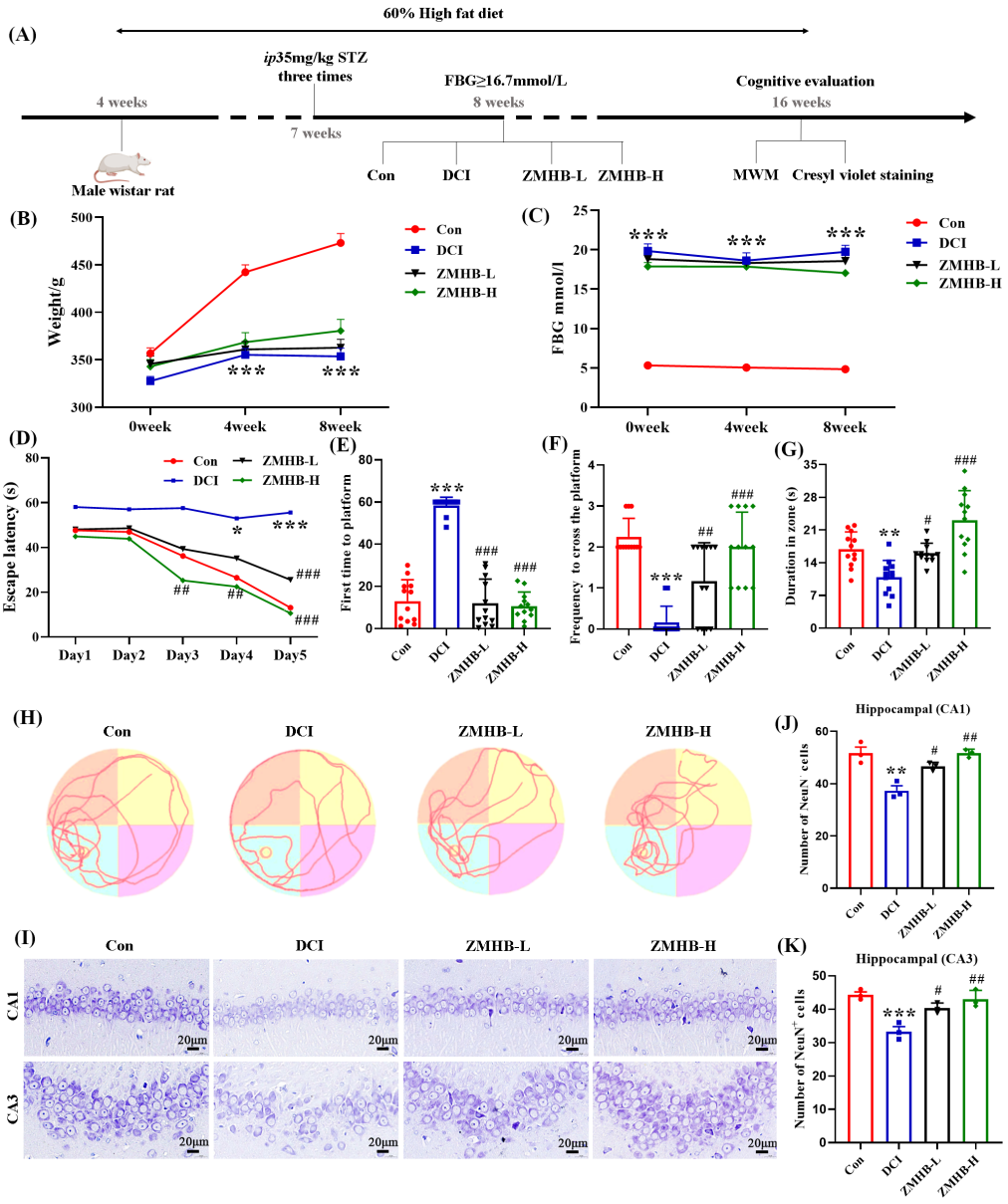

Figure 2. ZMHB improved the cognitive function of DCI rats. (**A**) Experimental workflow: Diabetic rats (induced by HFD + STZ, blood glucose concentration ≥ 16.7 mmol/L at 1 week post-modeling) were randomized into the DCI, ZMHB-L (2.16 g/kg), and ZMHB-H (4.32 g/kg) groups. (**B**) Body weights. (**C**) FBG. (**D–H**) Learning and memory functions were assessed by the MWM test after 8 weeks of treatment, including (**D**) 5-day escape latency during training and probe trial parameters after platform removal on Day 6: (**E**) first platform crossing latency, (**F**) frequency to cross the platform, (**G**) duration in target quadrant, and (**H**) representative swimming trajectories (n = 12). (**I**) Cresyl violet staining of the hippocampal CA1 and CA3 regions; scale bar = 20 μm (63×). (**J**) Neuronal count in CA1 (n = 3). (K) Neuronal count in CA3 (n = 3). The data are expressed as the means ± SDs. $^{*}P < 0.05$, $^{**}P < 0.01$, and $^{***}P < 0.001$ compared with the Con group; $^{\#}P < 0.05$, $^{\#\#}P < 0.01$, and $^{\#\#\#}P < 0.001$ compared with the DCI group.

(Figure 2E). Moreover, compared with Con rats, the DCI rats displayed fewer platform crossings and shorter dwell times in the target quadrant (Figures 2F and 2G). In contrast, ZMHB-treated rats exhibited significantly increased crossing frequencies and quadrant dwell times (Figures 2F and 2G). The results of the swimming trajectory analysis further supported these findings: Con rats persistently navigated toward the original platform position, whereas DCI rats swam irregularly. Strikingly, ZMHB-L- and ZMHB-H-treated animals showed improved directional movements and purposeful navigation (Figure 2H). Hippocampal CA1 and CA3 neuronal damage critically contributes to cognitive impairment. Cresyl violet staining revealed that the hippocampal neurons in the CA1 and CA3 regions of the DCI group were disorganized in terms of arrangement, reduced in number (Figures 2I-2K), irregular in morphology, and unevenly stained. However, the neurons in each treatment group were arranged neatly, their numbers significantly increased (Figures 2I-2K), their morphology was regular, and their staining was uniform. In summary, ZMHB alleviated cognitive dysfunction and hippocampal neuronal damage in a dose-dependent manner, with the efficacy of ZMHB-H

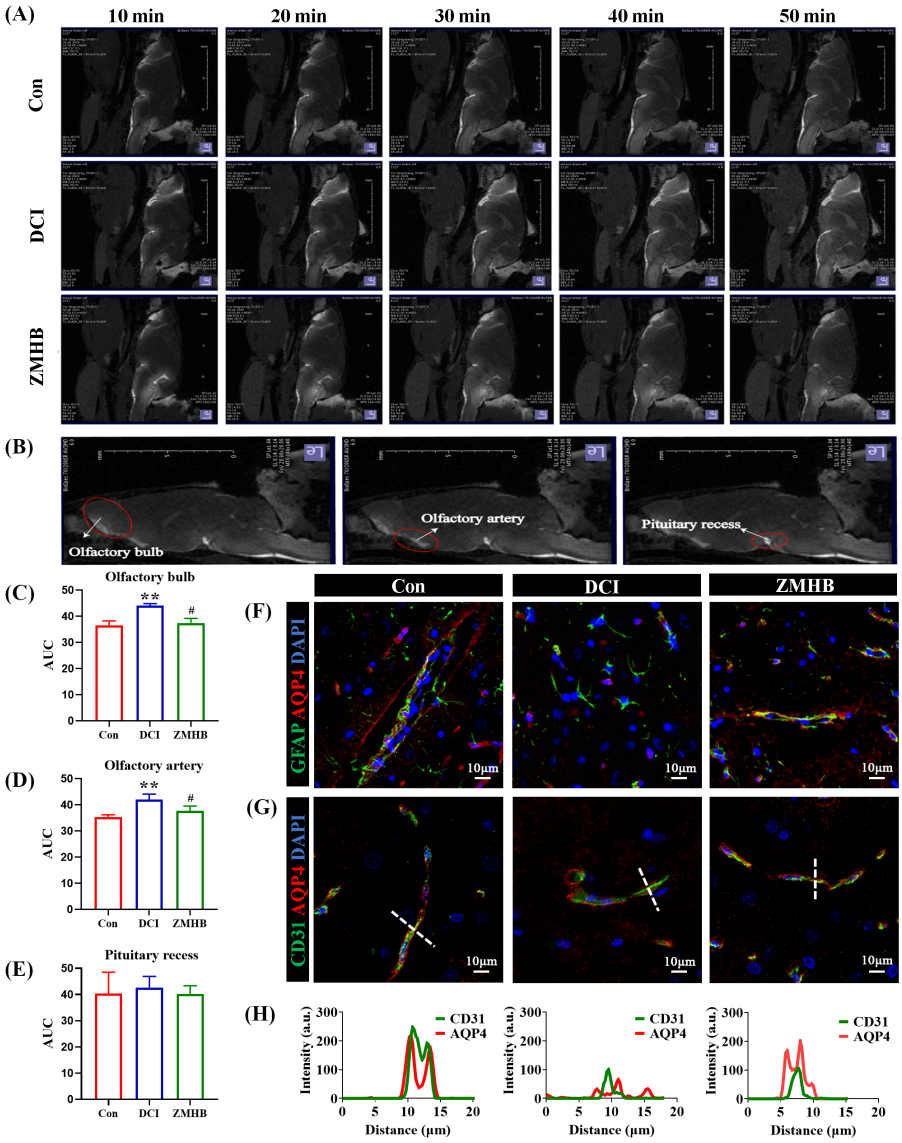

Figure 3. ZMHB enhanced GS clearance in DCI rats by maintaining AQP4 polarization. (**A**) Glymphatic system clearance function. (**B**) Gd-DTPA clearance rate. (**C-E**) Area under the curve (AUC) (n = 3). (**F**) Representative immunofluorescence images of the polarized distribution of AQP4 (red) in GFAP-positive astrocytes (green) within the cerebral cortex; scale bar = 10 μm (40×). (**G**) Representative immunofluorescence images of perivascular colocalization between AQP4 (red) and CD31 endothelial cells (green) in the cerebral cortex; scale bar = 10 μm (40×). (**H**) Quantitative expression of AQP4 under 20 μm vessel length. Data are expressed as the means ± SDs. $^{**}P < 0.01$ compared with the Con group; $^{\#}P < 0.05$ compared with the DCI group.

superior to that of ZMHB-L; thus, ZMHB-H was selected for subsequent investigations.

3.3. ZMHB enhanced GS clearance in DCI rats by maintaining AQP4 polarization

Modern medicine posits that impaired GS clearance constitutes the primary cause of learning and memory decline in diabetic rats (*6*), a mechanism congruent with the TCM pathogenesis theory of "toxin damaging brain collaterals". We detected GS clearance functioning through MRI, and the results revealed that in the Con group, the Gd-DTPA signal intensity peaked within 10-20 min post-injection and gradually decreased from 20 min onward. In contrast, the DCI group exhibited a peak Gd-DTPA signal intensity at 30 min post-injection, with no decreasing trend observed during the detection period, indicating a reduced cerebrospinal fluid–interstitial fluid (CSF–ISF) transport rate (Figure 3A). Additionally, the DCI group showed a significantly increased area under the curve (AUC) of the Gd-DTPA signal intensity in the olfactory bulb and olfactory artery regions, reflecting a decreased clearance rate and confirming GS dysfunction (Figures 3B-3E). Compared with the DCI group, the ZMHB group demonstrated a peak signal intensity at 20 min post-injection followed by a gradual decrease, a significantly increased CSF–ISF exchange rate (Figure 3A), markedly reduced AUC values in the olfactory

bulb and olfactory artery regions, and an increased Gd-DTPA clearance rate, suggesting that ZMHB improves GS clearance function (Figures 3B-3E). Considering that the distribution of AQP4 in perivascular astrocyte endfeet was the key histological basis of GS, we explored whether AQP4 participated in the regulation of DCI. Immunofluorescence analysis revealed that DCI rats exhibited a loss of polarized AQP4 distribution at perivascular astrocyte endfeet (GFAP), characterized by diffuse depolarized localization away from CD31-labeled vascular interfaces. ZMHB treatment restored astrocytic AQP4 polarization, as evidenced by AQP4 enrichment at perivascular endfeet (Figures 3F-3H). These findings indicate that ZMHB prevents and treats cognitive impairment by preserving AQP4 polarization to increase the clearance capacity of GS.

3.4. ZMHB restored AQP4 polarization in DCI rats through the exosomal pathway

Building on previous findings from our research group demonstrating that exosomes regulate AQP4 polarization to influence GS functionality (*24*), in this study, ZMHB was coadministered with the exosome release inhibitor GW4869 to elucidate the necessity of the exosomal pathway in the ZMHB-mediated restoration of AQP4 polarization. MWM tests demonstrated that ZMHB + GW4869 cotreatment abolished the ZMHB-induced improvements in learning and memory, as evidenced by prolonged escape latencies (Figure 4A), extended times to first reach the platform location (Figure 4B), reduced platform crossing frequencies (Figure 4C), shorter dwell times in the target quadrant (Figure 4D), and disorganized swimming trajectories (Figure 4E). Furthermore, GW4869 intervention eliminated the neuroprotective effects of ZMHB on hippocampal CA1/CA3 neurons, as shown by reduced neuronal density (Figures 4F-4H). Concurrently, ZMHB-induced restoration of AQP4 polarization at perivascular astrocyte endfeet was reversed, characterized by diffuse AQP4 distribution throughout astrocytes rather than localized perivascular clustering (Figures 4I-4K). These findings confirm that the exosomal pathway is essential for the ability of ZMHB to restore AQP4 polarization in DCI rats.

3.5. ZMHB ameliorated AQP4 depolarization in DCI rats by regulating serum-derived exosomal TIMP3-mediated MMP9/β-DG pathway

Circulating sExos are among the important sources of brain exosomes (*25*). To further investigate the mechanism of sExos in DCI, we isolated exosomes from the serum of experimental rats and characterized them using TEM, NTA, and western blotting. The sExos formed a double-layered membrane with a size distribution of 30–150 nm (Figures 5A and 5B), and tested positive for the exosome marker proteins, CD81 and TSG101 (Figure 5C). In summary, the circulating serum particles conformed to the characteristics of exosomes.

To elucidate the molecular mechanisms by which sExos regulate AQP4 polarization, we performed proteomics on the Con-sExos, DCI-sExos, and ZMHB-sExos groups. The results revealed 26 significantly upregulated proteins and 4 downregulated proteins in the ZMHB-sExos group, with TIMP3 expression markedly upregulated (Figure 5D-5F). The polarization of AQP4 is closely related to that of MMP9 (*13*), and TIMP3 is a natural inhibitor of MMP9 that can inhibit the activity of MMP9 and protect β-DG from degradation, thus supporting the polarization and function of AQP4. On the basis of the anchoring structure of AQP4 polarization and literature evidence, this study focused on the key protein TIMP3. Western blotting validation revealed that ZMHB significantly upregulated TIMP3 expression in the sExos group compared with that in the DCI-sExos group (Figures 5G and 5H), which is consistent with the proteomic findings. To explore how ZMHB restores AQP4 polarization in DCI rats, particularly its effects on the TIMP3-MMP9/β-DG pathway, we further analyzed the protein expressions in brain tissue. Western blotting results demonstrated that ZMHB intervention upregulated TIMP3 expression (Figures 5I and 5J) but downregulated the expressions of MMP9 and cleaved β-DG (Figures 5K-5N). Dual immunofluorescence staining of TIMP3/GFAP and β-DG/AQP4 revealed that ZMHB restored TIMP3 expression in astrocytes and enhanced β-DG-AQP4 colocalization (Figure 5O-5Q). These findings collectively suggest that ZMHB maintains astrocytic AQP4 polarization in DCI rats *via* the TIMP3-MMP9/β-DG pathway.

3.6. *In vitro* overexpression of TIMP3 improved the depolarization of AQP4 in astrocytes

To further validate the effects of serum exosomal TIMP3 on astrocytic AQP4 polarization, we induced a high-glucose injury model in astrocytes (Figure 6A) and treated both the Con and M groups with PKH26-labeled sExos (red fluorescence) for 24 h. Fluorescence imaging demonstrated effective exosome uptake by astrocytes, as indicated by the red intracellular signal (Figure 6C). The western blotting results demonstrated that the high-glucose environment both significantly suppressed TIMP3 expression in astrocytes and activated the abnormal MMP9-mediated β-DG cleavage pathway, leading to abnormally elevated ratios of the expressions of the AQP4 polarity markers M1/M23 (Figures 6D-6I). Notably, ZMHB-sExos and the TIMP3 small-molecule agonist MPT0B390 specifically upregulated TIMP3 protein levels, inhibited MMP9 activity, blocked β-DG cleavage, and ultimately restored the distribution of AQP4 polarization (Figures 6D-6I). Immunofluorescence

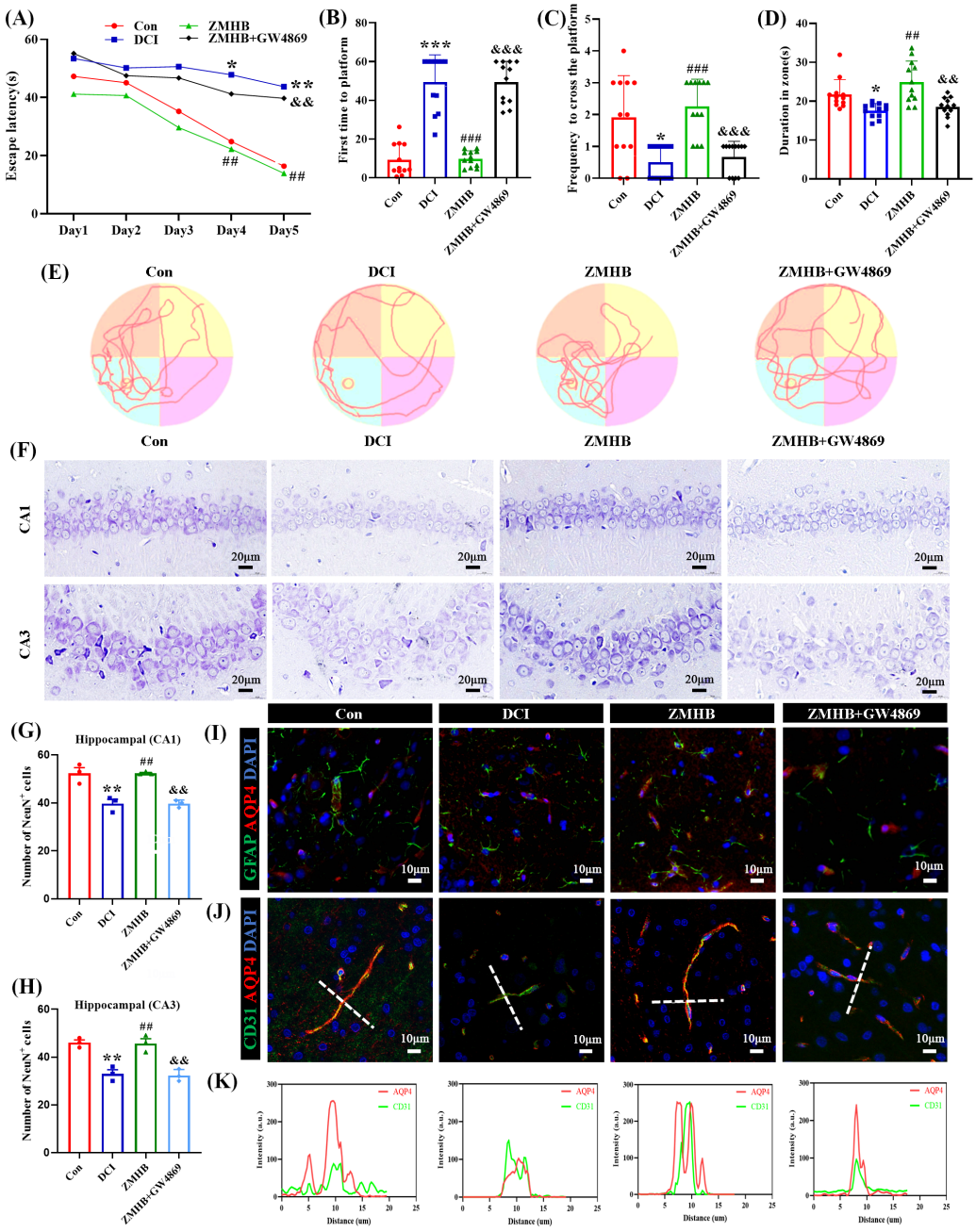

Figure 4. ZMHB restored AQP4 polarization in DCI rats through the exosomal pathway. Diabetic rats were randomized into DCI, ZMHB (4.32 g/kg), and ZMHB + GW4869 (4.32 g/kg + 1 mg/kg) groups. (**A-E**) Learning and memory functions were assessed by the MWM test after 8 weeks of treatment, including (**A**) 5-day escape latency during training and probe trial parameters after platform removal on Day 6: (**B**) first platform crossing latency, (**C**) frequency to cross the platform, (**D**) duration in target quadrant, and (**E**) representative swimming trajectories (n = 12). (**F**) Cresyl violet staining of the hippocampal CA1 and CA3 regions; scale bar = 20 μm (63×). (**G**) Neuronal count in CA1 (n = 3). (**H**) Neuronal count in CA3 (n = 3). (**I**) Representative immunofluorescence images of the polarized distribution of AQP4 (red) in GFAP-positive astrocytes (green) within the cerebral cortex; scale bar = 10 μm (40×). (**J**) Representative immunofluorescence images of perivascular colocalization between AQP4 (red) and CD31 endothelial cells (green) in the cerebral cortex; scale bar = 10 μm (40×). (**K**) Quantitative expression of AQP4 under 20 μm vessel length. Data are expressed as the means ± SDs. $^{*}P < 0.05$, $^{**}P < 0.01$, and $^{***}P < 0.001$ compared with the Con group; $^{\#\#}P < 0.01$ and $^{\#\#\#}P < 0.001$ compared with the DCI group; $^{\&\&}P < 0.01$ and $^{\&\&\&}P < 0.001$ compared with the ZMHB group.

staining further verified that ZMHB-sExos and MPT0B390 reversed the reduced expressions of AQP4, TIMP3, and β-DG that were caused by the high-glucose environment (Figures 6J and 6K). These findings establish the central role of the TIMP3-MMP9/β-DG pathway in the AQP4 polarization-mediated functional regulation of astrocytes.

4. Discussion

This study aimed to investigate the pathogenesis of DCI and the therapeutic effects of ZMHB from the perspective of the exosomal pathway. The results provide evidence that 1) ZMHB restored AQP4 polarization in DCI rats; 2) the exosomal pathway was essential for the ZMHB-

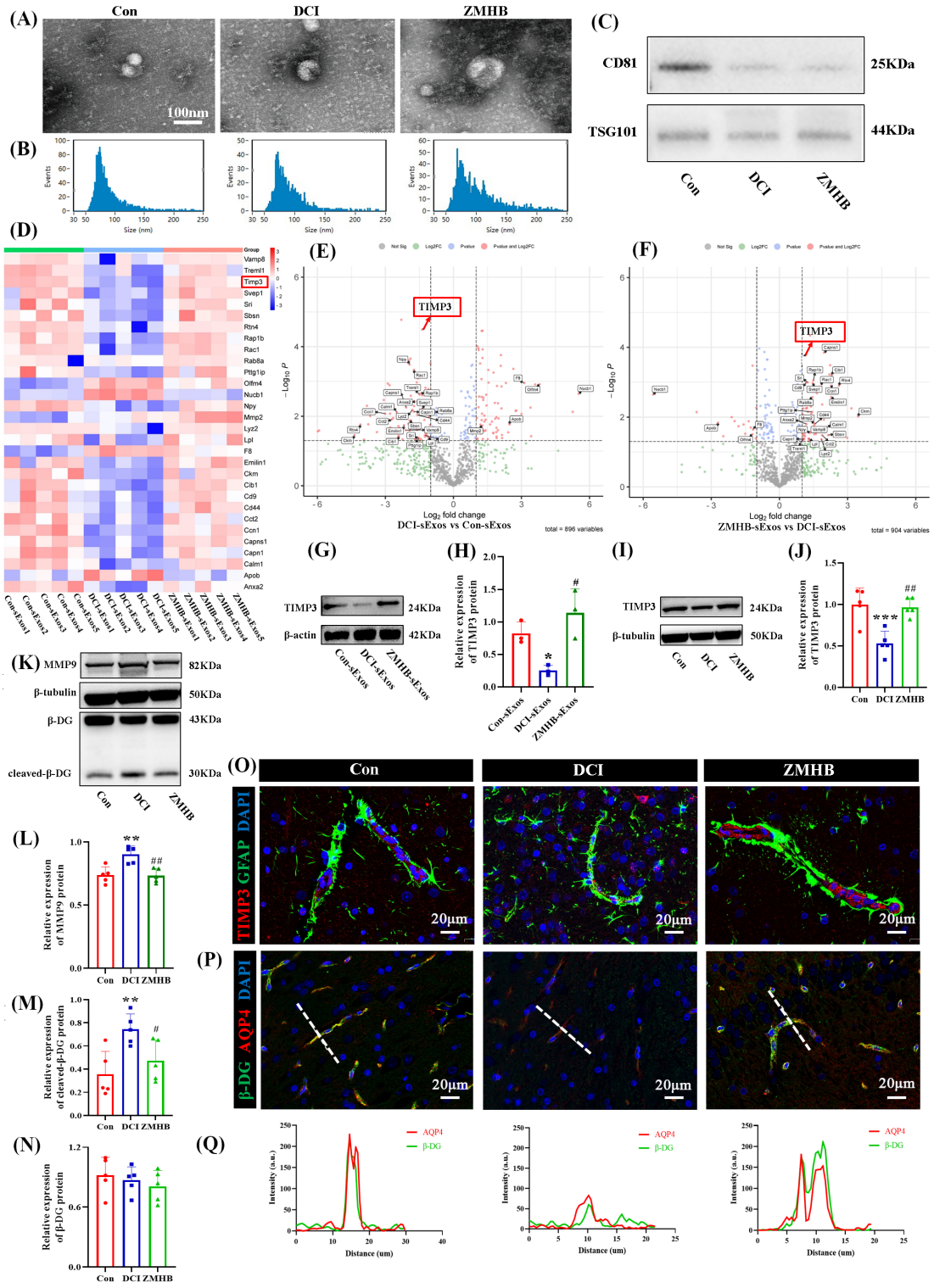

Figure 5. ZMHB ameliorated AQP4 depolarization in DCI rats by upregulating the serum-derived exosomal TIMP3-mediated MMP9/β-DG pathway. (**A**) Representative electron micrographs of sExos; scale bar = 100 nm. (**B**) Particle size distribution of sExos. (**C**) Expressions of the serum exosomal marker proteins CD81 and TSG101 ($n = 3$). (**D**) Hierarchical clustering heatmap of serum exosomal proteome profiles across the Con, DCI, and ZMHB groups, with red indicating higher expressions and blue indicating lower expressions ($n = 5$). (**E** and **F**) Volcano plot of differentially expressed exosomal proteins in DCI-sExos *vs.* Con-sExos (**E**) and in ZMHB-sExos *vs.* DCI-sExos (**F**), with the right quadrant indicating upregulated proteins (log2FC > 1, $P < 0.05$) and the left quadrant indicating downregulated proteins (log2FC < -1, $P < 0.05$) ($n = 5$). (**G** and **H**) The expressions of TIMP3 in sExos were detected by western blotting ($n = 3$). (**I** and **J**) TIMP3 expressions in whole-brain tissue were detected by western blotting ($n = 5$). (**K-N**) MMP9, cleaved-β-DG and β-DG expressions ($n = 5$) in whole-brain tissue were detected by western blotting. (**O**) TIMP3 (red) and GFAP (green) in cortical tissue sections from each group of rats were subjected to dual fluorescence staining; scale bar = 20 μm (40×). (**P**) The colocalization of AQP4 (red) and β-DG (green) in cortical tissue sections from rats in each group was determined using dual fluorescence staining; scale bar = 20 μm (40×). (**Q**) Linear intensity profiles of AQP4 and β-DG along 20 μm cortical regions (white dashed lines in P figure). Data are expressed as the means ± SDs. $^{*}P < 0.05$, $^{**}P < 0.01$, and $^{***}P < 0.001$ compared with the Con group; $^{\#}P < 0.05$ and $^{\#\#}P < 0.01$ compared with the DCI group.

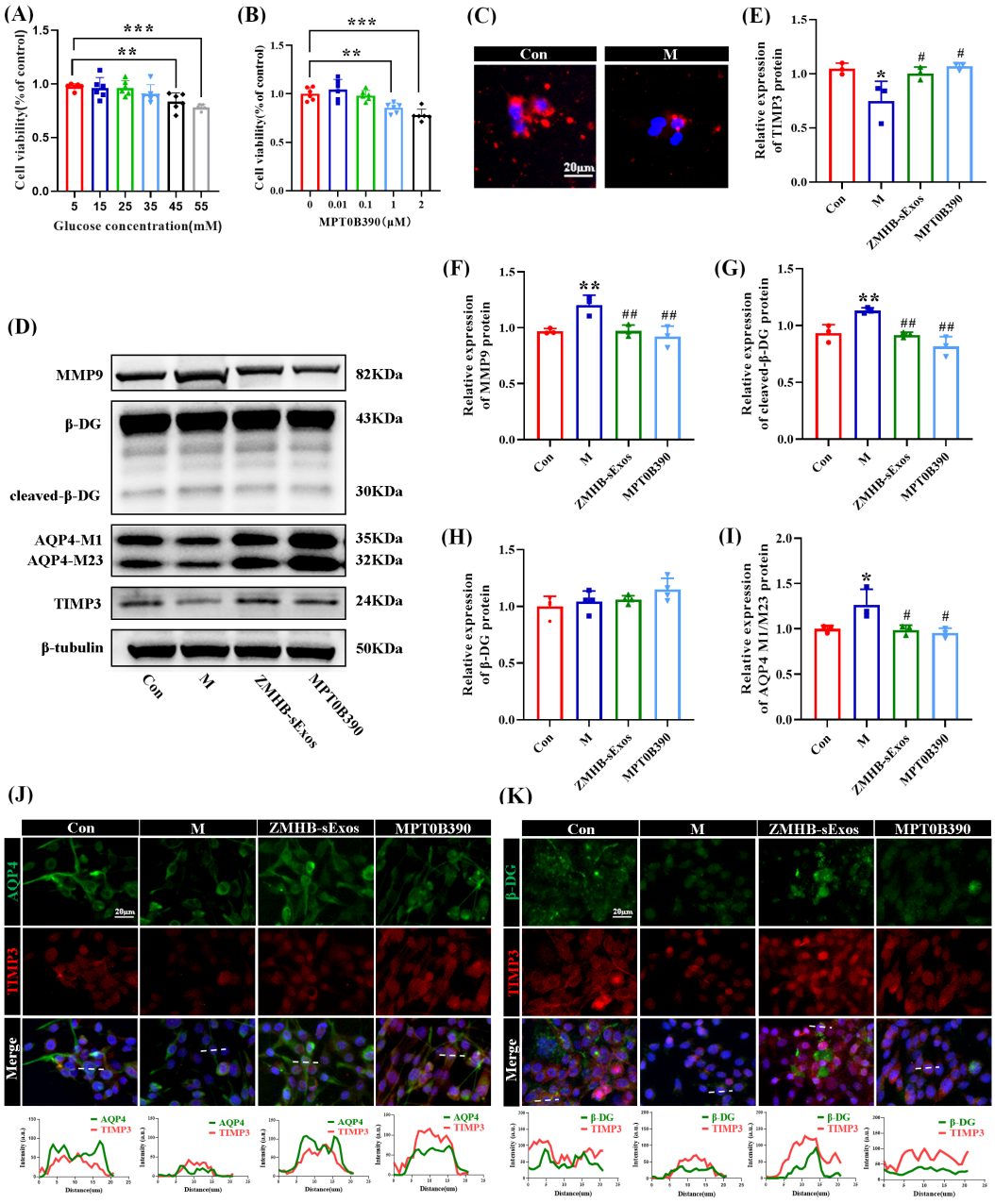

Figure 6. ***In vitro*** **overexpression of TIMP3 improved the depolarization of AQP4 in astrocytes.** (**A**) Murine astrocytes were subjected to glucose gradient screening (5–55 mM, 24 h) to induce hyperglycemic injury. The 45 mM dose (M: Model group) was determined to be optimal *via* a CCK-8 viability assay ($n = 6$). (**B**) Murine astrocytes were treated with a TIMP3 overexpression agent (0–2 μM) for 24 h under normal conditions. 0.1 μM was identified as the safe concentration with no cytotoxicity ($n = 6$). (**C**) Immunofluorescence analysis of the internalization of PKH26-labeled circulating serum-derived exosomes (red) by astrocytes. (**D-I**) TIMP3 (**E**), MMP9 (**F**), cleaved-β-DG (**G**), β-DG (**H**) and AQP4 M1/M23 (**I**) expression in astrocytes was detected by western blotting ($n = 3$). (**J-K**) Dual-labeling immunofluorescence analysis of protein colocalization in murine astrocytes. (**J**) AQP4 (green) and TIMP3 (red) colocalization after treatment with ZMHB-sExos or TIMP3 overexpression; scale bar = 20 μm (40×). (**K**) β-DG (green) and TIMP3 (red) colocalization after treatment with ZMHB-sExos or TIMP3 overexpression; scale bar = 20 μm (40×).

mediated restoration of AQP4 polarization in DCI rats; and 3) ZMHB upregulated peripheral exosomal TIMP3 expression and inhibited MMP9-mediated aberrant cleavage of β-DG, thereby restoring AQP4 polarization. These results not only confirm that dysregulated TIMP3-MMP9/β-DG/AQP4 signaling mediated by peripheral exosomes underlies DCI pathology but also demonstrate the potential of ZMHB as a therapeutic agent targeting this pathway. This study elucidates the modern scientific connotation of TCM pathogenesis "toxin damaging brain collaterals" from the perspective of AQP4 depolarization-mediated GS dysfunction, while identifying TIMP3 as a potential therapeutic target for reversing cognitive impairment in DCI patients.

Although ZMHB did not significantly affect body weight or FBG in DCI rats, it effectively alleviated neuronal damage and improved cognitive function. This therapeutic mechanism may involve the regulation of

hyperglycemia-induced pathological cascades by ZMHB, thereby improving cognitive function.

Related studies have shown that the clearance rate of interstitial fluid in the hippocampus and hypothalamus of diabetes patients is slow and that the function of the GS is abnormal, which may be an important reason for cognitive dysfunction (*8,26*). Most previous studies have focused on treating cognitive impairment by blocking the production of toxic substances such as amyloid-β (Aβ) (*27-29*), phosphorylated tau proteins (*30*), and advanced glycation end products (AGEs) (*31*) in brain tissue. In fact, these approaches have shown limited efficacy in halting cognitive decline. Recent evidence has indicated that diabetes may induce AQP4 depolarization in perivascular astrocytes (*32,33*), characterized by diffuse redistribution of AQP4 throughout the astrocytic soma (rather than polarized localization at perivascular endfeet) and an increased abundance of freely mobile tetrameric AQP4-M1 isoforms. This pathological redistribution disrupts cerebrospinal fluid flow dynamics, reduces the clearance efficiency of metabolic waste, and promotes the accumulation of toxic aggregates. Maintaining AQP4 polarization at astrocytic endfeet could restore GS inflow–outflow balance, increase cerebrospinal–interstitial fluid exchange, and provide a novel strategy for toxin clearance, offering new perspectives for preventing cognitive impairment. Guided by this premise, we investigated the association between AQP4 dysregulation-mediated GS dysfunction and DCI progression. Mechanistically, ZMHB ameliorates DCI by promoting AQP4 polarization to restore the GS clearance efficiency, which aligns with the TCM pathogenesis of "toxin damaging brain collaterals", potentially establishing the modern pathological basis for this TCM theory. Nevertheless, the regulatory mechanisms underlying AQP4 spatial redistribution in DCI require further exploration.

Previous studies have confirmed the pharmacological efficacy of ZMHB in restoring the distribution of AQP4 polarization in DCI rats, but its limited bioavailability in the brain (*34*), suggests that this effect may be mediated through peripheral regulatory mechanisms. Additionally, research has demonstrated that peripheral-derived exosomes can mediate GS clearance function by regulating the distribution of AQP4 polarization (*24*). For example, Wang *et al.* suggested that peripheral adipose tissue-derived exosomes could cause synaptic loss and cognitive impairment (*35*). On the basis of these findings, we investigated the role of the exosomal pathway in the ZMHB-mediated maintenance of AQP4 polarization by coadministering ZMHB with the exosome release inhibitor GW4869. The results showed that GW4869 partially decreased the efficacy of ZMHB in maintaining AQP4 polarization, consequently diminishing its ability to improve cognition and provide neuroprotection in DCI rats. These findings confirm that the delivery of peripheral-derived exosomes into the brain is critical for the ability of ZMHB to restore the distribution of AQP4 polarization.

Exosomes can achieve intercellular information transmission (*36-38*) by transferring various substances such as functional proteins, nucleic acids, and lipids (*39*). This study focused on exosomal functional proteins, and through proteomics screening, it was found that 26 proteins were significantly upregulated and 4 proteins were downregulated in the ZMHB-sExos group, with TIMP3 expression being significantly upregulated. Previous studies have shown that the distribution of polarized AQP4 partially depends on the complete dystroglycan complex (DGC)-like complex, which includes β-DG, α-synaptic nutrients, and dystrophin protein 71 (Dp71) (*40*). Si *et al.* reported that stable binding of β-DG to AQP4 could maintain polarization on the terminal feet of astrocytes (*13*). Mutations or defects in β-DG lead to impaired localization and function of AQP4, highlighting the importance of β-DG in anchoring AQP4 (*41*). The matrix metalloproteinase MMP9 degrades extracellular matrix (ECM) components. TIMP3 is a natural inhibitor of MMP9, which can inhibit the activity of MMP9, protect β-DG from degradation, and maintain the connection between cells and the ECM, thus supporting the polarization and function of AQP4. Multiple studies have shown that β-DG can be cleaved by MMP9 in various disease models (*15,16,42*). Under pathological conditions, downregulation of MMP9 blocker TIMP3 could activate MMP9. Combined with the anchoring structure of AQP4 polarization and existing evidence in the literature, our findings indicate that TIMP3 in circulating sExos is a key protein that regulates AQP4 polarization. ZMHB specifically upregulated TIMP3 levels in both sExos and brain tissues, which is consistent with the proteomics results. We therefore propose that brain-targeted delivery of serum-derived exosomal TIMP3 constitutes the central mechanism through which ZMHB maintains AQP4 polarization and alleviates DCI. Through *in vivo* experiments, we further investigated the regulatory effects of ZMHB on the TIMP3-MMP9/β-DG pathway. The results demonstrated that ZMHB promoted the entry of TIMP3 from circulating sExos into the brain, preventing β-DG from being cleaved by MMP9 and thereby maintaining the polarization of AQP4 in astrocytes. Overall, our data support the hypothesis that ZMHB restores AQP4 depolarization in DCI rats by modulating the exosomal TIMP3-mediated MMP9/β-DG pathway.

It should be noted that the primary aim of this study was to validate the existence of the "TIMP3-MMP9/β-DG-AQP4" signaling axis at a core level. While the high-glucose-treated astrocyte model used herein, as a classic *in vitro* system, provided key evidence supporting this central mechanism, we clearly recognize that this monoculture model cannot fully recapitulate the complexity of multicellular interactions within the

neurovascular unit (NVU)—such as those involving vascular endothelial cells, microglia, and neurons—in the *in vivo* DCI environment. For instance, the absence of brain microvascular endothelial cells, which play critical roles in blood-brain barrier (BBB) function, cytokine secretion, and responses to hyperglycemic stress, underscores the necessity for future studies to employ more complex models to explore the complete regulatory network of this pathway within the NVU. Therefore, utilizing co-culture models of astrocytes with brain microvascular endothelial cells or microglia, and even developing three-dimensional brain organoid models, will be important future directions for comprehensively elucidating this signaling axis. Notwithstanding these limitations, the evidence obtained from our simplified high-glucose astrocyte model still provides preliminary yet crucial support for the central role of serum exosomal TIMP3. To further confirm the effects of serum exosomal TIMP3 on astrocytic AQP4 polarization, MPT0B390 was applied to astrocytes, revealing that TIMP3 is a critical target for AQP4 polarization. Treatment of astrocytes with sExos specifically increased TIMP3 protein levels, inhibited MMP9 activity, blocked β-DG cleavage, and ultimately restored the distribution of AQP4 polarization. These findings establish the central role of the TIMP3-mediated MMP9/β-DG pathway in regulating astrocyte functions that are mediated by AQP4 polarization.

This study focuses on elucidating the integrated mechanism by which the TCM formula ZMHB alleviates DCI through the exosomal TIMP3-MMP9/β-DG-AQP4 axis. It is important to note that as a multi-component system, a comprehensive understanding of ZMHB's pharmacological material basis relies on in-depth analysis of its single active ingredients. Existing research suggests that common constituents of ZMHB (such as alkaloids, flavonoids, and saponins) possess the potential to regulate intercellular communication *via* exosomal pathways. For instance, berberine, a typical alkaloid, has been shown to modulate miR-182-5p expression in astrocyte-derived exosomes in neurological disease models, thereby suppressing neuroinflammation (*43*). In the context of diabetic nephropathy, it also inhibits the high glucose-induced transfer of TGFβ1 from mesangial cells to podocytes *via* exosomes, protecting podocyte function (*44*). Furthermore, Zhao *et al.* found that berberine-containing herbs can modulate changes in insulin target organs by downregulating miR-29-b, exerting anti-diabetic effects (*45*). Notably, the regulation of MMP activity *via* exosomes represents a common mechanism shared by multiple active components. For example, the primary flavonoid component of *Scutellaria baicalensis*, baicalein, has been demonstrated to effectively inhibit the expression of MMP-2 and MMP-9 in various pathological models, which provides mechanistic insight into how flavonoid components may stabilize the extracellular matrix and protect neurological function through the regulation of MMPs (*46,47*). Similarly, saponin components also exhibit the ability to influence pathological processes through exosomes. In studies on ginsenosides, Ginsenoside Rg1 (Rg1) can induce mesenchymal stem cells to secrete exosomes containing the NOTCH1 ring, promoting macrophage M2 polarization *via* NOTCH signaling activation and thereby ameliorating diabetic cardiomyopathy (*48*). Concurrently, Rg1 can inhibit exosomal miR-21 release, enhance TIMP3 expression, and regulate MMP activity, consequently protecting BBB integrity (*49*)—a mechanism that shows significant relevance and convergence with the TIMP3-MMP9/β-DG-AQP4 axis central to this study. In summary, future research should integrate techniques such as UPLC–Q–TOF–MS to systematically analyze the chemical composition of ZMHB and further screen for key active components using *in vitro* models to validate their upstream regulatory effects on exosomal TIMP3. This research path, progressing from the "holistic formula" to "single components", will deepen the understanding of the modernized mechanisms of TCM.

In summary, we demonstrated that exosomal protein transfer-mediated regulation of AQP4 depolarization-induced GS dysfunction constitutes the pathological mechanism of the TCM theory, "toxin damaging brain collaterals". ZMHB regulates the expression of TIMP3 in circulating sExos and its uptake in the brain, thereby restoring AQP4 polarization through the MMP9/β-DG pathway, improving GS function, and preventing DCI. These findings establish a modern scientific framework for the TCM pathogenesis of "toxin damaging brain collaterals" in DCI and provide a novel therapeutic strategy for its prevention and treatment.

Certainly, the current research also has several limitations. The primary issue is that the upstream molecular mechanisms through which ZMHB regulates TIMP3 remain unresolved. Second, an important unresolved aspect is that the existence of an exosomal cargo component (*e.g.*, miRNA)-AQP4 regulatory axis remains to be conclusively established. Furthermore, the cellular origins of the peripherally derived exosomes need to be systematically elucidated. Finally, it should be noted that, although this study confirmed at the cellular level that ZMHB-sExos can regulate AQP4 polarization *via* the TIMP3-MMP9/β-DG pathway, it did not directly verify through *in vivo* experiments whether peripheral injection of ZMHB-sExos alone is sufficient to fully recapitulate the overall therapeutic efficacy of ZMHB.

To address the aforementioned limitations, future research could proceed as follows: Regarding the upstream regulatory mechanisms, we speculate that ZMHB may increase TIMP3 synthesis by activating transcription factors (*e.g.*, SP1) or enhancing translation at the source cell level (*50*); or promote its selective sorting by modulating the ESCRT complex or sphingomyelinase activity during exosome biogenesis

(*51,52*). Subsequent mechanistic studies could be designed accordingly: for the first pathway, SP1 inhibitors or siRNA could be used in cellular models to observe whether ZMHB's upregulating effect is blocked; for the second pathway, changes in the expression or localization of key ESCRT proteins (*e.g.*, Alix, TSG101) following ZMHB treatment could be examined to verify their involvement. Meanwhile, to validate whether other regulatory components exist in exosomes, miRNA sequencing could be employed to unbiasedly screen for differentially expressed miRNAs in ZMHB-sExos, and dual-luciferase reporter assays, cellular functional experiments, and exosomal *in vivo* transfer techniques could be utilized to systematically verify whether they directly target AQP4 and affect its polarization. Elucidating the cellular origins of peripherally derived exosomes requires systematically investigating which cell types these TIMP3-enriched exosomes originate from. These exosomes likely derive from multiple metabolically active organs modulated by ZMHB: for example, adipocytes, which play a central role in energy metabolism and endocrine regulation and whose secreted exosomes have been confirmed to participate in adipose-brain communication (*53*); hepatocytes, as the primary sites of drug metabolism and protein synthesis, are a potential important source of exosomal TIMP3; mesenchymal stem cell-derived exosomes, reported to possess favorable biocompatibility and BBB crossing potential, are also candidate mediators in neurodegenerative disease research (*54*); additionally, blood cells and vascular endothelial cells are direct contributors to circulating exosomes. To this end, single-exosome multi-omics analysis, tissue-specific TIMP3 knockdown models, and CRISPR-based lineage tracing could be used to clarify their cellular origins. Most critically, it is essential to isolate sExos from the serum of ZMHB-treated donor animals, inject them alone into DCI model recipients, and comprehensively evaluate their effects on improving cognition and providing neuroprotection. These studies will establish a complete causal chain from peripheral regulation to central effects, comprehensively revealing the systemic mechanism of action of ZMHB.

5. Conclusion

In conclusion, this study confirmed that ZMHB could effectively alleviate cognitive dysfunction of in diabetic rats. Mechanistically, this study revealed that abnormal downregulation of TIMP3 triggers β-DG lysis, which is the molecular mechanism of AQP4 depolarization in DCI. Serum exosomal TIMP3 from the ZMHB group entered the brain, inhibiting the activity of MMP9 in astrocytes and preventing β-DG from being cleaved, thereby restoring the polarization of AQP4 and exerting neuroprotective effects on DCI. The results of this study indicate that ZMHB is effective and safe and may be a promising drug for treating DCI.

Acknowledgements

Zhimu and Huangbo were identified by professor Lin Ma (Tianjin University of Traditional Chinese Medicine).

Funding: This work was supported by the Foundation of National Natural Science Foundation of China (82174112), the Science and Technology Project of Haihe Laboratory of Modern Chinese Medicine (22HHZYSS00015), the State Key Laboratory of Component-based Chinese Medicine (CBQM2022102) and the Eyas Research Project of Tianjin University of Traditional Chinese Medicine (XJS2022207).

Ethics approval: This experiment passed the ethical review of animal experiments at Tianjin University of Traditional Chinese Medicine (TCM-LAEC2021152). All experiments were performed in accordance with relevant guidelines and regulations.

Conflict of Interest: The authors have no conflicts of interest to disclose.

References

1. Dove A, Shang Y, Xu W, Grande G, Laukka EJ, Fratiglioni L, Marseglia A. The impact of diabetes on cognitive impairment and its progression to dementia. Alzheimers Dement. 2021; 17:1769-1778.
2. Rizzo MR, Di Meo I, Polito R, Auriemma MC, Gambardella A, di Mauro G, Capuano A, Paolisso G. Cognitive impairment and type 2 diabetes mellitus: Focus of SGLT2 inhibitors treatment. Pharmacol Res. 2022; 176:106062.
3. Zanotto C, Simão F, Gasparin MS, Biasibetti R, Tortorelli LS, Nardin P, Gonçalves CA. Exendin-4 Reverses Biochemical and Functional Alterations in the Blood-Brain and Blood-CSF Barriers in Diabetic Rats. Mol Neurobiol. 2017; 54:2154-2166.
4. Baumgart M, Snyder HM, Carrillo MC, Fazio S, Kim H, Johns H. Summary of the evidence on modifiable risk factors for cognitive decline and dementia: A population-based perspective. Alzheimers Dement. 2015; 11:718-726.
5. Tuligenga RH, Dugravot A, Tabák AG, Elbaz A, Brunner EJ, Kivimäki M, Singh-Manoux A. Midlife type 2 diabetes and poor glycaemic control as risk factors for cognitive decline in early old age: a post-hoc analysis of the Whitehall II cohort study. Lancet Diabetes Endocrinol. 2014; 2:228-235.
6. Benveniste H, Liu X, Koundal S, Sanggaard S, Lee H, Wardlaw J. The Glymphatic System and Waste Clearance with Brain Aging: A Review. Gerontology. 2019; 65:106-119.
7. Kim YK, Nam KI, Song J. The Glymphatic System in Diabetes-Induced Dementia. Front Neurol. 2018; 9:867.
8. Zhang L, Chopp M, Jiang Q, Zhang Z. Role of the glymphatic system in ageing and diabetes mellitus impaired cognitive function. Stroke Vasc Neurol. 2019; 4:90-92.
9. Silva I, Silva J, Ferreira R, Trigo D. Glymphatic system,

AQP4, and their implications in Alzheimer's disease. Neurol Res Pract. 2021; 3:5.
10. Ward R, Li W, Abdul Y, Jackson L, Dong G, Jamil S, Filosa J, Fagan SC, Ergul A. NLRP3 inflammasome inhibition with MCC950 improves diabetes-mediated cognitive impairment and vasoneuronal remodeling after ischemia. Pharmacol Res. 2019; 142:237-250.
11. Ran Q, Tian H, Lin J, Wang H, Wang B, Chen Z, Song D, Gong C. Mesenchymal Stem Cell-Derived Exosomes: A Novel Approach to Diabetes-Associated Cognitive Impairment. J Inflamm Res. 2023; 16:4213-4228.
12. Jia L, Zhu M, Kong C, *et al*. Blood neuro-exosomal synaptic proteins predict Alzheimer's disease at the asymptomatic stage. Alzheimers Dement. 2021; 17:49-60.
13. Si X, Dai S, Fang Y, Tang J, Wang Z, Li Y, Song Z, Chen Y, Liu Y, Zhao G, Zhang B, Pu J. Matrix metalloproteinase-9 inhibition prevents aquaporin-4 depolarization-mediated glymphatic dysfunction in Parkinson's disease. J Adv Res. 2024; 56:125-136.
14. Jäkel L, Kuiperij HB, Gerding LP, Custers EEM, van den Berg E, Jolink WMT, Schreuder F, Küsters B, Klijn CJM, Verbeek MM. Disturbed balance in the expression of MMP9 and TIMP3 in cerebral amyloid angiopathy-related intracerebral haemorrhage. Acta Neuropathol Commun. 2020; 8:99.
15. Zhu B, Cao A, Chen C, Zhou W, Luo W, Gui Y, Wang Q, Xu Z, Wang J. MMP-9 inhibition alleviates postoperative cognitive dysfunction by improving glymphatic function *via* regulating AQP4 polarity. Int Immunopharmacol. 2024; 126:111215.
16. Yuan Y, Peng W, Lei J, Zhao Y, Zhao B, Li Y, Wang J, Qu Q. AQP4 Endocytosis-Lysosome Degradation Mediated by MMP-9/β-DG Involved in Diabetes Cognitive Impairment. Mol Neurobiol. 2024; 61:8438-8453.
17. Sun H, Li TJ, Sun LN, Qiu Y, Huang BB, Yi B, Chen WS. Inhibitory effect of traditional Chinese medicine Zi-Shen Pill on benign prostatic hyperplasia in rats. J Ethnopharmacol. 2008; 115:203-208.
18. Li XN, Zhang A, Sun H, Song Y, Zou D, Wang X. Rapid discovery of absorbed constituents and metabolites in rat plasma after the oral administration of Zi Shen Wan using high-throughput UHPLC-MS with a multivariate analysis approach. J Sep Sci. 2016; 39:4700-4711.
19. Xue A, Zhao D, Zhao C, Li X, Yang M, Zhao H, Zhao C, Lei X, Wu J, Zhang N. Study on the neuroprotective effect of Zhimu-Huangbo extract on mitochondrial dysfunction in HT22 cells induced by D-galactose by promoting mitochondrial autophagy. J Ethnopharmacol. 2024; 318:117012.
20. Shi J, Yin Q, Zhang L, Wu Y, Yi P, Guo M, Li H, Yuan L, Wang Z, Zhuang P, Zhang Y. Zi Shen Wan Fang Attenuates Neuroinflammation and Cognitive Function *Via* Remodeling the Gut Microbiota in Diabetes-Induced Cognitive Impairment Mice. Front Pharmacol. 2022; 13:898360.
21. Yin Q, Zhang L, Han X, Zhang H, Wang F, Qin X, Zhuang P, Zhang Y. Zi Shen Wan Fang regulates kynurenine metabolism to alleviate diabetes-associated cognitive impairment *via* activating the skeletal muscle PGC1α-PPARα signaling. Phytomedicine. 2022; 99:154000.
22. Valente T, Gella A, Solé M, Durany N, Unzeta M. Immunohistochemical study of semicarbazide-sensitive amine oxidase/vascular adhesion protein-1 in the hippocampal vasculature: pathological synergy of Alzheimer's disease and diabetes mellitus. J Neurosci Res. 2012; 90:1989-1996.
23. Sasaki-Hamada S, Sacai H, Oka JI. Diabetes onset influences hippocampal synaptic plasticity in streptozotocin-treated rats. Neuroscience. 2012; 227:293-304.
24. Zhang L, Li D, Yi P, Shi J, Guo M, Yin Q, Liu D, Zhuang P, Zhang Y. Peripheral origin exosomal microRNAs aggravate glymphatic system dysfunction in diabetic cognitive impairment. Acta Pharm Sin B. 2023; 13:2817-2825.
25. Saint-Pol J, Gosselet F, Duban-Deweer S, Pottiez G, Karamanos Y. Targeting and Crossing the Blood-Brain Barrier with Extracellular Vesicles. Cells. 2020; 9:851.
26. Jiang Q, Zhang L, Ding G, Davoodi-Bojd E, Li Q, Li L, Sadry N, Nedergaard M, Chopp M, Zhang Z. Impairment of the glymphatic system after diabetes. J Cereb Blood Flow Metab. 2017; 37:1326-1337.
27. Chen Z, Zhong C. Decoding Alzheimer's disease from perturbed cerebral glucose metabolism: implications for diagnostic and therapeutic strategies. Prog Neurobiol. 2013; 108:21-43.
28. Li H, Luo Y, Xu Y, Yang L, Hu C, Chen Q, Yang Y, Ma J, Zhang J, Xia H, Li Y, Yang J. Meloxicam Improves Cognitive Impairment of Diabetic Rats through COX2-PGE2-EPs-cAMP/pPKA Pathway. Mol pharmaceutics. 2018; 15:4121-4131.
29. Zhang T, Pan BS, Zhao B, Zhang LM, Huang YL, Sun FY. Exacerbation of poststroke dementia by type 2 diabetes is associated with synergistic increases of beta-secretase activation and beta-amyloid generation in rat brains. Neuroscience. 2009; 161:1045-1056.
30. Jayaraj RL, Azimullah S, Beiram R. Diabetes as a risk factor for Alzheimer's disease in the Middle East and its shared pathological mediators. Saudi J Biol Sci. 2020; 27:736-750.
31. Tang Y, Yu C, Wu J, Chen H, Zeng Y, Wang X, Yang L, Mei Q, Cao S, Qin D. Lychee seed extract protects against neuronal injury and improves cognitive function in rats with type II diabetes mellitus with cognitive impairment. Int J Mol Med. 2018; 41:251-263.
32. Chiu CD, Chen CC, Shen CC, Chin LT, Ma HI, Chuang HY, Cho DY, Chu CH, Chang C. Hyperglycemia exacerbates intracerebral hemorrhage *via* the downregulation of aquaporin-4: temporal assessment with magnetic resonance imaging. Stroke. 2013; 44:1682-1689.
33. Zhang L, Chopp M, Zhang Y, Xiong Y, Li C, Sadry N, Rhaleb I, Lu M, Zhang ZG. Diabetes Mellitus Impairs Cognitive Function in Middle-Aged Rats and Neurological Recovery in Middle-Aged Rats After Stroke. Stroke. 2016; 47:2112-2118.
34. Zheng Y, Zhang Y, Geng S, Xu M, Yin Q, Song L, Zhuang P, Zhang Y. Identification of the constituents and metabolites in rats after oral administration of Zi Shen Formula by UPLC-Q-TOF/MS combined pattern recognition analysis. Biomed Chromatogr. 2018; 32. doi: 10.1002/bmc.4060.
35. Wang J, Li L, Zhang Z, Zhang X, Zhu Y, Zhang C, Bi Y. Extracellular vesicles mediate the communication of adipose tissue with brain and promote cognitive impairment associated with insulin resistance. Cell Metab. 2022; 34:1264-1279.e1268.
36. Liu W, Bai X, Zhang A, Huang J, Xu S, Zhang J. Role of Exosomes in Central Nervous System Diseases. Front Mol Neurosci. 2019; 12:240.
37. Datta Chaudhuri A, Dasgheyb RM, DeVine LR, Bi H, Cole RN, Haughey NJ. Stimulus-dependent modifications

in astrocyte-derived extracellular vesicle cargo regulate neuronal excitability. Glia. 2020; 68:128-144.
38. Jean-Toussaint R, Tian Y, Chaudhuri AD, Haughey NJ, Sacan A, Ajit SK. Proteome characterization of small extracellular vesicles from spared nerve injury model of neuropathic pain. J Proteomics. 2020; 211:103540.
39. Lu Y, Zhang J, Han B, Yu Y, Zhao W, Wu T, Mao Y, Zhang F. Extracellular vesicles DJ-1 derived from hypoxia-conditioned hMSCs alleviate cardiac hypertrophy by suppressing mitochondria dysfunction and preventing ATRAP degradation. Pharmacol Res. 2023; 187:106607.
40. Waite A, Brown SC, Blake DJ. The dystrophin-glycoprotein complex in brain development and disease. Trends Neurosci. 2012; 35:487-496.
41. Gondo A, Shinotsuka T, Morita A, Abe Y, Yasui M, Nuriya M. Sustained down-regulation of β-dystroglycan and associated dysfunctions of astrocytic endfeet in epileptic cerebral cortex. J Biol Chem. 2014; 289:30279-30288.
42. Wang Z, Li Y, Wang Z, Liao Y, Ye Q, Tang S, Wei T, Xiao P, Huang J, Lu W. Edaravone Maintains AQP4 Polarity *Via* OS/MMP9/β-DG Pathway in an Experimental Intracerebral Hemorrhage Mouse Model. Mol Neurobiol. 2024; 61:7639-7658.
43. Ding W, Gu Q, Liu M, Zou J, Sun J, Zhu J. Astrocytes-derived exosomes pre-treated by berberine inhibit neuroinflammation after stroke *via* miR-182-5p/Rac1 pathway. Int Immunopharmacol. 2023; 118:110047.
44. Wang YY, Tang LQ, Wei W. Berberine attenuates podocytes injury caused by exosomes derived from high glucose-induced mesangial cells through TGFβ1-PI3K/AKT pathway. Eur J Pharmacol. 2018; 824:185-192.
45. Zhao HL, Sui Y, Qiao CF, *et al*. Sustained antidiabetic effects of a berberine-containing Chinese herbal medicine through regulation of hepatic gene expression. Diabetes. 2012; 61:933-943.
46. Chandrashekar N, Selvamani A, Subramanian R, Pandi A, Thiruvengadam D. Baicalein inhibits pulmonary carcinogenesis-associated inflammation and interferes with COX-2, MMP-2 and MMP-9 expressions *in-vivo*. Toxicol Appl Pharmacol. 2012; 261:10-21.
47. He HJ, Lv ZY, Li ZY, Zhang LY, Liao Q, Zheng HQ, Su WY, Rao SQ, Yu XB, Wu ZD. Efficacy of combined treatment with albendazole and baicalein against eosinophilic meningitis induced by Angiostrongylus cantonensis in mice. J Helminthol. 2011; 85:92-99.
48. Zhen J, Bai J, Liu J, Men H, Yu H. Ginsenoside RG1-induced mesenchymal stem cells alleviate diabetic cardiomyopathy through secreting exosomal circNOTCH1 to promote macrophage M2 polarization. Phytother Res. 2024; 38:1745-1760.
49. Zhai K, Duan H, Wang W, Zhao S, Khan GJ, Wang M, Zhang Y, Thakur K, Fang X, Wu C, Xiao J, Wei Z. Ginsenoside Rg1 ameliorates blood-brain barrier disruption and traumatic brain injury *via* attenuating macrophages derived exosomes miR-21 release. Acta Pharm Sin B. 2021; 11:3493-3507.
50. Bernot D, Barruet E, Poggi M, Bonardo B, Alessi MC, Peiretti F. Down-regulation of tissue inhibitor of metalloproteinase-3 (TIMP-3) expression is necessary for adipocyte differentiation. J Biol Chem. 2010; 285:6508-6514.
51. Vietri M, Radulovic M, Stenmark H. The many functions of ESCRTs. Nat Rev Mol Cell Biol. 2020; 21:25-42.
52. Hessvik NP, Llorente A. Current knowledge on exosome biogenesis and release. Cell Mol Life Sci. 2018; 75:193-208.
53. Wang J, Li L, Zhang Z, Zhang X, Zhu Y, Zhang C, Bi Y. Extracellular vesicles mediate the communication of adipose tissue with brain and promote cognitive impairment associated with insulin resistance. Cell Metab. 2022; 34:1264-1279.e8.
54. Kandeel M, Morsy MA, Alkhodair KM, Alhojaily S. Mesenchymal Stem Cell-Derived Extracellular Vesicles: An Emerging Diagnostic and Therapeutic Biomolecules for Neurodegenerative Disabilities. Biomolecules. 2023; 13:1250.

Received September 23, 2025; Revised November 25, 2025; Accepted December 6, 2025.

[§]These authors contributed equally to this work.

**Address correspondence to:*
Qingsheng Yin, Yanjun Zhang and Pengwei Zhuang, Tianjin University of Traditional Chinese Medicine, Jinghai District, Tianjin, 301617, China.
E-mail: carrysable@163.com (QSY), zyjsunye@163.com (YJZ) and zhuangpengwei@163.com (PWZ)

Released online in J-STAGE as advance publication December 17, 2025.

Original Article

DOI: 10.5582/ddt.2025.01095

Real-world use of non-oral administration of oral anticancer agents *via* the simple suspension method in Japanese patients with cancer: A nationwide claims-based analysis

Hiroaki Ohta, Takeo Yasu*

Department of Medicinal Therapy Research, Education and Research Unit for Comprehensive Clinical Pharmacy, Meiji Pharmaceutical University, Tokyo, Japan.

SUMMARY: The enteral administration of drugs as suspensions is a potential alternative route for patients with dysphagia. The simple suspension method is commonly used in Japan; however, nationwide data are lacking. This study aimed to investigate the real-world use and potential impact of oral anticancer agent (OAA) suspensions in patients with dysphagia in Japan. A large Japanese administrative claims database was used in this retrospective study (April 2014 to August 2023). Patients with cancer who had nasogastric, gastrostomy, or jejunostomy tubes and received OAAs during non-oral intake periods were included. These periods were defined using procedural codes, and it was assumed that the prescribed drugs were suspended. Three frequently used drugs (temozolomide, lenvatinib, and osimertinib) were analyzed. Patients were divided into suspension and non-suspension groups using propensity score matching, and overall survival (OS) was compared using the Kaplan–Meier method. Among 25,252 patients with feeding tubes, 126 received OAAs during the non-oral period. The median age was 76 years, and 62% had gastrostomy tubes. Temozolomide was the most common drug suspension, followed by lenvatinib and osimertinib. No significant difference in OS was observed between the temozolomide and lenvatinib groups. However, OS of the osimertinib suspension group was shorter than that of the non-suspension group ($p = 0.047$). This large-scale study of OAA suspensions in Japan suggests that drug suspensions may support continued anticancer treatment in patients with dysphagia. However, drug stability and exposure risks should be considered. Further evidence and more specific guidelines are required to ensure safe and effective use.

Keywords: anticancer drug suspensions, enteral administration, dysphagia, Japanese cohort

1. Introduction

The development and widespread use of oral anticancer agents (OAAs) in recent years have led to an increase in outpatient cancer treatment. This shift offers advantages, such as reduced hospital visits and decreased physical and psychological burden, thereby maintaining the patients' quality of life. However, ensuring patient adherence is crucial for maximizing the efficacy of oral therapies (*1*). Older individuals and patients with advanced cancer often experience dysphagia, making oral administration challenging with potential treatment interruptions. In Japan, the clinical burden of dysphagia has been increasing; for example, the incidence of aspiration pneumonia, which is a major complication of dysphagia, rose by 53.7% between 2005 and 2019, with the majority of cases observed in individuals aged 70 years or older (*2*). Alternatively, OAA suspensions can be administered *via* feeding tubes.

In Japan, the simple suspension method (SSM), developed in 1997 and officially recognized in 2020, is now reimbursed under the Japanese medical insurance system (*3*). SSM involves suspension of tablets and capsules in warm water without physical crushing, further improving the stability and reducing the risk of exposure for healthcare providers and caregivers. However, data on the feasibility, stability, and pharmacokinetics of individual OAAs in suspension remain limited, highlighting the need for evidence-based, safe, and effective use (*3*). Treatment decisions should consider the therapeutic goals (*e.g.*, adjuvant or palliative chemotherapy), patient condition, available alternatives, and patient and family preferences. Pharmacists and other healthcare professionals should provide support from a pharmaceutical perspective, including safety evaluations and pharmacokinetics.

Japan has a rapidly aging society, with a growing population of individuals aged ≥ 85.0 years. This

population is experiencing increased rates of age-related comorbidities, including stroke, dementia, and Parkinson's disease, which impair swallowing and increase the risk of dysphagia (*4,5*). In these patients, a low prognostic nutritional index is associated with increased mortality, and many of them also have cancer (*6*). The number of older patients with cancer and dysphagia is expected to increase, necessitating systems to support cases where oral drug administration is challenging. However, the real-world use of OAA suspensions in Japan remains unexplored. Understanding the current clinical practices is critical for optimizing decisions regarding drug selection and administration, formulation strategies, guideline development, and patient support systems.

This study aimed to investigate the real-world use of OAA suspensions in patients unable to receive oral medications in clinical settings. This method is considered off-label, and we assumed that it would be rarely practiced. Therefore, we used a large Japanese administrative claims database to clarify its real-world use, patient characteristics, and potential impact on outcomes.

2. Materials and Methods

2.1. Study design and data source

This retrospective study examined the real-world use of OAA suspensions in Japan. Data were obtained from the DeSC, a commercial administrative claims repository provided by DeSC Healthcare, Inc. (Tokyo, Japan; *https://desc-hc.co.jp/*). As of October 2022, the database contained the information of approximately 12 million insured individuals. It integrates information from three major health insurance schemes under Japan's mandatory universal healthcare system: Kenpo (for employees of large corporations), Kokuho (for non-employees, retirees, and their dependents), and the Koki Koreisha Iryo Seido (for individuals aged ≥ 75.0 years). Collectively, these schemes cover 9.8% of the Japanese population and offer a comprehensive nationwide overview of healthcare utilization.

2.2. Study population

Of the 1,838,927 patients with a confirmed diagnosis of cancer (based on International Statistical Classification of Diseases and Related Health Problems [ICD-10] codes starting with "C," excluding suspected cases) between April 2014 and August 2023, we included those who underwent nasogastric tube (NGT), gastrostomy, or jejunostomy tube placement and were prescribed OAAs during the non-oral intake period. Patients who were prescribed orally disintegrating tablets, dispersible tablets, or powders were excluded.

The index date was defined as the first day on which an OAA suspension was administered. As this study aimed to describe the status of suspension administration rather than conduct a longitudinal follow-up, treatment progress or prognosis following suspension administration were not assessed. Patients with data available for < 30 days before the index date were excluded (*7,8*).

We extracted data on age, sex, cancer type, comorbidities (excluding suspected diagnoses) on the index date; OAAs prescribed during the non-oral intake period; NGT, gastrostomy or jejunostomy tube placement; and feeding data during hospitalization.

2.3. Impact of the administered OAA suspensions

First, we identified the three most frequent combinations of OAA suspensions and cancer types. For each combination, we classified patients into a suspension group (who received OAA suspensions at least once during the treatment period) and non-suspension group (who never received OAA suspensions). We extracted the following data and compared overall survival (OS) between the two groups: age, sex, and cancer type at the time of initial OAA prescription; confirmed (non-suspected) disease names, prescription records, and medical procedures from 180 days before the initial prescription; and disease name, prescription records, medical procedures, and mortality data following the initial prescription. The index date was defined as the start date of the OAA prescription, and the end of the observation period was defined as the date of death or censoring (Figure 1). OAAs were prescribed during the non-oral intake period; data on NGT, gastrostomy, or jejunostomy tube placement and feeding data during hospitalization were also obtained.

2.4. Definitions of the non-oral intake period and OAA suspensions

In this study, we utilized claims data from the Japanese medical insurance system, using procedure codes as indicators to indirectly identify patients' treatment status and clinical conditions. These codes are standardized classifications used by medical institutions for reimbursement purposes and are calculated based on specific medical procedures or patient conditions. In Japan, a meal fee is charged each time a patient consumes food orally during hospitalization. Similarly, when a patient is unable to eat orally and receives liquid nutrition *via* a tube, a different meal fee applicable to non-oral intake is applied.

The non-oral intake period was defined as the duration during which the procedure code indicating enteral nutrition through a feeding tube (Procedure Code J120 from the Japanese Health Insurance System) was recorded after NGT, gastrostomy, or jejunostomy tube placement (Procedure Codes J0342, K664, and K725).

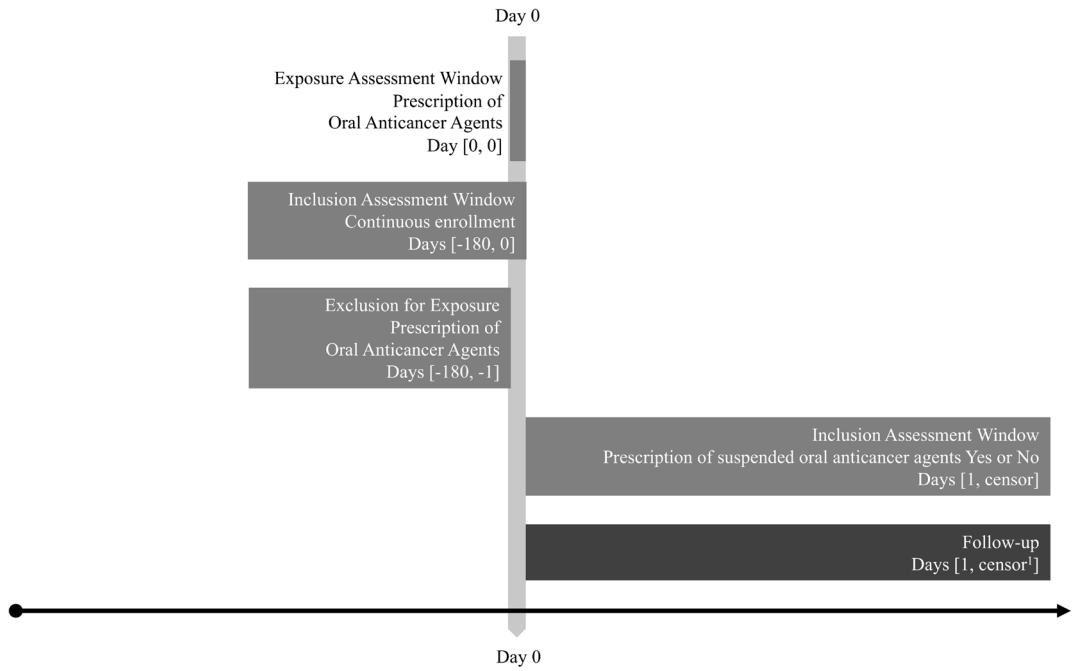

[1] Censor on death, deregistration from health insurance, or end of study period

Figure 1. Study design applied to the information in the commercial claims database with data observability lines to evaluate the impact of the administration of oral anticancer agent suspensions on overall survival.

Any OAA prescribed during this non-oral intake period was considered to be administered *via* suspension.

2.5. Outcomes

2.5.1. Survey of the real-world use of OAA suspensions in Japan

We assessed the clinical characteristics of patients who were administered OAA suspensions, including sex, age, cancer type, route of administration of the OAA suspension, and comorbidities at the time of suspension administration.

2.5.2. Review of alternative routes for OAAs

A summary of product characteristics (SPC) from Japan, European Medicines Agency (EMA), and U.S. Food and Drug Administration (FDA) was made. We reviewed the latest SPC issued by the Japanese regulatory authority, EMA, and FDA for each OAA administered as a suspension during the study period to determine whether suspension or crushing methods for administration were mentioned.

2.5.3. Impact of OAA suspension administration on survival

Among the combinations of OAA suspensions and cancer types, the three most frequently prescribed combinations were identified. Patients were categorized into the suspension and non-suspension groups, and OS was compared from the date of the initial prescription of the OAA until death or censoring.

2.6. Statistical analysis

We evaluated the prescription trends of OAA suspensions during hospitalization between April 2014 and August 2023. Actual usage patterns based on the clinical characteristics of the patients at the time of the initial suspension administration were summarized using descriptive statistics. Continuous variables are presented as medians with interquartile ranges (IQR). Suspension and non-suspension groups were compared using the Mann–Whitney *U* test. Categorical variables are expressed as frequencies and percentages (n [%]). We conducted a survival comparison between the suspension and non-suspension groups using 1:2 propensity score matching for the three most frequently prescribed OAA suspensions (*9*). Kaplan–Meier survival curves were plotted, and the log-rank test was used for comparisons. All analyses were performed using EZR (version 2.9-1; Saitama Medical Center, Jichi Medical University, Saitama, Japan) (*10*). Statistical significance was set at $p < 0.05$.

2.7. Ethical approval

This study was conducted according to the principles outlined in the Declaration of Helsinki (as revised in 2013) and was approved by the Ethics Committee of Meiji Pharmaceutical University (April 14, 2025/ No.202466).

3. Results

3.1. Survey of the real-world use of OAA suspensions in Japan

Between April 2014 and August 2023, 25,252 patients registered in DeSC underwent NGT, gastrostomy, or jejunostomy tube placement. Among them, 126 patients were prescribed OAAs during the non-oral intake period (Figure 2), 62.0% underwent gastrostomy tube placement, and 38.0% underwent NGT placement. No patient who underwent jejunostomy tube placement received OAA suspensions. The median patient age was 76.0 years and 53.2% were men. Brain tumors were the most common primary cancer (23.0%), followed by lung cancer (20.6%), leukemia (15.1%), and thyroid cancer (14.3%) (Table 1).

Thirty-one different OAAs were administered as a suspension. The most common drug suspensions included temozolomide (29 cases), lenvatinib (18 cases), osimertinib (14 cases), imatinib (eight cases), and gefitinib, estramustine, and capecitabine (five each) (Table 2). The route of administration varied depending on the drug used. Temozolomide and imatinib were more typically administered *via* NGT, whereas lenvatinib, osimertinib, gefitinib, estramustine, and capecitabine were mainly administered *via* gastrostomy tubes.

3.2. Review of alternative routes for OAAs based on SPCs from Japan, EMA, and FDA

There were no descriptions of alternative administration methods involving suspension or crushing for non-oral routes in the Japanese SPCs for all 31 OAAs administered by the suspension method. For lenvatinib, osimertinib, imatinib, gefitinib, capecitabine, tepotinib, and nilotinib, the SPCs from the FDA and EMA included instructions on alternative administration methods. Ibrutinib and bosutinib had such instructions only in the FDA SPC, whereas afatinib had instructions only in the EMA documentation. Additionally, while case reports have documented the non-oral administration of tirabrutinib, alectinib, erlotinib, TS-1, and venetoclax, the Japanese, FDA, or EMA SPCs did not include instructions for the preparation for non-oral administration.

3.3. Impact of the administration of OAA suspension on survival

The three most frequent combinations of OAA suspensions and cancer types were temozolomide

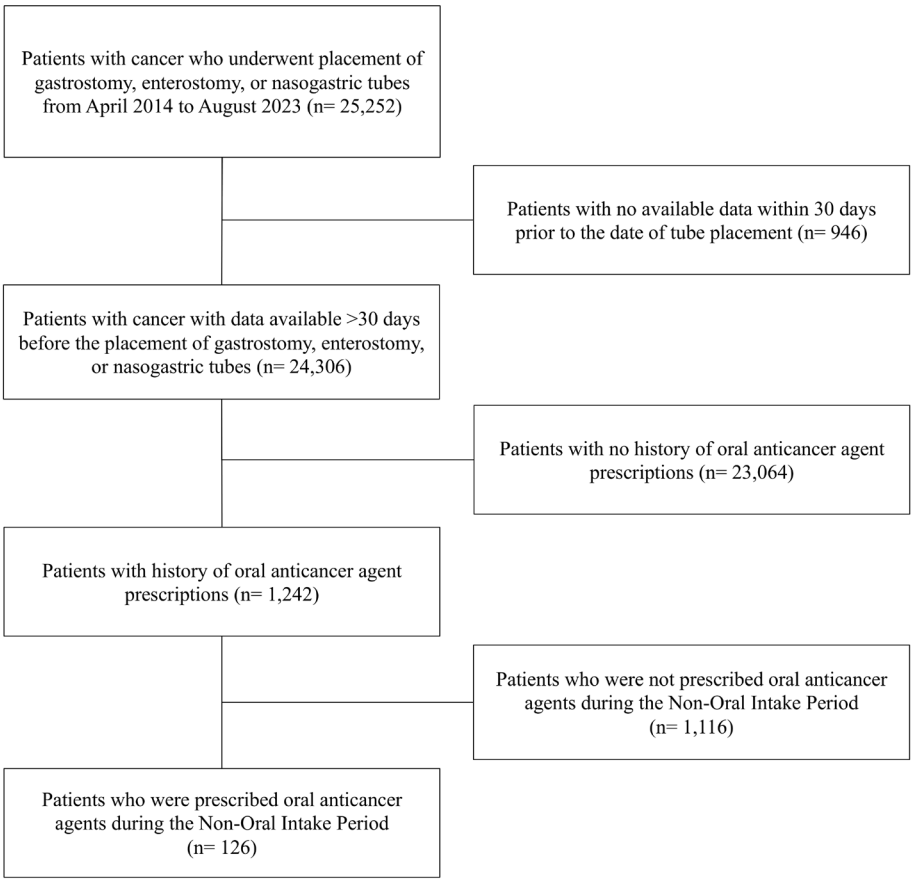

Figure 2. Flowchart of patients included in the study.

Table 1. Patient characteristics

	Total, n (%) 126
Male sex	67 (53.2)
Age: median (IQR)	76.0 (71.0–80.0)
Type of cancer	
Brain and central nervous system	29 (23.0)
Lung	26 (20.6)
Leukemia	19 (15.1)
Thyroid	18 (14.3)
Non-Hodgkin lymphoma	7 (5.6)
Prostate	6 (4.8)
Stomach	5 (4.0)
Gastrointestinal stromal tumor	4 (3.2)
Multiple myeloma	4 (3.2)
Breast	2 (1.6)
Liver	1 (0.8)
Uterine leiomyosarcoma	1 (0.8)
Esophagus	1(0.8)
Renal	1 (0.8)
Larynx	1 (0.8)
Colon	1 (0.8)
Route of administration	
Gastrostomy	78 (61.9)
Nasogastric tube	48 (38.1)
CCI on the index date	
Cerebral vascular accident	41 (32.5)
Metastatic cancer	38 (30.2)
Peptic ulcer	37 (29.4)
Congestive heart failure	31 (24.6)
Pulmonary disease	31 (24.6)
Diabetes	19 (15.1)
Renal disease	11 (8.7)
Liver disease	7 (5.6)
Acute myocardial infarction	4 (3.2)
Paraplegia	4 (3.2)
Diabetes complications	3 (2.4)
Peripheral vascular disease	3 (2.4)
Connective tissue disorder	2 (1.6)
Dementia	2 (1.6)
Severe liver disease	1 (0.8)

IQR, interquartile range; CCI, Charlson comorbidity index.

for brain and central nervous system (CNS) tumors, lenvatinib for thyroid cancer, and osimertinib for lung cancer. Patient backgrounds before and after 1:2 propensity score matching for these three combinations are shown in Table 3. Using sex, age, and treatment duration as covariates, all standardized differences between the two groups were < 1 after matching. Figure 3 presents the results of the survival analysis following propensity score matching. For temozolomide and lenvatinib, survival did not differ between the suspension and non-suspension groups. In contrast, the osimertinib suspension group had a shorter survival duration than the non-suspension group ($p = 0.047$).

4. Discussion

To our knowledge, this is the first study to clarify the real-world use of OAA suspensions using a large Japanese administrative claims database. Temozolomide was the most commonly used agent, followed by lenvatinib and osimertinib, with most administered through gastrostomy tubes. No Japanese SPC included instructions for suspension, although FDA and EMA SPCs offered some guidance. OS did not differ significantly between the suspension and non-suspension groups for temozolomide and lenvatinib. However, for osimertinib, the suspension group showed significantly shorter OS compared to the non-suspension group. This finding should be interpreted with caution, as the selection of patients for suspension administration likely reflects a more advanced disease status, poor performance status, or terminal-stage care. These potential confounding factors were not fully adjusted for in the propensity score matching. Therefore, this result should be viewed as an observational finding, rather than as evidence of harmful impact or ineffectiveness of suspension administration.

Patients who received suspensions were predominantly older adults (median age 76.0 years), aligning with the findings of Sako *et al*., who reported a median age of 80.0 years among patients undergoing gastrotomy or jejunostomy tube placements (*11*). They also noted cerebrovascular disease, aspiration pneumonia, dementia, neuromuscular disease, and malignancy as the key underlying conditions. Similarly, in this study, many patients who underwent NGT or gastrostomy tube placement were found to have comorbidities other than malignancies, including cerebrovascular accidents, metastatic cancer, peptic ulcers, congestive heart failure, and pulmonary disease. In contrast, only two patients (1.6%) had dementia during the initiation of OAA suspension, possibly indicating a reluctance to administer chemotherapy to patients with dementia. Boakye *et al*. reported that dementia was the comorbidity most strongly associated with non-receipt of chemotherapy compared to other conditions, such as heart failure or stroke (*12*).

Temozolomide suspension, the most frequently used agent, remains physically and chemically stable for up to 14 days under refrigeration (*13*). The temozolomide suspension developed by Annereau *et al.* by decapsulating the capsule contents is suitable for administration *via* NGT (*14*). However, SPCs for temozolomide from Japan, the FDA, and EMA do not include information regarding alternative administration methods for patients who cannot orally consume the drug. This omission may be attributed to the availability of an injectable formulation of temozolomide developed specifically for such patients (*15*). Nevertheless, only one of the 29 patients receiving oral temozolomide in our study was switched to the injectable form. Given its proven stability (*13,14*), temozolomide suspension may retain sufficient efficacy. Survival analysis comparing the suspension and non-suspension groups of patients with brain and CNS tumors revealed no significant differences in OS. Prophylactic gastrostomy tube placement in patients with head and neck cancer helps in maintaining adequate nutritional status (*16*). Therefore, in this study,

Table 2. Types of oral anticancer agent suspensions

Oral anticancer agent suspensions	Type of cancer	n	Route of administration	n	Japan	FDA	EMA	Case Report
Temozolomide	Brain and central nervous system	29	Gastrostomy	12	None	None	None	None
			Nasogastric tube	17				
Lenvatinib	Thyroid	17	Gastrostomy	16	None	○	○	○
	Liver	1	Nasogastric tube	2				
Osimertinib	Lung	14	Gastrostomy	12	None	○	○	○
			Nasogastric tube	2				
Imatinib	Leukemia	4	Gastrostomy	3	None	○	○	○
	Gastrointestinal stromal tumor	4	Nasogastric tube	5				
Gefitinib	Lung	5	Gastrostomy	4	None	○	○	○
			Nasogastric tube	1				
Estramustine	Prostate	5	Gastrostomy	5	None	None	Not approved	None
			Nasogastric tube	0				
Capecitabine	Stomach	3	Gastrostomy	3	None	○	○	None
	Colon	1	Nasogastric tube	2				
	Esophagus	1						
Tirabrutinib	Non-Hodgkin lymphoma	4	Gastrostomy	2	None	Not approved	Not approved	○
			Nasogastric tube	2				
Tegafur/Uracil	Breast	2	Gastrostomy	4	None	Not approved	Not approved	None
	Prostate	1	Nasogastric tube	0				
	Larynx	1						
Cyclophosphamide	Leukemia	1	Gastrostomy	0	None	None	Not approved	None
	Multiple myeloma	1	Nasogastric tube	3				
	Non-Hodgkin lymphoma	1						
Dasatinib	Leukemia	3	Gastrostomy	1	None	None	None	None
			Nasogastric tube	2				
Melphalan	Multiple myeloma	3	Gastrostomy	2	None	None	Not approved	None
			Nasogastric tube	1				
Alectinib	Lung	2	Gastrostomy	1	None	None	None	○
			Nasogastric tube	1				
Ibrutinib	Leukemia	1	Gastrostomy	1	None	○	None	○
	Non-Hodgkin lymphoma	1	Nasogastric tube	1				
Erlotinib	Lung	2	Gastrostomy	2	None	None	None	○
			Nasogastric tube	0				
Dacomitinib	Lung	2	Gastrostomy	2	None	None	None	None
			Nasogastric tube	0				
TS-1	Stomach	2	Gastrostomy	2	None	Not approved	None	○
			Nasogastric tube	0				
Tretinoin	Leukemia	2	Gastrostomy	0	None	None	Not approved	None
			Nasogastric tube	2				
Bosutinib	Leukemia	2	Gastrostomy	1	None	○	None	None
			Nasogastric tube	1				

FDA, U.S. Food and Drug Administration; EMA, European Medicines Agency.

Table 2. Types of oral anticancer agent suspensions (continued)

Oral anticancer agent suspensions	Type of cancer	n	Route of administration	n	Japan	FDA	EMA	Case Report
Ponatinib	Leukemia	2	Gastrostomy	2	None	None	None	None
			Nasogastric tube	0				
Afatinib	Lung	1	Gastrostomy	1	None	None	○	None
Axitinib	Renal	1	Nasogastric tube	1	None	None	None	None
Sorafenib	Thyroid	1	Gastrostomy	1	None	None	None	None
Trifluridine and Tipiracil	Colon	1	Gastrostomy	1	None	None	None	None
Tepotinib	Lung	1	Nasogastric tube	1	None	○	○	None
Nilotinib	Leukemia	1	Nasogastric tube	1	None	○	○	None
Nintedanib	Leukemia	1	Gastrostomy	1	None	None	None	None
Pazopanib	Uterine leiomyosarcoma	1	Nasogastric tube	1	None	None	None	None
Procarbazine	Non-Hodgkin lymphoma	1	Nasogastric tube	1	None	None	Not approved	None
Venetoclax	Leukemia	1	Nasogastric tube	1	None	None	None	○
Methotrexate	Leukemia	1	Gastrostomy	1	None	None	Not approved	None

FDA, U.S. Food and Drug Administration; EMA, European Medicines Agency.

prophylactic gastrostomy tube placement may have enabled continued treatment with suspensions, thereby contributing to survival.

Lenvatinib suspension has been administered *via* NGT with favorable outcomes in patients with thyroid cancer (*17,18*). This may explain the frequent use of lenvatinib in our thyroid cancer cohort. The FDA and EMA SPCs describe this method, although no randomized trials or bioequivalence data are available. In our study, OS did not differ significantly between the lenvatinib suspension and non-suspension groups among patients with thyroid cancer. Multiple case reports support the effectiveness of enteral lenvatinib in thyroid cancer (*17,18*). In particular, for anaplastic thyroid cancer, rapid tumor growth in the neck may prevent oral intake of medications, and enteral administration of lenvatinib suspension reduces the tumor size and improves prognosis (*18*). Similar to previous case reports, we found that among patients receiving lenvatinib, the median duration from treatment initiation to the start of suspension administration was 2.5 days (IQR: 0.0–59.8), suggesting that oral intake challenges often emerged at an early stage during therapy. Despite early difficulties in oral intake, treatment may be continued through alternative administration of suspensions. This potential continuation of therapy may have contributed to no significant differences in OS between the suspension and non-suspension groups, suggesting that suspension did not adversely affect survival.

Cases of osimertinib administration *via* suspension have been reported (*19,20*). This method is described in SPCs by the FDA and EMA, similar to lenvatinib. However, the efficacy and bioequivalence of osimertinib suspension have not been validated. Notably, patients with lung cancer receiving osimertinib suspension had significantly shorter survival compared to those receiving it intact. The median time from treatment initiation to suspension administration was longer in the osimertinib group (median: 668.5 days; IQR: 106.2–1129.8) than in the temozolomide (median: 17.0 days, IQR: 8.0–72.0; p value = 0.005) and lenvatinib (median: 19.0 days, IQR: 0.5–158.8, p value = 0.049) groups. Furthermore, brain metastases were observed in four of the 10 patients in the osimertinib suspension group. Considering the high CNS penetrability and efficacy of osimertinib against leptomeningeal metastases (*21*), many patients in this group were likely unable to receive the medication orally because of terminal disease progression and poor general health. Patients with lung cancer and leptomeningeal metastases frequently present with poor performance status (PS) and dysphagia (*20*), which may contribute to their shorter survival. These background factors underscore the importance of not attributing the shorter survival observed in the osimertinib suspension group to the administration method itself. Rather, they highlight the need for clinical awareness of the severe condition of such patients. This study was a descriptive

Table 3. Characteristics of patients treated with the top three oral anticancer drugs before and after propensity score matching

	Before propensity score matching			After propensity score matching		
	Suspension group	Non-suspension group	SMD	Suspension group	Non-suspension group	SMD
Temozolomide						
Total, n	1145			63		
n	23	1122		21	42	
Male sex	12 (52.2)	591 (52.7)	0.010	11 (52.4)	22 (52.4)	< 0.001
Age: median (IQR)	79.0 (76.0–80.0)	76.0 (68.0–80.0)	0.709	78.0 (76.0–80.0)	78.0 (76.0–80.0)	0.007
Treatment duration: median (IQR)	160.0 (51.0–310.0)	155.5 (42.0–337.0)	0.121	160.0 (47.0–308.0)	155.5 (47.3–309.3)	0.002
Lenvatinib						
Total, n	537			30		
n	12	525		10	20	
Male sex	4 (33.3)	194 (37.0)	0.076	3 (30.0)	6 (30.0)	< 0.001
Age: median (IQR)	76.0 (70.0–80.0)	76.0 (69.0–81.0)	0.208	76.0 (69.0–80.3)	76.0 (70.3–80.0)	0.030
Treatment duration: median (IQR)	177.0 (16.8–550.3)	246.0 (50.0–627.0)	0.337	177.0 (34.3–609.8)	156.5 (19.5–565.3)	0.015
Osimertinib						
Total, n	5116			30		
n	10	5106		10	20	
Male sex	3 (30.0)	1763 (34.6)	0.097	3 (30.0)	6 (30.0)	< 0.001
Age: median (IQR)	74.0 (70.3–79.3)	78.0 (72.0–82.0)	0.346	74.0 (70.3–79.3)	74.0 (71.0–79.0)	< 0.001
Treatment duration: median (IQR)	222.0 (31.8–465.5)	269.5 (74.0–609.0)	0.341	222.0 (31.8–465.5)	213.5 (36.8–423.8)	0.011

SMD; standardized mean difference; IQR, interquartile range.

Drug Discoveries & Therapeutics. 2025; 19(6):378-388. www.ddtjournal.com

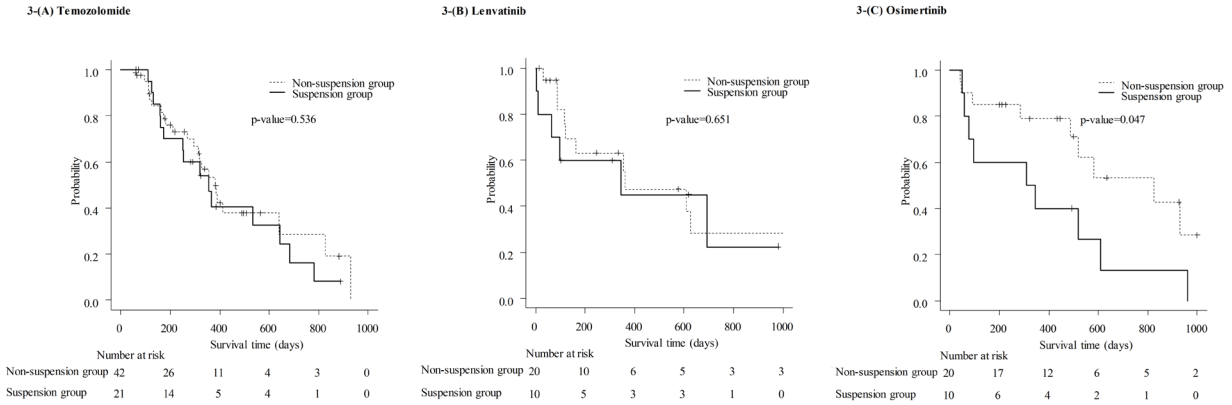

Figure 3. Kaplan–Meier curves for overall survival. (A) Patients with brain and central nervous system tumors treated with temozolomide; (B) Patients with thyroid cancer treated with lenvatinib; (C) Patients with lung cancer treated with osimertinib.

investigation of the nationwide use of the suspension method for OAAs and was not designed to directly assess the efficacy or safety. Nonetheless, by leveraging large-scale claims data, it evaluated treatment practices in under-represented populations in real-world settings, such as those with dysphagia and poor general health. Suspension administration may enable continued therapy when oral intake is difficult, provided the patient's overall condition is carefully considered. Multidimensional patient assessments and pharmacotherapeutic strategies tailored to individual preferences and treatment goals are essential. Insights from this study may support informed decision-making in complex clinical scenarios.

Regarding imatinib, adequate plasma concentrations were achieved *via* suspension through a gastrostomy tube (*22*). Case reports have documented that gefitinib administration *via* either a gastrostomy tube or NGT causes tumor shrinkage (*23-25*). No serious adverse events were reported. Pharmacokinetic studies demonstrated no significant differences in the area under the curve and maximum plasma concentration between the suspensions and intact formulations (*26*). The pharmacokinetics, efficacy, and safety of imatinib and gefitinib were evaluated when administered *via* suspension through enteral feeding tubes, and the results support suspension as an alternative route. Conversely, although estramustine and capecitabine are frequently administered as a suspension, case reports or pharmacokinetic studies on the efficacy or safety of their suspension are lacking. For drugs such as TS-1, alectinib, ibrutinib, erlotinib, tirabrutinib, and venetoclax, case reports where suspensions were administered *via* enteral routes have shown treatment efficacy in tumor reduction or improvement in PS (*27-36*). However, these reports were limited to individual cases, and comprehensive data on the stability, absorption, and long-term safety of suspensions are lacking. Therefore, from a pharmacist's perspective, proactively recommending a suspension of OAAs is challenging.

Suspension of OAAs is an important alternative route for patients who cannot swallow because of dysphagia or other medical conditions. Several case reports have supported its efficacy (*17-20,23-25,27-36*), and some SPCs explicitly describe alternative administration procedures. However, the risks of exposure to healthcare providers and caregivers during preparation remain understudied. When capsules or tablets are opened and crushed, drug particles may become airborne, risking contact with skin, mucosa, or inhalation (*37*), which is particularly concerning for highly toxic agents. The National Institute for Occupational Safety and Health and the American Society of Health-System Pharmacists strongly recommend the use of biological safety cabinets and personal protective equipment when preparing these agents (*38,39*). In Japan, the SSM minimizes exposure risk by avoiding tablets. However, studies evaluating the extent of exposure associated with the preparation and administration of OAA suspensions using this method are lacking. Therefore, careful handling is warranted during preparation and administration. Future research should address the stability of each suspension and the associated exposure risks to establish safe preparation methods and administration protocols.

This study has some limitations. First, the claims database lacks detailed information on cancer stage, PS, and rationale for suspension administration, limiting casual interpretation. Second, we could not identify patients who received anticancer suspensions orally without tube placement, or those receiving enteral therapy alongside total parenteral nutrition. Third, data on suspension methods (*e.g.*, use of SSM, medium used, preparation steps, or tube type) were unavailable. In addition, the definition of "suspension administration" in this study was inferred based on the overlap between the health insurance procedure codes for enteral nutrition and records of oral anticancer agent prescriptions. However, direct confirmation was not possible as specific prescription orders or procedure records were

not available. This indirect classification method may have introduced misclassification bias and limited the precision of identifying true suspension administration. Therefore, these results should be interpreted taking into account the potential for exposure misclassification inherent in claims-based analyses. These limitations are inherent in claims-based studies. Future studies using clinical records are warranted to validate these findings.

In summary, for patients with cancer experiencing dysphagia, suspension administration offers a valuable treatment option. However, drug stability, safety, and exposure risk must be considered. Scientific evidence remains limited for many agents, highlighting the need for careful, individualized clinical judgement. Healthcare professionals must manage suspension therapy comprehensively, including indication, preparation, safety measures, and caregiver education. Accumulating pharmacological evidence and developing evidence-based guidelines tailored to clinical practice will be essential for safe and effective implementation.

Funding: None.

Conflict of Interest: The authors have no conflicts of interest to disclose.

References

1. Kav S, Fleury M, Fernandez-Ortega P, Manzullo EF, Kerr KA, DeGennaro R, Ginex PK. 15 years supporting adherence to oral anti-cancer treatment: use of the MASCC Oral Agent Teaching Tool (MOATT) worldwide, a review for the future. Support Care Cancer. 2025; 33:229.
2. Tomonaga I, Koseki H, Imai C, Shida T, Nishiyama Y, Yoshida D, Yokoo S, Osaki M. Incidence and characteristics of aspiration pneumonia in the Nagasaki Prefecture from 2005 to 2019. BMC Pulm Med. 2024; 24:191.
3. Abe T, Kusakabe S, Naoi M, Suzuki T, Sagara A, Hiraide M, Sano M, Nakayama T. Evaluation of the simple suspension method for oral anticancer drugs. Yakugaku Zasshi. 2024; 144:441-445.
4. Dziewas R, Beck AM, Clave P, Hamdy S, Heppner HJ, Langmore SE, Leischker A, Martino R, Pluschinski P, Roesler A, Shaker R, Warnecke T, Sieber CC, Volkert D, Wirth R. Recognizing the importance of dysphagia: stumbling blocks and stepping stones in the twenty-first century. Dysphagia. 2017; 32:78-82.
5. Martino R, Foley N, Bhogal S, Diamant N, Speechley M, Teasell R. Dysphagia after stroke: incidence, diagnosis, and pulmonary complications. Stroke. 2005; 36:2756-2763.
6. Pei R, Wang D. Prognostic nutritional index negative associated with mortality in older Japanese patients with dysphagia. Front Nutr. 2025; 12:1586248.
7. ASGE Standards of Practice Committee; Jain R, Maple JT, *et al*. The role of endoscopy in enteral feeding. Gastrointest Endosc. 2011; 74:7-12.
8. Volkert D, Berner YN, Berry E, *et al*. ESPEN Guidelines on Enteral Nutrition: Geriatrics. Clin Nutr. 2006; 25:330-360.
9. Austin PC. Statistical criteria for selecting the optimal number of untreated subjects matched to each treated subject when using many-to-one matching on the propensity score. Am J Epidemiol. 2010; 172:1092-1097.
10. Kanda Y. Investigation of the freely available easy-to-use software 'EZR' for medical statistics. Bone Marrow Transplant. 2013; 48:452-458.
11. Sako A, Yasunaga H, Horiguchi H, Fushimi K, Yanai H, Uemura N. Prevalence and in-hospital mortality of gastrostomy and jejunostomy in Japan: a retrospective study with a national administrative database. Gastrointest Endosc. 2014; 80:88-96.
12. Boakye D, Nagrini R, Ahrens W, Haug U, Gunther K. The association of comorbidities with administration of adjuvant chemotherapy in stage III colon cancer patients: a systematic review and meta-analysis. Ther Adv Med Oncol. 2021; 13:1758835920986520.
13. Trissel LABRF, Zhang YB, Koontz SEPB. Temozolomide stability in extemporaneously compounded oral suspensions. Int J Pharm Compd. 2006; 10:396-399.
14. Annereau M, Hinterlang M, Bienayme H, Vassal G, Pinon A, Schmitt M, Denis L, Lemarchand C, Martin L, Lemare F, Abbou S, Bastid J, Tortolano L. Development of a hospital compounded, taste-masked, temozolomide oral suspension and 5-year real-life experience in treating paediatric patients. Pharmaceuticals (Basel). 2022; 15:555.
15. Diez BD, Statkevich P, Zhu Y, Abutarif MA, Xuan F, Kantesaria B, Cutler D, Cantillon M, Schwarz M, Pallotta MG, Ottaviano FH. Evaluation of the exposure equivalence of oral versus intravenous temozolomide. Cancer Chemother Pharmacol. 2010; 65:727-734.
16. Almeida ND, Yu H, Iovoli AJ, Fang M, Schrand TV, Pepin A, Gupta V, Wooten KE, Markiewicz MR, McSpadden RP, Hicks WL, Jr., Farrugia MK, Singh AK. Prophylactic gastrostomy tube during chemoradiation for head and neck cancer decreases weight loss but increases rate of tube use beyond six months. Oral Oncol. 2025; 160:107136.
17. Molinaro E, Viola D, Viola N, Falcetta P, Orsolini F, Torregrossa L, Vagli P, Ribechini A, Materazzi G, Vitti P, Elisei R. Lenvatinib administered *via* nasogastric tube in poorly differentiated thyroid cancer. Case Rep Endocrinol. 2019; 2019:6831237.
18. Kawano F, Yonekawa T, Yamaguchi H, Shibata N, Tashiro K, Ikenoue M, Munakata S, Higuchi K, Tanaka H, Sato Y, Hosokawa A, Takeno S, Nakamura K, Nanashima A. Nasogastric administration of lenvatinib solution in a mechanically ventilated patient with rapidly growing anaplastic thyroid cancer. Endocrinol Diabetes Metab Case Rep. 2020; 2020.
19. Tani N, Takatsuka S, Kataoka N, Kunimatsu Y, Tsutsumi R, Sato I, Tanimura M, Nakano T, Tanimura K, Kato D, Takeda T. Nasogastric administration of osimertinib suspension for an epidermal growth factor receptor-mutated lung cancer causing an esophageal stricture: case report. Ann Palliat Med. 2022; 11:1542-1545.
20. Takeda T, Itano H, Takeuchi M, Nishimi Y, Saitoh M, Takeda S. Osimertinib administration *via* nasogastric tube in an EGFR-T790M-positive patient with leptomeningeal metastases. Respirol Case Rep. 2017; 5:e00241.
21. Ballard P, Yates JW, Yang Z, *et al*. Preclinical comparison of osimertinib with other EGFR-TKIs in EGFR-mutant NSCLC brain metastases models, and early evidence of clinical brain metastases activity. Clin Cancer Res. 2016; 22:5130-5140.

22. Fiebrich-Westra HB, Visser O, Francken AB, Smolders EJ. Alternative routes of drug administration: exposure of imatinib using different formulations. Cancer Chemother Pharmacol. 2025; 95:45.
23. Okuda T, Hayashi H, Fujita M, Yoshioka H, Tasaki T, Nakagawa K, Kato A. Administration of gefitinib *via* nasogastric tube effectively improved the performance status of a patient with lung adenocarcinoma-derived meningeal carcinomatosis. Int Cancer Conf J. 2014; 3:211-214.
24. Suzumura T, Yonesaka K, Tsukuda H, Fukuoka M. Successful gefitinib treatment administration *via* gastrostomy tube in a patient with non-small cell lung cancer with dysphagia. BMJ Case Rep. 2014; 2014:bcr2013202705.
25. Uruga H, Moriguchi S, Takahashi Y, Ogawa K, Murase K, Mochizuki S, Hanada S, Takaya H, Miyamoto A, Morokawa N, Kishi K. Gefitinib successfully administered in a lung cancer patient with leptomeningeal carcinomatosis after erlotinib-induced pneumatosis intestinalis. BMC Cancer. 2018; 18:825.
26. Cantarini MV, McFarquhar T, Smith RP, Bailey C, Marshall AL. Relative bioavailability and safety profile of gefitinib administered as a tablet or as a dispersion preparation *via* drink or nasogastric tube: results of a randomized, open-label, three-period crossover study in healthy volunteers. Clin Ther. 2004; 26:1630-1636.
27. Okita A, Miyade Y, Okano K. Effective management of an advanced gastric cancer patient by TS-1 combined chemotherapy using nasojejunal tube and successful transfer to home care after percutaneous transesophageal gastro-tubing (PTEG): a case report. Acta Med Okayama. 2010; 64:67-70.
28. Hirano K, Nakamura K, Hasegawa M. Pharmacokinetics and adverse event of TS-1 administered through gastrostomy. Gan To Kagaku Ryoho. 2005; 32:859-862.
29. Hagiike M, Tsuboi Y, Akamoto S, Yachida S, Izuishi K, Karasawa Y, Goda F, Okada S, Usuki H, Maeta H. TS-1 therapy *via* intestinal catheter used for tube feeding in a patient with gastric cancer after total gastrectomy. Gan To Kagaku Ryoho. 2005; 32:1033-1036.
30. Thomas QD, Pautas M, Guilhaume MN, Fiteni F, Ge T, Girard N. Enteral administration of alectinib for ALK-positive non-small cell lung cancer in an elderly patient: A case report. Medicine (Baltimore). 2021; 100:e27611.
31. Kanai O, Kim YH, Nakatani K, Fujita K, Mio T. Nasogastric tube-administered alectinib achieved long-term survival in a crizotinib-refractory nonsmall cell lung cancer patient with a poor performance status. Clin Case Rep. 2017; 5:927-930.
32. Alsuliman T, Belghoul M, Choufi B. Ibrutinib treatment through nasogastric tube in a comatose patient with central nervous system localization of mantle cell lymphoma. Case Rep Hematol. 2018; 2018:5761627.
33. Bosch-Barrera J, Sais E, Lorencio C, Porta R, Izquierdo A, Menendez JA, Brunet J, Sirvent JM, Rosell R. Successful empirical erlotinib treatment of a mechanically ventilated patient newly diagnosed with metastatic lung adenocarcinoma. Lung Cancer. 2014; 86:102-104.
34. Yoshioka H, Okuda T, Nakao T, Fujita M, Takahashi JC. Experience with tirabrutinib in the treatment of primary central nervous system lymphoma that is difficult to treat with standard treatment. Anticancer Res. 2022; 42:4173-4178.
35. Yoshioka H, Okuda T, Nakao T, Fujita M, Takahashi JC. Experience with nasogastric tube administration of tirabrutinib in the treatment of an elderly patient with primary central nervous system lymphoma. Int Cancer Conf J. 2021; 10:290-293.
36. Sato H, Kobayashi T, Fujita N, Yamashita T, Kitadate A, Yoshioka T, Nara M, Kameoka Y, Miura M, Takahashi N. Safe administration and pharmacokinetic monitoring of crushed venetoclax tablets with posaconazole and clarithromycin *via* percutaneous endoscopic gastrostomy tube in a patient with acute myeloid leukemia. Cancer Chemother Pharmacol. 2022; 90:279-284.
37. Sugiura S, Asano M, Kinoshita K, Tanimura M, Nabeshima T. Risks to health professionals from hazardous drugs in Japan: a pilot study of environmental and biological monitoring of occupational exposure to cyclophosphamide. J Oncol Pharm Pract. 2011; 17:14-19.
38. Managing Hazardous Drug Exposures: Information for Healthcare Settings. *https://www.cdc.gov/niosh/docs/2023-130/default.html* (accessed December 4, 2025).
39. Power LA, Coyne JW. ASHP guidelines on handling hazardous drugs. Am J Health Syst Pharm. 2018; 75:1996-2031.

Received September 9, 2025; Revised December 4, 2025; Accepted December 8, 2025.

**Address correspondence to:*
Takeo Yasu, Department of Medicinal Therapy Research, Education and Research Unit for Comprehensive Clinical Pharmacy, Meiji Pharmaceutical University, Tokyo 204-8588, Japan.
E-mail: yasutakeo@my-pharm.ac.jp

Released online in J-STAGE as advance publication December 11, 2025.

Original Article

DOI: 10.5582/ddt.2025.01096

Disproportionality and time-to-onset analyses of drug-induced weight gain using the Japanese Adverse Drug Event Report database

Naohito Ide[1,*], Rika Shibata[1], Ken-ichi Sako[2], Tomoji Maeda[2]

[1] Department of Practical Pharmacy, Nihon Pharmaceutical University, Saitama, Japan;
[2] Department of Clinical Pharmacology, Nihon Pharmaceutical University, Saitama, Japan.

SUMMARY: Drug-induced weight gain is a clinically important adverse event that can lead to obesity, metabolic syndrome, cardiovascular disease, and reduced treatment adherence. Although several drug classes are known to cause weight gain, the onset timing and underlying mechanisms remain incompletely understood. This study aimed to investigate signals and evaluate time to onset of drug-induced weight gain using the Japanese Adverse Drug Event Report (JADER) database. We analyzed JADER data from April 2004 to June 2025, and in the disproportionality analysis reporting odds ratios with 95% confidence intervals were calculated. Time to onset was also assessed, and Weibull distribution analysis was applied to evaluate onset patterns. Among 975,869 reports, 814 cases of drug-induced weight gain were identified. Signals were detected for known drugs such as antipsychotics, pregabalin, and pioglitazone, as well as for drugs without weight gain listed in their package inserts, including benzodiazepines. Pregabalin showed the earliest median onset at 19 days (early failure), followed by olanzapine and risperidone at 1–2 months, pioglitazone at 2 months, and clozapine at 6 months, all classified as random failure types. This study demonstrated that drug-induced weight gain varies by drug class in both onset timing and mechanisms. These findings underscore the need for careful weight monitoring during treatment, particularly early with pregabalin and long-term with clozapine and pioglitazone. Prospective studies are warranted to clarify causal relationships and clinical implications.

Keywords: weight gain, Japanese Adverse Drug Event Report database, disproportionality analysis, time to onset, Weibull distribution

1. Introduction

Drug-induced weight gain is a clinically important adverse event, as it can lead to obesity, metabolic syndrome, and cardiovascular disease, as well as reduced quality of life and treatment adherence (*1*). Several drug classes are known to cause weight gain, including second-generation antipsychotics, antiepileptic drugs, antidepressants, and antidiabetic agents such as thiazolidinediones (*2*). Although these associations are well recognized, the risk profiles differ across drug classes, and the onset timing and underlying mechanisms remain incompletely understood.

Previous pharmacovigilance studies using spontaneous reporting systems (SRS), such as the US Food and Drug Administration Adverse Event Reporting System (FAERS) and the Japanese Adverse Drug Event Report (JADER) database, have provided valuable insights (*3*-*6*). For example, Ahmed *et al.* investigated drug-induced weight gain using FAERS (*7*), but their study was limited to a descriptive analysis of the number of reported cases and did not evaluate onset patterns in detail. Comprehensive analyses of drug-induced weight gain using SRS databases remain scarce.

Therefore, the aim of this study was to investigate drug-induced weight gain using JADER. Specifically, we sought to identify signals through disproportionality analysis and to evaluate the time to onset of weight gain. By clarifying these aspects, our findings may contribute to improved monitoring and management of drug-induced weight gain in clinical practice.

2. Materials and Methods

2.1. Data source

We obtained data from the JADER database, which is managed by the Pharmaceuticals and Medical Devices

Agency (PMDA). The JADER database contains fully anonymized data submitted by healthcare professionals and pharmaceutical companies. The database is structured into 4 tables: "Demo", "Drug", "Reac", and "Hist". The "Demo" table includes basic patient information, such as age, sex, and reporting year. The "Drug" table contains details on drug administration, including the drug name, route of administration, start and end dates, dosage, and classification of involvement in adverse reactions (*e.g.*, suspected, concomitant, or interaction). The "Reac" table contains adverse events, outcomes, and onset dates, and the "Hist" table contains information on patient medical history. We downloaded the JADER database for April 2004 to June 2025 from the PMDA website (*https://www.info.pmda.go.jp/fukusayoudb/CsvDownload.jsp*) on August 4, 2025. We analyzed patient age and sex, reporting year, drug name, administration start date, adverse event onset date, and clinical outcome.

2.2. Definition of adverse reactions

Adverse events in the JADER database are categorized using the preferred terms (PTs) from the Japanese version of the Medical Dictionary for Regulatory Activities (MedDRA/J). In this study, we extracted adverse events by using the PTs in MedDRA/J ver. 28.0. In this study, we defined the PT names (PT codes) for weight gain as "weight gain" (10047899) and "abnormal weight gain" (10000188).

2.3. Target drugs

Only cases of weight gain for which drug involvement was classified as "suspected" were included in the analysis. We analyzed the drugs for which there were 10 or more reports of weight gain.

2.4. Signal detection

The reporting odds ratio (ROR) is used by the PMDA and the Netherlands Pharmacovigilance Center to detect signals of adverse events in SRS (*8*). The ROR, along with its 95% confidence interval (95% CI), is a quantification of the disproportionality in adverse event reporting between groups (*9*). Therefore, the ROR is conceptually analogous to the odds ratio in case–control studies, representing the odds of exposure in reported cases compared with non-cases.

We calculated the ROR and 95% CI for weight gain adverse reactions (Figure 1); the signal of adverse reactions was considered to be positive when the lower limit of the 95% CI was greater than 1.

2.5. Analysis of time to onset

When a positive signal for weight gain was detected in the disproportionality analysis, we analyzed the time to onset. Cases were excluded if either the start date of drug administration or the onset date of the adverse event was unavailable. Cases were also excluded if the time to onset of the adverse event exceeded 1,095 days (*i.e.*, 3 years). Time to onset was analyzed for cases with 5 or more reports after exclusion. The time to onset was defined as the difference between the start date of drug administration and the onset date of weight gain, plus 1. To evaluate the pattern of onset, we used the Weibull distribution model and examined the Weibull shape parameters (*10,11*). Weibull shape parameters characterize the distribution of failure rates over time, where failure rates correspond to the onset of adverse events. The scale parameter α indicates the distribution breadth, with larger values representing a wider spread. The shape parameter β describes whether the hazard rate is increasing, decreasing, or constant over time. If the scale parameter β is equal to 1 or the 95% CI includes 1, the frequency of adverse events is considered to remain constant overtime; if β exceeds 1 and its 95% CI does not include 1, the frequency is assumed to increase over time; and if β is less than 1 and its 95% CI does not include 1, the frequency is assumed to decrease over time.

2.6. Ethical considerations

This study was conducted in accordance with the ethical principles of the Declaration of Helsinki and the Ethical Guidelines for Medical and Health Research Involving Human Subjects. The database used in this

	Target adverse events	Other adverse events	Total
Target drugs	a	b	a+b
Other drugs	c	d	c+d
Total	a+c	b+d	a+b+c+d

Reporting odds ratio (ROR) = (a/c)/(b/d) = ad/bc

95% Confidence interval = $\exp(\ln(ROR) \pm 1.96 \sqrt{1/a + 1/b + 1/c + 1/d})$

Figure 1. Two-by-two contingency table for disproportionality analysis.

study is completely anonymized. Therefore, the study was reviewed by the Ethics Committee of Nihon Pharmaceutical University, but it has been confirmed that ethical approval is not required.

2.7. Statistical analysis

All statistical analyses were performed with JMP Student Edition (SAS Institute Inc., Cary, NC, USA).

3. Results

3.1. Descriptive analysis of adverse reactions with weight gain

The JADER database contains a total of 975,869 cases, of which 814 cases were drug-induced weight gain. The characteristics and clinical outcomes of the patients with drug-induced weight gain and the specialties of the reporters are shown in Table 1. The number of male and female patients was similar. Patient age ranged from young to elderly, and the distribution across age groups did not differ significantly. Approximately 80% of reporters were medical professionals such as physicians and pharmacists, while a minority were consumers. The clinical outcomes were mostly good, but 16.8% of patients did not recover. The number of reports was relatively low before 2010, followed by a sharp increase in 2011 and a peak in 2014 (70 cases) (Figure 2). Since 2011, the number of reports generally remained above 30 cases per year. Although some fluctuations were observed, the overall reporting frequency after 2011 was consistently higher compared with the earlier period.

3.2. Signal detection of weight gain

The number of reports of weight gain as an adverse event for each drug, the RORs, and whether weight gain is described in the package insert are shown in Figure 3. Among the drugs without weight gain listed in the package insert, signals were detected for bromazepam, limaprost alfadex, sennoside, prednisolone, flunitrazepam, etizolam, zolpidem, furosemide, diclofenac, and ciclosporine.

Table 1. Characteristics of patients with drug-induced weight gain in the Japanese Adverse Drug Event Report database

Items	n	%
Sex		
Male	358	44.0
Female	430	52.8
Unknown	26	3.2
Age group, years		
< 10	16	2.0
10-19	20	2.5
20-29	52	6.4
30-39	87	10.7
40-49	109	13.4
50-59	103	12.7
60-69	98	12.0
70-79	110	13.5
80-89	62	7.6
90-99	14	1.7
Unknown	143	17.6
Specialty of the reporters		
Healthcare professional	641	78.7
Consumer	167	20.5
Unknown	6	0.7
Clinical outcome		
Good outcome		
Recovery	132	16.2
Improvement	163	20.0
Poor outcome		
Sequelae	0	0.0
Unrecovered	137	16.8
Death	3	0.4
Unknown	379	46.6

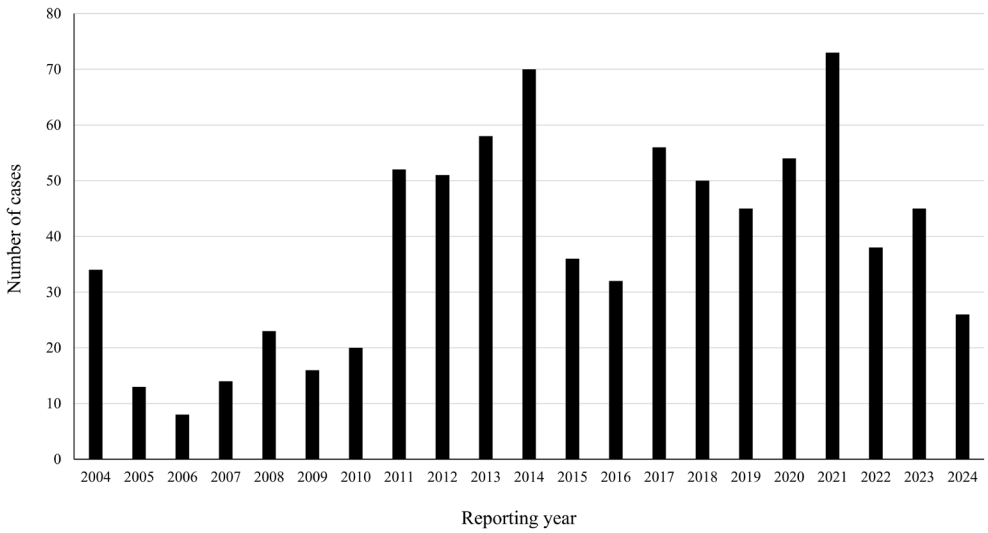

Figure 2. Yearly number of cases of drug-induced weight gain.

3.3. Time to onset of weight gain

The median time to onset for pregabalin was the earliest at 19 days, showing an early failure pattern (Table 2). For antipsychotic drugs, the median time to onset was approximately 1 to 2 months for olanzapine and risperidone but about 6 months for clozapine. The onset pattern of all antipsychotic drugs was classified as random failure. The median time to onset of pioglitazone was approximately 2 months, and the pattern was also random failure.

4. Discussion

Ahmed *et al.* investigated drug-induced weight gain using FAERS (*7*); however, their study only described the number of adverse event reports. In contrast, in the present study we conducted a disproportionality analysis of drug-induced weight gain using Japanese pharmacovigilance data and additionally examined the time to onset.

Many of the drugs for which signals were detected already listed weight gain in their package inserts and are widely recognized to be associated with weight gain. These include antipsychotics such as olanzapine and clozapine, antiepileptic drugs such as pregabalin and valproic acid, antidepressants such as mirtazapine and paroxetine, and tyrosine kinase inhibitors such as lorlatinib and imatinib.

However, signals were also detected for drugs that did not list weight gain in their package inserts, with benzodiazepines accounting for the majority of these signals. Sleep medications such as benzodiazepines are often used concomitantly with antipsychotics (*12*), suggesting that the signals detected for these drugs may be attributable to confounding. As a supplementary analysis, we investigated concomitant medications in 45 reports of weight gain associated with bromazepam, etizolam, zolpidem, and flunitrazepam. Notably, in 41 of these reports (91.1%), antipsychotics or other drugs known to induce weight gain were listed as "suspected drugs." This finding strongly suggests that the signals observed for benzodiazepines and zolpidem are likely attributable to confounding by concomitant antipsychotic medications rather than a direct effect of benzodiazepines and zolpidem themselves.

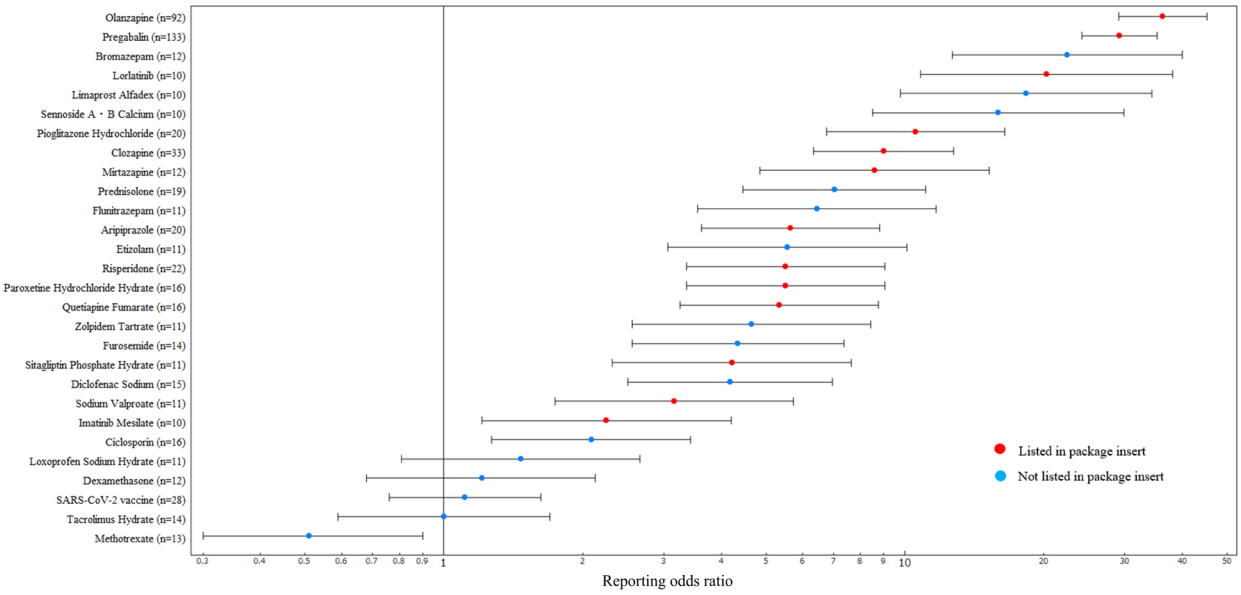

Figure 3. Reporting odds ratio and 95% confidence interval of weight gain, and whether or not included in the package insert.

Table 2. Time to onset and Weibull parameters of drug-induced weight gain

Drug	Cases, n	Median time to onset, days	IQR	Weibull scale parameter		Weibull shape parameter		
				α	95% CI	β	95% CI	Pattern
Pregabalin	35	19	9-91	47.14	28.57-75.84	0.74	0.56-0.94	Early failure
Olanzapine	22	52	16-121	84.12	47.97-143.04	0.85	0.60-1.13	Random failure
Clozapine	21	184	89-309	231.57	150.02-350.62	1.11	0.76-1.53	Random failure
Risperidone	5	39	16-296	96.33	18.07-473.65	0.69	0.32-1.19	Random failure
Pioglitazone Hydrochloride	9	64	45-499	199.68	80.41-465.61	0.88	0.50-1.39	Random failure

CI: confidence interval; IQR: interquartile range.

In previous reports, approximately 60% of patients were female (*7*), whereas in this study the ratio of males to females was nearly equal. In addition, while about 60% of reports in the previous study were submitted by consumers (*7*), approximately 80% of reports in our study originated from healthcare professionals. It has been reported that women are more conscious of weight loss behaviors and treatment than men (*13*). For adverse events that are readily recognized by patients themselves, such as weight gain, there may be substantial differences in reporting patterns between FAERS and JADER, as observed in the present study, and further investigation is warranted in this respect.

In the time-to-onset analysis, pregabalin showed a short onset time of approximately 3 weeks and was classified as an early failure type. Pregabalin is known to cause adverse events such as somnolence and dizziness, and several studies have investigated these adverse events using JADER and FAERS (*4,14*). However, there are few reports focusing on weight gain as an adverse event associated with pregabalin.

Previous reports on pregabalin have indicated that weight gain of 7% or more from baseline is generally observed within 1 to 2 months (*15*), whereas in the present study the time to onset appeared to be earlier. However, because this study used an SRS database, the specific amount of weight gain was not available, and therefore a direct comparison is not possible. Nevertheless, our findings suggest that weight gain associated with pregabalin may occur at an early stage of treatment.

The mechanisms underlying pregabalin-induced weight gain are not fully understood. One proposed explanation is that pregabalin increases food intake by inhibiting dopamine function in the lateral hypothalamic area (*16*). In addition, pregabalin has been reported to inhibit the α2δ1 subunit of calcium channels, thereby promoting appetite (*17*), and to suppress glutamate release, resulting in decreased corticotropin-releasing hormone levels and increased food intake (*18*). Further studies are needed to clarify these mechanisms.

Second-generation antipsychotic drugs such as olanzapine, clozapine, and risperidone have been reported to cause weight gain within 2 weeks to approximately 3 months (*2*), with olanzapine and clozapine being most strongly associated. In the present study, signals of weight gain were detected for the antipsychotics olanzapine, clozapine, risperidone, aripiprazole, and quetiapine. The median time to onset of weight gain was 1 to 2 months for risperidone and olanzapine, consistent with previous reports, but was longest for clozapine at 184 days. Results of the Weibull distribution analysis indicated that all were classified as random failure types, suggesting that weight gain may occur over an extended period, particularly with clozapine.

The mechanism by which second-generation antipsychotics cause weight gain is thought to involve their actions on multiple receptors, including dopamine receptors D1, D2, and D4; 5-hydroxytryptamine (serotonin) receptors 1A, 2A, 2C, 6, and 7; histamine receptor H1; and muscarinic acetylcholine receptor M3, leading to increased appetite and subsequent weight gain (*19*). Olanzapine and clozapine have higher affinity for serotonin, histamine, and muscarinic receptors than for dopamine receptors, which may explain their stronger appetite-stimulating effects and greater impact on weight gain (*19*). Therefore, careful monitoring of body weight is warranted during long-term treatment with second-generation antipsychotics, particularly clozapine, given the potential for progressive weight gain over time.

Pioglitazone-induced weight gain has been reported to increase significantly within 2 months (*20*). The median onset time in this study was approximately 2 months, which was similar to the previously reported results. Weight gain induced by pregabalin and second-generation antipsychotics is attributed to increased appetite. However, thiazolidinediones, including pioglitazone, are associated with fluid retention and increased fat mass. Thiazolidine increases insulin sensitivity and binds to peroxisome proliferator-activated receptor gamma receptors, which increases fat mass and leads to weight gain (*21*). It also causes fluid retention by reducing sodium excretion in the distal tubules (*22*), which leads to weight gain.

This study has several limitations. First, it was conducted using the JADER database, an SRS. As with other studies employing similar databases, it was not possible to calculate the incidence of adverse events, and inaccuracies or underreporting in the registered data may have been present (*4*). Second, in the time-to-onset analysis, many reports lacked information on the start date of drug administration or the onset date of adverse events, resulting in a limited number of analyzable cases. Because the Weibull distribution is sensitive to outliers in small samples, its accuracy may decrease under such conditions (*23*); therefore, caution may be warranted when interpreting onset patterns. Third, the potential influence of concomitant medications was not assessed. As noted previously, although weight gain signals were detected for benzodiazepines and zolpidem, they are likely attributable to concomitant use of antipsychotics. To overcome these limitations, prospective clinical trials or well-designed case–control studies are required.

In conclusion, this study identified signals and evaluated the time to onset of drug-induced weight gain using the JADER database. Signals were detected not only for well-known drugs such as antipsychotics and pregabalin but also for drugs without weight gain listed in their package inserts. Pregabalin showed early onset at approximately 3 weeks, whereas clozapine exhibited a later onset at around 6 months. These findings underscore the importance of careful weight monitoring during treatment and highlight the need for prospective studies to clarify causal relationships.

Funding: None.

Conflict of Interest: The authors have no conflicts of interest to disclose.

References

1. Jallon P, Picard F. Bodyweight gain and anticonvulsants. Drug Saf. 2001; 24:969-978.
2. Anekwe CV, Ahn YJ, Bajaj SS, Stanford FC. Pharmacotherapy causing weight gain and metabolic alteration in those with obesity and obesity-related conditions: a review. Ann N Y Acad Sci. 2024; 1533:145-155.
3. Ide N, Sako KI, Takigawa M, Tanaka H. Risk and time-to-onset of acute kidney injury with vancomycin plus piperacillin-tazobactam combination: analysis using JADER. In Vivo. 2024; 38:1436-1442.
4. Kato H, Koseki T, Kondo M. Occurrence of somnolence and respiratory depression induced by pregabalin and mirogabalin use and the influence of opioid treatment using the Japanese adverse drug event report database. Pharmazie. 2024; 79:169-172.
5. Liu Q, Wang Y, Hu P, He P. Abortion adverse events associated with adalimumab, etanercept, ustekinumab, and dupilumab during pregnancy: A pharmacovigilance study based on FDA adverse event reporting system. Drug Discov Ther. 2025; 19:160-173.
6. Yang L, Zhang W, Shen X, Liu M, Wu M, Xiao D. Fosfomycin-associated adverse events: A disproportionality analysis of the FDA Adverse Event Reporting System. Drug Discov Ther. 2025; 19:1-9.
7. Ahmed NJ, Alshehri AM, Almalki ZS, Alahmari A. Drug-induced weight gain in the last 10 years: a descriptive study. Pharmazie. 2022; 77:299-301.
8. Van Puijenbroek EP, Bate A, Leufkens HGM, Lindquist M, Orre R, Egberts ACG. A comparison of measures of disproportionality for signal detection is spontaneous reporting systems for adverse drug reactions. Pharmacoepidemiol Drug Saf. 2002; 11:3-10.
9. Katsuhara Y, Ogawa T. Acute renal failure, ketoacidosis, and urogenital tract infections with SGLT2 inhibitors: signal detection using a Japanese spontaneous reporting database. Clin Drug Investig. 2020; 40:645-652.
10. Asano H, Noguchi Y, Kimura M, Usami E, Yoshimura T. Pituitary-related adverse events and onset patterns caused by immune checkpoint inhibitors: analysis using the Japanese adverse drug event report database. Medicina (Kaunas). 2023; 59:1963.
11. Sauzet O, Carvajal A, Escudero A, Molokhia M, Cornelius VR. Illustration of the weibull shape parameter signal detection tool using electronic healthcare record data. Drug Saf. 2013; 36:995-1006.
12. Wu CS, Lin YJ, Liu SK. Benzodiazepine use among patients with schizophrenia in Taiwan: a nationwide population-based survey. Psychiatr Serv. 2011; 62:908-914.
13. Muscogiuri G, Verde L, Vetrani C, Barrea L, Savastano S, Colao A. Obesity: a gender-view. J Endocrinol Invest. 2024; 47:299-306.
14. Mukai R, Hasegawa S, Umetsu R, Nakao S, Shimada K, Uranishi H, Masuta M, Suzuki H, Nishibata Y, Nakamura M. Evaluation of pregabalin-induced adverse events related to falls using the FDA adverse event reporting system and Japanese adverse drug event report databases. J Clin Pharm Ther. 2019; 44:285-291.
15. Cabrera J, Emir B, Dills D, Murphy TK, Whalen E, Clair A. Characterizing and understanding body weight patterns in patients treated with pregabalin. Curr Med Res Opin. 2012; 28:1027-1037.
16. Ikeda H, Yonemochi N, Ardianto C, Yang L, Kamei J. Pregabalin increases food intake through dopaminergic systems in the hypothalamus. Brain Res. 2018; 1701:219-226.
17. Taylor CP, Angelotti T, Fauman E. Pharmacology and mechanism of action of pregabalin: the calcium channel α2–δ (alpha2–delta) subunit as a target for antiepileptic drug discovery. Epilepsy Res. 2007; 73:137-150.
18. Micheva KD, Taylor CP, Smith SJ. Pregabalin reduces the release of synaptic vesicles from cultured hippocampal neurons. Mol Pharmacol. 2006; 70:467-476.
19. Grajales D, Ferreira V, Valverde ÁM. Second-generation antipsychotics and dysregulation of glucose metabolism: beyond weight gain. Cells. 2019; 8:1336.
20. Smith SR, Jonge LD, Volaufova J, Li Y, Xie H, Bray GA. Effect of pioglitazone on body composition and energy expenditure: a randomized controlled trial. Metabolism. 2005; 54:24-32.
21. Ko KD, Kim KK, Lee KR. Does weight gain associated with thiazolidinedione use negatively affect cardiometabolic health? J Obes Metab Syndr. 2017; 26:102-106.
22. Zanchi A, Chiolero A, Maillard M, Nussberger J, Brunner HR, Michel Burnier M. Effects of the peroxisomal proliferator-activated receptor-γ agonist pioglitazone on renal and hormonal responses to salt in healthy men. J Clin Endocrinol Metab. 2004; 89:1140-1145.
23. Safari MAM, Masseran N, Majid MHA, Tajuddin RRM. Robust estimation of the three parameter weibull distribution for addressing outliers in reliability analysis. Sci Rep. 2025; 15:11516.

Received September 11, 2025; Revised December 3, 2025; Accepted December 7, 2025.

**Address correspondence to:*
Naohito Ide, Department of Pharmaceutical Sciences, Nihon Pharmaceutical University, 10281 Komuro, Ina-Machi, Kitaadachi-Gun, Saitama, 362-0806, Japan.
E-mail: n-ide@nichiyaku.ac.jp

Released online in J-STAGE as advance publication December 11, 2025.

Original Article

DOI: 10.5582/ddt.2025.01101

Verification of the protective effect of transfecting brain-derived neurotrophic factor and B-cell lymphoma 2 genes on retina ganglion cells in a rat model of optic nerve injury

Zijia Zhao[1], Yuan Fang[1], Gezhi Xu[1], Jiawei Xiong[1], Xiaofen Mo[1,2,3], Jiawen Fan[1,*]

[1] Eye Institute and Department of Ophthalmology, Eye & ENT Hospital, Fudan University, Shanghai, China;
[2] NHC Key Laboratory of Myopia (Fudan University); Key Laboratory of Myopia, Chinese Academy of Medical Sciences, Shanghai, China;
[3] Shanghai Key Laboratory of Visual Impairment and Restoration, Shanghai, China.

SUMMARY: This pilot study investigated the protective effect of transfecting brain-derived neurotrophic factor (*BDNF*) and B-cell lymphoma 2 (*bcl-2*) genes in retinal ganglion cells (RGCs) using *in vivo* electroporation in an adult rat optic nerve transection model. Sprague-Dawley rats were randomly divided into five groups: BDNF(+)/bcl-2(+), BDNF(+), bcl-2(+), empty plasmid (EP), and no surgery (NS). The plasmids were intravitreally injected and electroporated into the left eye. Seven days later, optic nerve transection was performed in all groups except the NS group. Protein expression was examined using Western blotting, RGC survival was quantified using 1,1'-dioctadecyl-3,3,3',3'-tetramethyl-indocarbocyanine perchlorate (DiI) retrograde labeling, and apoptosis was assessed using terminal deoxynucleotidyl transferase dUTP nick end labeling (TUNEL) at multiple time points (7, 14, and 28 d after transfection). A significantly higher number of DiI (+) RGCs and lower number of apoptotic cells were observed in the BDNF(+)/bcl-2(+), BDNF(+), and bcl-2(+) groups compared to those in the EP group at all time points. The number of DiI (+) RGCs in the three treatment groups was significantly lower than that in the NS group. However, there were no significant differences among the three treatment groups. The protective effects of gene transfection tended to be strongest in the BDNF(+)/bcl-2(+) group, followed by the BDNF(+) group and then the bcl-2(+) group. Thus, all gene transfection treatments had a protective effect against the loss of DiI(+) RGCs induced by optic nerve transection but did not result in full recovery. This study also confirmed the value of *in vivo* electroporation. The findings of this pilot study provide a working base for the development of gene therapy for blinding optic nerve disorders.

Keywords: electroporation, gene therapy, retinal ganglion cells, brain-derived neurotrophic factor, bcl-2

1. Introduction

Degeneration and death of retinal ganglion cells (RGCs) are observed in many blinding optic nerve disorders, with glaucoma being the most prevalent. Loss of RGCs contributes substantially to the development of irreversible vision loss (*1,2*). After optic nerve injury, axonal disruption triggers apoptotic RGC death, which is difficult to ameliorate with currently available treatments. Experimental studies have shown that if the optic nerve axon is compressed or severed, its connected ganglion cells will initiate apoptosis (*3*). Multiple mechanisms have been reported to be involved in the degeneration and death of RGCs, including intraocular pressure-independent oxidative stress, axonal transport disruption, neurotrophic factor deprivation, and activation of apoptotic and autophagic pathways (*4,5*).Currently, efficient treatments for RGC-related optic nerve injuries are insufficient. Accordingly, the development of novel treatments with satisfactory safety and efficacy has been an urgent task for ophthalmologists. Quigley proposed that the promotion of RGC growth, along with the prevention of apoptosis, is efficient in terms of protecting RGCs (*6*). Our previous work confirmed that transfection of the brain-derived neurotrophic factor (*BDNF*) gene into RGCs using an improved *in vivo* electroporation technique has a high transfection efficiency. Moreover, transfection of *BDNF* gene *per se* had protective effects on rat RGCs after optic nerve amputation (*7*).

Gene therapy has emerged as a promising strategy to protect RGCs by delivering neuroprotective or anti-apoptotic genes into RGCs; however, most existing studies have only focused on a single factor and have seldom observed multiple factors. For example, overexpression of BDNF *via* viral or other vectors results in significant RGC rescue; however, it only achieves

transient efficacy (*8*). Anti-apoptotic factors, such as members of the B-cell lymphoma (bcl) family (including bcl-2 and bcl-XL), oppose intrinsic apoptotic pathways. However, studies combining bcl-2 and neurotrophins in animal models of RGC injury are limited (*9*).

Based on the aforementioned information, we hypothesized that transfecting the *BDNF* (a neurotrophic factor) gene, the *bcl-2* gene (an anti-apoptotic gene), or co-transfecting both might result in yield protective effects in RGCs following optic nerve transection. Our main aim was to test whether transfection of *BDNF*, transfection of *bcl-2*, or co-transfection of both might result in better RGC survival and reduce cellular apoptosis. We believe that the findings of this pilot study will be helpful in developing a novel and effective gene therapy for the treatment of optic nerve injury.

2. Materials and Methods

2.1. Animals

Male Sprague-Dawley (SD) rats (9 weeks of age; weight, 200-250 g) were housed in a temperature-controlled room. The animals were kept on a 12-hour light-dark schedule and had free access to food and water. The treatment of all animals conformed to the National Institute of Health Principles of Laboratory Animal Care, the Association for Research in Vision and Ophthalmology (ARVO) Statement of the Use of Animals in Ophthalmic and Vision Research, and local institutional guidelines. All experiments were approved and supervised by the Ethics Committee for the Welfare of Laboratory Animals of the Eye and ENT Hospital of Fudan University (approval number: 2023DW003).

2.2. Plasmid construction and preparation

The plasmid vector, pbcl-2-green fluorescent protein (GFP), carrying the *bcl-2* and *GFP* genes, was obtained from the Institute of Neurobiology (Fudan University, Shanghai, China). The plasmid was transfected into *Escherichia coli* DH 5α competent cells, multiplied by culturing the *E. coli* cells, and then isolated and purified using an EndoFree Plasmid Maxi Kit (Qiagen, Santa Clarita, CA, USA). The plasmid was dissolved in Tris-HCl buffer with ethylenediaminetetraacetic acid (TE buffer) (Qiagen, Hilden, Germany) at a concentration of 2.5 μg/μL.

Plasmid pRc/cytomegalovirus (CMV) BDNF, containing mouse *BDNF* cDNA with a fragment length of 750 bp, was combined as previously described (*7*). Primers were designed and synthesized for amplification. The upstream primer sequence was 5'-ATG ACC ATC CTT TTC CTT ACT ATG-3', and the downstream primer sequence was 5'-CCA CTA TCT TCC CCT TTT AAT GG-3' (synthesized by Shanghai Sangon Biotech Co., Ltd., Shanghai, China). A polymerase chain reaction (PCR) reaction (consisting of 30 cycles at 94°C for 30 s, 57°C for 30 s, and 72°C for 40 s) was used to amplify the target genes. The resulting PCR product, approximately 750 bp in length, was electrophoresed on a 1% agarose gel, and the PCR product was purified.

The ligation reaction was performed in a final volume of 5 μL, containing 1 μL of purified PCR product, 1 μL of salt solution, 2 μL of sterile water, and 1 μL of TOPO vector provided in the GFP Fusion Protein Topoisomerase (TOPO) Expression Kit (NT-GFP Fusion TOPO TA Expression Kit; Invitrogen).

The reaction mixture was incubated at room temperature for 5 min and then transferred to ice. Then, 2 μL of the reaction mixture was added to competent *E. coli* cells and mixed gently. The mixture was incubated on ice for 30 min, subjected to heat shock for 30 s at 42°C, and then returned to ice. After adding 250 μL of Super Optimal broth with Catabolite repression (SOC) medium, the tube was capped, and the mixture was incubated at 37°C with shaking at 250 rpm for 1 h. After incubation, the cells were spread on pre-prepared Luria–Bertani Agar (LBA) plates, which were then placed in a 37°C incubator overnight. The next day, bacterial colonies on the plates were marked and single colonies were selected. Each colony was used as a template and subjected to PCR using the upstream primer for BDNF (as mentioned earlier) and the downstream primer BGH provided by the vector plasmid (5'-TAG AAG GCA CAG TCG AGG-3'). The PCR conditions were the same as those described previously (*7*). The PCR products were then electrophoresed, and colonies with bands of approximately 850 bp were considered positive. Positive colonies were streaked again to obtain single clones.

Single colonies from the streaked plates were transferred into LB medium containing ampicillin and incubated on a shaker at 37°C and 250 rpm overnight. A portion of the bacterial culture was stored, and the remaining portion was sent to Shanghai Sangon Biotech Co., Ltd. for sequencing. After sequencing, the stored bacterial culture was used to expand and extract plasmids using an Endofree Plasmid Purification Maxi kit (Qiagen). The purity of the plasmids was checked, and the concentration was adjusted to 2.5 μg/μL in 1 mM Tris-EDTA (TE) buffer (Qiagen).

2.3. Animal grouping, intravitreal injections, and electroporation

The entire grouping and experimental protocols are shown in Figure 1A. In rats, deep anesthesia was induced using an intraperitoneal injection of 500 mg of urethane, 11 mg of ketamine, and 14 mg of xylazine per kilogram of body weight (*7*). Subsequently, the left eye and left optic nerve (ON) were exposed (Figure 1B). The intraocular pressure was initially reduced through paracentesis before the surgery. A 31-gauge (G) needle was used to create a tiny hole in the rats' sclera,

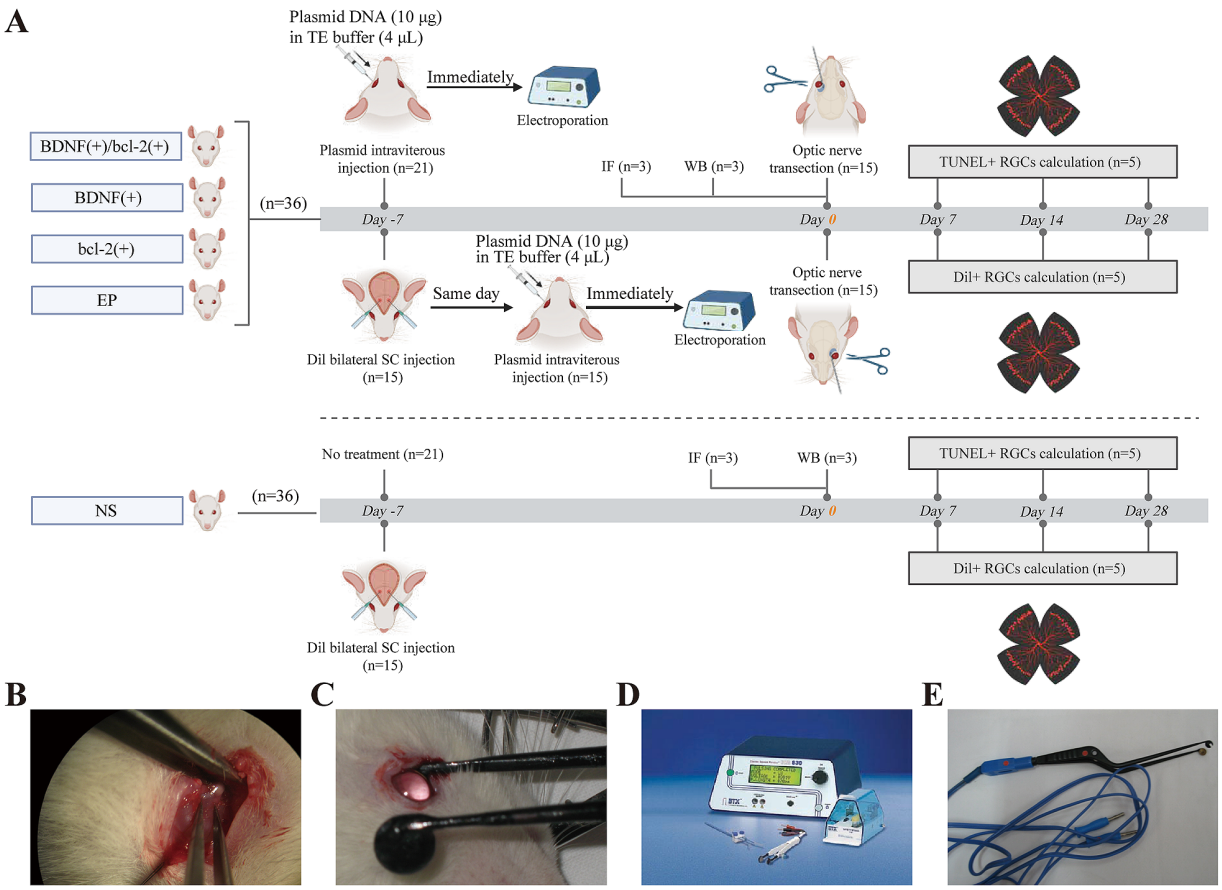

Figure 1. Diagram of the experimental protocol. (**A**) Entire grouping and experimental protocol; (**B**) Optic nerve exposure during surgery; (**C**) Self-developed electrodes, with the cathode connected to the corneal electrode and the anode connected to the scleral electrode; (**D**) ECM830 electroporator from BTX; (**E**) Self-developed electrode for rat experiments. bcl-2, B-cell lymphoma 2; BDNF, brain-derived neurotrophic factor; Dil, 1,1'-dioctadecyl-3,3,3',3'-tetramethyl-indocarbocyanine perchlorate; EP, empty plasmid; IF, immunofluorescence; NS, no surgery; RGC, retinal ganglion cell; SC, superior colliculi; TE buffer, Tris-HCl buffer with ethylenediaminetetraacetic acid; TUNEL, terminal deoxynucleotidyl transferase dUTP nick end labeling; WB, Western blotting.

positioned 0.5 to 1.0 mm posterior to the limbus. The tip of the 31G needle was observed after entering the vitreous at a 40 to 50-degree angle through the dilated pupil. Subsequently, 10 μg of plasmid DNA in 4 μL of TE buffer was gently injected into the vitreous body (*10,11*).

Subsequently, the eye was immediately held and grasped using forceps-type electrodes, with the cathode connected to the corneal electrode and anode connected to the scleral electrode (Figure 1C), as previously described (*11,12*). Square-wave pulses lasting 99 ms were then applied, with a field strength of 12 V/cm, and five pulses were delivered. This process was repeated twice with a 5-min interval between applications using an Electro Square Porter T820 device (BTX, Holliston, Massachusetts, USA) (Figures 1D and E). Rats that received 4 μL of the *BDNF* gene before electroporation were referred to as the BDNF(+) group. Rats receiving 4 μL of the *bcl-2* gene solution before electroporation were referred to as the bcl-2(+) group. Rats receiving 2 μL of the *BDNF* gene and 2 μL of the *bcl-2* gene along with electroporation were referred to as the BDNF(+)/bcl-2(+) group, and those rats injected with 4 μL of plasmid pRc/CMV with electroporation but containing no *BDNF* cDNA or *bcl-2* cDNA were referred to as the empty plasmid (EP) group. Rats that did not receive an intravitreal injection were referred to as the no surgery (NS) group.

2.4. Fluorescence observation in retinal whole mounts

To confirm the transfection of *BDNF* and *bcl-2* into RGCs, connected GFP fluorescence was observed in the rat retina in the BDNF(+) (n = 3), bcl-2(+) (n = 3), BDNF(+)/bcl-2(+) (n = 3), EP (n = 3), and NS (n = 3) groups. One week after *in vivo* electroporation, all rats were killed by intracardiac perfusion of 4% paraformaldehyde in 0.1 M PBS under deep ether anesthesia. The left eyeball was then immediately removed, post-fixed in 4% paraformaldehyde for one hour, and then placed in phosphate-buffered saline (PBS) at 4°C. For the observation of fluorescence in retinal wholemounts, retinas were isolated and cut into a four-leaf clover structure within 24 h after eyeball isolation.

Retinas were then mounted using glycerol buffer and observed under a fluorescence microscope (Leica, Wetzlar, Hesse, Germany) to visualize the expression of green fluorescent protein.

2.5. Western blotting (WB)

WB was performed to study the changes in *BDNF* and *bcl-2* gene expression. Treated retinal tissues were lysed using RIPA buffer (Sigma-Aldrich, St. Louis, MO, USA.) with protease and phosphatase inhibitors (Roche, Basel, Switzerland). Protein concentrations were measured using bicinchoninic acid assays (QuantiPro BCA Assay kit, Sigma-Aldrich). Lysate proteins were separated on NuPAGE Novex 4–12% Bis-Tris 1 mm-thick mini-gels (Life Technologies, Carlsbad, CA, USA) by electrophoresis and then transferred to polyvinylidene fluoride (PVDF) membranes (Millipore, Billerica, MA, USA) for blotting. The membranes were incubated overnight at 4°C with affinity-purified rabbit polyclonal anti-human BDNF (N-20, Santa Cruz Biotechnology, Santa Cruz, CA, USA) and mouse monoclonal anti-human bcl-2 (bcl-2-100, Invitrogen) primary antibodies. After three washes in tris-buffered saline (TBS)-T (0.1% Tween 20 in TBS), the membranes were incubated with horseradish peroxidase-labeled secondary antibodies (Cell Signaling, Danvers, MA, USA) diluted 1:1,000 in TBS-T for 2 h at room temperature and washed again in TBS-T. Detection was performed using enhanced chemiluminescence (ECL; Amersham Pharmacia Biotech, Uppsala, Sweden). β-actin (Cell Signaling#4967, 1:2,000) served as the loading control. Protein bands were observed using an IMAGE READER LAS-3000 imaging system (Fujifilm, Tokyo, Japan) and analyzed using the software IMAGE READER LAS-3000 (V2.2, Fujifilm).

2.6. Transection of the optic nerves

Optic nerve transection was performed to induce RGC apoptosis 7 d after intravitreal injection combined with electroporation, as described earlier (*13*). The protocol was improved by our group and implemented in all groups except the NS group. Briefly, the rats were anesthetized with 1 mL/kg of ketamine and 0.0625 g/kg of xylazine *via* intramuscular injection. After anesthesia, the orbital tissues were re-isolated and the optic nerve was exposed. A sharp blade was used to open the optic nerve sheath to expose the optic nerve and avoid blood vessels. Micro-scissors were used to cut the optic nerve at a position approximately 1.0 mm and 1.5 mm behind the eye, and a segment of approximately 0.5 mm was removed to ensure complete transection of the optic nerve. The orbital tissues were carefully restored, and the conjunctiva was sutured. The fundus was observed using indirect ophthalmoscopy through dilated pupils to confirm normal retinal circulation.

2.7. Retrograde tracing of 1,1'-dioctadecyl-3,3,3',3'-tetramethyl-indocarbocyanine perchlorate (DiI) to count living RGCs after optic nerve transection

Retrograde tracing of DiI refers to a method used to retrogradely trace the projections of neurons using DiI fluorescent labeling. In this technique, DiI dye is injected into the target area, and the labeled neurons are subsequently observed in a retrograde manner based on their inherent fluorescence properties, both near the injection site and distant from the injection site. This approach is widely used in neuroscience research, enabling researchers to gain insights into the connections and neural circuits of neurons (*14,15*). We used DiI (Molecular Probes, Invitrogen) dissolved in *N*,*N*-dimethylformamide (DMF). Fifteen randomly selected SD rats from each group were anesthetized with an intramuscular injection of 1 mL/kg ketamine and 0.0625 g/kg xylazine and then fixed in a stereotaxic apparatus. The skin on the top of the head was incised to expose the skull, and bilateral holes were drilled at the corresponding positions of the dorsal lateral geniculate nucleus using an electric drill. According to Paxinos' rat brain stereotaxic atlas (*16*), the superior colliculi (SC) was localized 20 mm anterior to the bregma, 12 mm lateral to the midline, and at a depth of 32 mm. A total of 5 μL of DiI at a concentration of 150 μg/μL was injected into each side using a 10-μL microsyringe. After the injection, the scalp was sutured layer by layer. On the same day as the DiI injection, a combination of intravitreal injection of the plasmid and *in vivo* electroporation was performed.

Seven days after retrograde tracing with DiI, the optic nerves were transected as described above. Five rats from each group at each time point were euthanized 7, 14, and 28 d after optic nerve transection. Retinal wholemounts were prepared as described in the 'Fluorescence observation' section above. Wholemounts were sealed with glycerol buffer and observed under a fluorescence microscope (DRM model; Leica) to visualize DiI-labeled positive RGCs. Images were collected and analyzed using the software QWin (V3, Leica) to calculate the area and number of RGCs. Calculations were performed in four quadrants, with the optic disc at the center. In each quadrant, DiI-labeled positive cells were counted at 1.5, 2.5, and 3.5 mm from the center, with a total of 12 regions for observation and counting in each sample (*7*). The results were calculated and converted to the number of surviving RGCs per square millimeter of the area.

2.8. Terminal deoxynucleotidyl transferase dUTP nick end labeling (TUNEL) staining

To analyze RGC apoptosis 7, 14, and 28 d after optic nerve transection, five rats from each group at each time point were euthanized, and retinal tissue paraffin sections (six sections per eye) were prepared. After pretreatment,

an *In Situ* Apoptosis Detection Kit (R&D Systems, Minneapolis, MN, USA) was used for proteinase K digestion and terminal deoxynucleotidyl transferase (TdT) labeling, followed by biotin-labeled fluorescence conjugation. The sections were then sealed with 20% glycerol buffer and observed under a fluorescence microscope to identify the apoptotic RGCs. The number of apoptotic RGCs per millimeter of length was counted and calculated for each group.

2.9. Statistical analysis

In this study, statistical analyses were performed using the software SPSS (V 29.0.1.0, IBM, Chicago, IL, USA) and GraphPad Prism 10 (V10.2.3, GraphPad Software, MA, US). Each experiment was performed in triplicate. The normal distribution of the data was confirmed using the Shapiro-Wilk test. Data are expressed as the mean ± standard deviation (SD). Comparisons between the two groups were done using paired or unpaired *t*-tests. Statistical evaluation among multiple groups was done using one-way analysis of variance (ANOVA) followed by Bonferroni's test. Statistical significance was set at $P < 0.05$.

3. Results

3.1. Confirmation of *BDNF* and *bcl-2* gene expression in RGCs

As shown in Figure 2, no green fluorescence of GFP was observed in the NS and EP groups (Figure 2A). In contrast, distinct green fluorescence signals were detected in the BDNF(+), bcl-2(+), and BDNF(+)/bcl-2(+) groups 7 d after electroporation and plasmid transfection (Figure 2B). Accordingly, expression of the *BDNF* and *bcl-2* genes in RGCs was confirmed

3.2. Verification of gene expression after transfection of the *BDNF* and *bcl-2* genes

Figure 3 shows the results of gene transfection 7 d after plasmid transfection, as indicated by WB. The BDNF(+) group exhibited the highest expression of BDNF protein compared to the other groups, and the BDNF(+)/bcl-2(+) group also had a higher level of BDNF protein expressed than the bcl-2(+), EP, and NS groups (Figures 3A and 3C), indicating successful transfection of the *BDNF* gene. The bcl-2(+) group exhibited the highest level of bcl-2 protein expression compared to the other groups, and the BDNF(+)/bcl-2(+) group also exhibited a higher level of bcl-2 protein expression than the BDNF(+), EP, and NS groups (Figures 3B and 3D), indicating successful transfection of the *bcl-2* gene. Thus, the BDNF(+), bcl-2(+), and BDNF(+)/bcl-2(+) groups were successfully established and could be used for subsequent experiments (Figure 3).

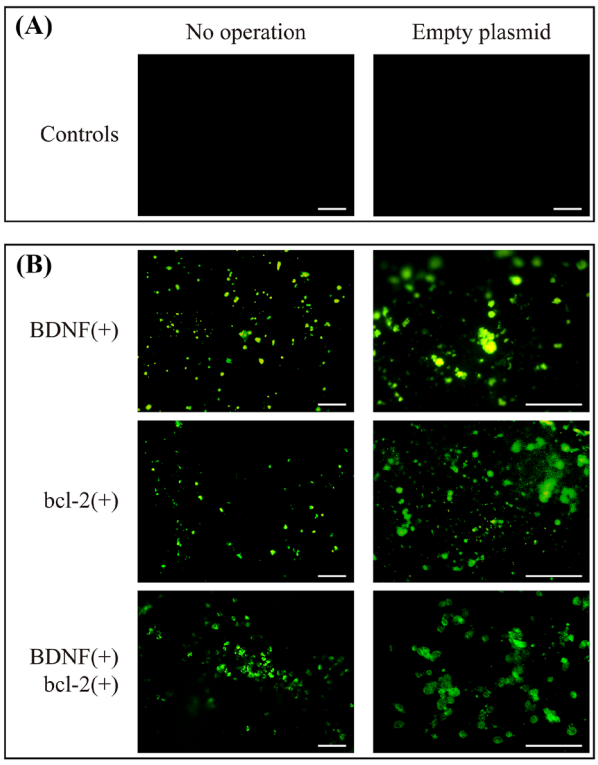

Figure 2. Analysis of gene expression 7 d after electroporation and plasmid transfection. (**A**) Images from controls. The column on the left shows an image of no surgery (NS), and the column on the right shows an image of the empty plasmid (EP). (**B**) Images from the BDNF (+), bcl-2 (+), and BDNF (+)/bcl-2 (+) groups. The column on the left is at a magnification of 1×, and the column on the right is at a magnification of 2×. Scale bar = 100 μm. bcl-2, B-cell lymphoma 2; BDNF, brain-derived neurotrophic factor.

3.3. Verification of the morphological manifestation of Dil-labeled (Dil(+)) RGCs in the NS group

Figures 4A–4C depict the morphological manifestation of DiI(+) RGCs at different sites in the retina, namely the central retina (Figure 4A), parafoveal retina (Figure 4B), and peripheral retina (Figure 4C). The DiI(+) RGCs observed in the central retina had a diameter of 7–10 μm (Figure 4A), which increased from the central to the peripheral region (Figures 4B and 4C). In the peripheral retina, the diameter of the cells was 9–13 μm with a plump shape (Figure 4C). Figure 4D shows the density of DiI(+) RGCs in the central retina at 7, 14, and 28 d. There were significant differences in cellular density at 7, 14, and 28 d. The stability of DiI(+) RGCs was confirmed in the NS group, indicating that it was suitable for use as a blank control.

3.4. Verification of the protective effects of transfecting the genes *BDNF*, *bcl-2*, and *BDNF* plus *bcl-2* on the loss of DiI(+) RGCs induced by optic nerve transection

Figure 5 shows the effects of transfecting the genes *BDNF*, *bcl-2*, and *BDNF* plus *bcl-2* 7, 14, and 28 d later. As shown in Figure 1A, the number of DiI(+) RGCs in

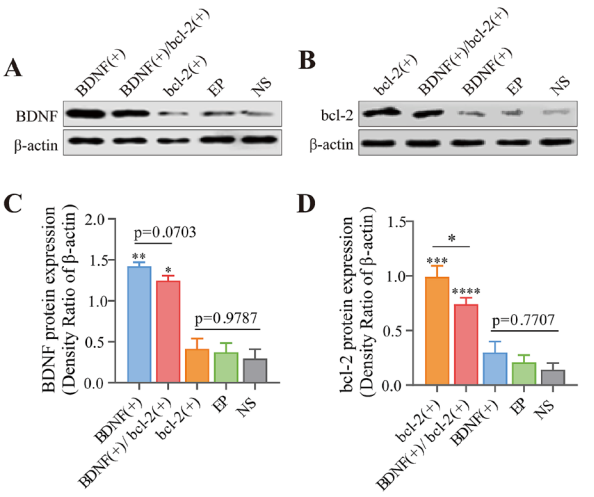

Figure 3. Expression of BDNF and bcl-2 7 d after gene transfection. (**A**) BDNF expression. The BDNF(+) and BDNF(+)/bcl-2(+) groups had higher levels of BDNF expression than the bcl-2(+), EP, and NS groups. (**B**) bcl-2 expression. The bcl-2(+) and BDNF(+)/bcl-2(+) groups had higher levels of bcl-2 expression than the BDNF(+), EP, and NS groups. (**C**) Quantitative data on BDNF expression. BDNF protein expression in the BDNF(+) and BDNF(+)/bcl-2(+) groups was significantly upregulated compared to that in the control group but did not differ significantly in the bcl2(+), EP, and NS control groups. (**D**) Quantitative data on bcl-2 expression. bcl-2 protein expression in the bcl-2(+) and BDNF(+)/bcl-2(+) groups was significantly higher than that in the control group but did not differ significantly in the BDNF(+), EP, and NS control groups. *means $P < 0.05$, **means $P < 0.01$ and ***means $P < 0.001$, ****means $P < 0.0001$, (vs NS control group). n = 3/group. Independent repeats = 2 samples. bcl-2, B-cell lymphoma 2; BDNF, brain-derived neurotrophic factor; EP, empty plasmid; NS, no surgery.

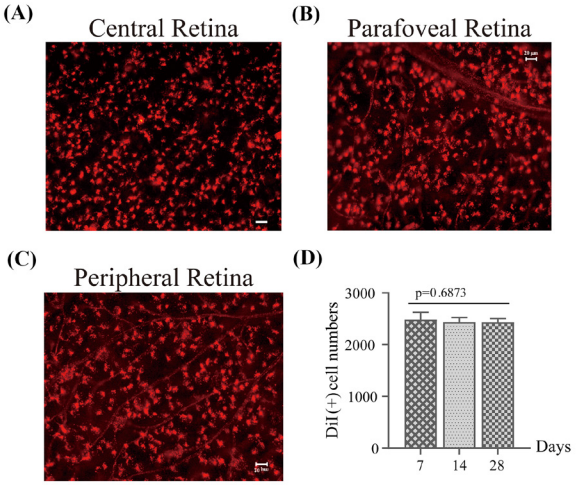

Figure 4. Morphology of DiI(+) RGCs in the retina of the NS group. (**A**) RGCs in the central retina (around the optic nerve) were small, with a diameter of 7-10 μm, and densely distributed. (**B**) RGCs in the parafoveal retina were slightly larger, with a diameter of 9-11 μm, and distributed more sparsely than those in the central retina. (**C**) RGCs in the peripheral retina were larger, with a diameter of 9-13 μm, and sparsely distributed. (**D**) There were no significant differences in the NS group at the three experimental time points (one-way ANOVA, $P = 0.6873$). Scale bar = 20 μm. DiI, 1,1'-dioctadecyl-3,3,3',3'-tetramethyl-indocarbocyanine perchlorate; NS, no surgery; RGC, retinal ganglion cell.

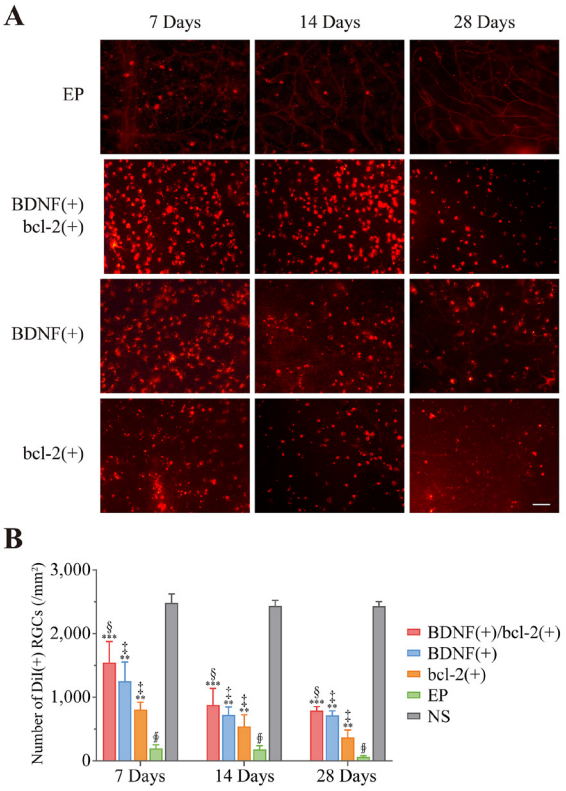

Figure 5. Transfecting the genes *BDNF*, *bcl-2*, and *BDNF* plus *bcl-2* enhanced survival of DiI(+) RGCs. (A) Images of DiI(+) RGCs at 7, 14, and 28 d after gene transfection. The EP group had the lowest number of DiI(+) RGCs (bright-red cells). The BDNF(+)/bcl-2(+), BDNF(+), and bcl-2(+) groups exhibited higher numbers of DiI(+) RGCs. Scale bar = 50 μm. (**B**) Quantitative data on the number of DiI(+) RGCs 7, 14, and 28 d after gene transfection. **$P <$ 0.01 and ***$P < 0.001$, *vs.* EP group. $^{‡}P < 0.01$, $^{§}P < 0.001$ and $^{¶}P <$ 0.0001, *vs.* NS group. bcl-2, B-cell lymphoma 2; BDNF, brain-derived neurotrophic factor; EP, empty plasmid; DiI, 1,1'-dioctadecyl-3,3,3',3'-tetramethyl-indocarbocyanine perchlorate; NS, no surgery; RGC, retinal ganglion cell.

the BDNF(+)/bcl-2(+), BDNF(+), and bcl-2(+) groups gradually decreased over time. At the same timepoint, the BDNF(+)/bcl-2(+) group had the highest number of cells. The number of cells was greatest in the BDNF(+)/bcl-2(+) group, followed by the BDNF(+) group and then the bcl-2(+) group. The EP group had the lowest number of cells. Apoptotic cells (reduced cell volume, condensed nuclei, and loose cytoplasm) were observed, and their number increased with time (Figure 5A). Figures 5B shows the quantitative data on cell counts. Trends were similar at the three time points. The number of DiI(+) RGCs in the BDNF(+)/bcl-2(+), BDNF(+), and bcl-2(+) groups was significantly greater than that in the EP group and lower than that in the NS group. This result indicates that all gene transfection treatments resulted in protective effects against the loss of DiI(+)-labeled RGCs induced by optic nerve transection but did not result in full recovery. The number of DiI(+) RGCs tended to be greatest in the BDNF(+)/bcl-2(+) group, followed by the BDNF(+) group and then the bcl-2(+) group, there were no significant differences among these three groups

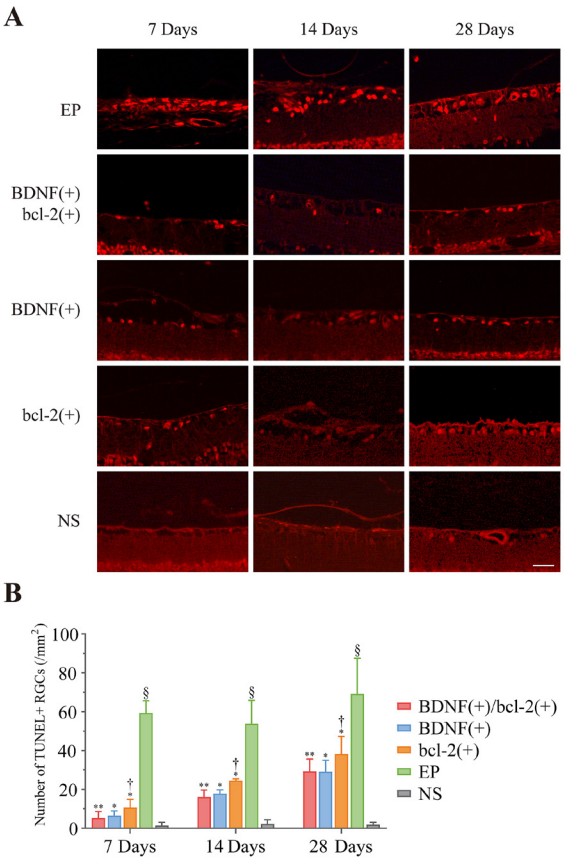

Figure 6. Transfecting the genes *BDNF*, *bcl-2*, and *BDNF* plus *bcl-2* reduced apoptosis of RGCs (TUNEL(+) cells). (A) Images of TUNEL(+) cells 7, 14, and 28 d after gene transfection. The EP group had the highest number of apoptotic cells (TUNEL staining, bright-red cells). The BDNF(+)/bcl-2(+), BDNF(+), and bcl-2(+) groups had fewer apoptotic cells, and no apoptotic cells were found in the NS group. Scale bar = 20μm. **(B)** Quantitative data on TUNEL(+) cells at 7, 14, and 28 d after gene transfection. $^{*}P < 0.05$, $^{**}P < 0.01$ and $^{***}P < 0.001$, *vs.* EP group. $^{\dagger}P < 0.05$ and $^{\S}P < 0.001$ *vs.* NS group. bcl-2, B-cell lymphoma 2; BDNF, brain-derived neurotrophic factor; EP, empty plasmid; NS, no surgery; RGC, retinal ganglion cell; TUNEL, terminal deoxynucleotidyl transferase dUTP nick end labeling.

(Figure 5B).

TUNEL-positive apoptotic RGCs were also observed in the same experimental system. Figure 6A shows the changes in apoptotic RGCs over the period of transfection. Figure 6B shows the cell counts of TUNEL+ cells in each group (Figure 6). Trends were similar at the three time points, namely the number of TUNEL+ cells in the BDNF(+)/bcl-2(+), BDNF(+), and bcl-2(+) groups was significantly lower than that in the EP group and higher than that in the NS group. There were no significant differences among the three treatment groups. However, cellular apoptosis tended to be least prevalent in the BDNF(+)/bcl-2(+) but greater in the BDNF(+) group and even greater in the bcl-2(+) group; the number of DiI(+) RGCs followed the reverse of that trend.

The productive effects of gene transfection were verified based on the observation of DiI (+) and TUNEL(+) cells.

4. Discussion

This study revealed that transfection of the *BDNF* and *bcl-2* genes and co-transfection of both genes *via in vivo* electroporation significantly improved the survival of RGCs and reduced cellular apoptosis. The protective effects on DiI(+) RGCs were significant in these three groups but full recovery was not achieved. Thus, the protective effects of transfection with the genes *BDNF* and *bcl-2* and co-transfection with both genes on the loss of RGCs induced by optic nerve transection were verified. There were no significant differences among the groups with transfection of the genes *BDNF*, *bcl-2*, and *BDNF* plus *bcl-2*, but protective effects tended to be strongest in the BDNF(+)/bcl-2(+) group, followed by the BDNF(+) group and then the bcl-2(+) group. To extent known, this is the first study to verify the effects of gene transfection with a neurotrophic support-related gene, an anti-apoptosis-related gene, and co-transfection of both genes in animals that underwent optic nerve transection. We believe that the findings of the present study are pivotal to the development of a novel gene treatment for RGC-related optic nerve injury.

After electroporation and plasmid transfection for 7 d, the expression of BDNF(+), bcl-2(+), and BDNF(+)/bcl-2(+) was clearly observed (Figure 2), indicating that *in vivo* electroporation can result in the successful transfection and co-transfection of the *BDNF* and *bcl-2* genes into RGCs. Co-transfection of the *BDNF* and *bcl-2* genes *via in vivo* electroporation was developed in our previous study (*7*). We found that BDNF expression was significantly upregulated by transfection with the *BDNF* gene, but not by transfection with the *bcl-2* gene. Likewise, the expression of bcl-2 was significantly upregulated by transfection with *bcl-2*, but not by transfection with the *BDNF* gene. However, transfection of *BDNF*(+)/*bcl-2*(+) upregulated both (Figure 3). Transfection of the genes *BDNF*, *bcl-2*, and *BDNF* plus *bcl-2* resulted in significant protective effects (less reduction in/apoptosis of DiI(+) cells). The number of RGCs in the three treatment groups was significantly higher than that in the EP group but still lower than that in the NS group, indicating that the treatments were effective but did not result in full recovery. There were no significant differences among the BDNF (+), bcl-2 (+), and BDNF (+)/bcl-2 (+) groups, but efficiency tended to be highest in the BDNF(+)/bcl-2(+) group (Figure 5). Analysis of apoptosis yielded coincident results, namely there were significantly fewer apoptotic cells (TUNEL+) in the BDNF(+), bcl-2(+), and BDNF(+)/bcl-2(+) groups than in the EP group, and there were no significant differences among the three treatment groups. However, the protective effects of transfection tended to be strongest in the BDNF(+)/bcl-2(+) group (Figure 6). These results partly agree with the findings of previous studies, in which the administration of BDNF and anti-apoptotic Z-DEVD_fmk (*17*) and the combination

of bcl-2 and growth-related protein-43 promoted the regeneration of vertebrate peripheral nerve axons (*18*). We demonstrated that co-transfection of the *BDNF* and *bcl-2* genes did not result in better efficiency than transfection of *BDNF* or *bcl-2* alone. Thus, this study did not observe any synergistic effects of neurotrophic support genes and anti-apoptotic therapy. However, the survival of DiI(+) RGCs tended to be greater in the BDNF(+)/bcl-2(+) group while it tended to have fewer apoptotic cells (*vs.* transfection of *BDNF* or *bcl-2* alone). Indeed, the quantity of transfected plasmids of each gene in the BDNF(+)/bcl-2(+) group was only half that of the groups with transfection of a single gene. These trends imply that co-transfection has a better efficacy than that of transfection alone. This warrants further verification. In addition, we observed that the protective effects diminished over time. As indices, the number of RGCs and apoptotic cells exhibited similar trends. Confirmation of this phenomenon requires a longer follow-up period in future studies.

The main limitation of this study was the small sample size in each experimental group. This may have led to biased conclusions. In addition, the follow-up period was only 28 d, and the long-term effects were unclear. These issues should be addressed in future studies.

5. Conclusion

In conclusion, this study demonstrated that transfection of the *BDNF* and *bcl-2* genes and co-transfection of both genes significantly enhanced retinal ganglion cell survival and reduced apoptosis in animals *via in vivo* electroporation. Accordingly, results confirmed the protective effects of transfection of these genes on the loss of RGCs. These findings imply that gene therapy is a promising strategy for treating traumatic and degenerative optic neuropathies. Approaches to translate this strategy into clinical applications are highly anticipated. Moreover, results confirmed the value of *in vivo* electroporation. This study provides a foundation for further use of gene therapy in blinding optic nerve disorders. Future studies should focus on exploring the underlying signaling networks, observing long-term functional outcomes, and exploring potential clinical applications.

Funding: This study was supported by the Shanghai Pujiang Talent Program Project - Class A (Research and Development Category) (22PJ1401500) in China.

Conflict of Interest: The authors have no conflicts of interest to disclose.

References

1. Quigley HA. Glaucoma. Lancet. 2011; 377:1367-1377.
2. Calkins DJ. Critical pathogenic events underlying progression of neurodegeneration in glaucoma. Prog Retin Eye Res. 2012; 31:702-719.
3. Levin LA, Gordon LK. Retinal ganglion cell disorders: Types and treatments. Prog Retin Eye Res. 2002; 21:465-484.
4. Si Z, Fan Y, Wang M, Zhao J, Zhang Y, Liu D, Zheng Y. The role of RGC degeneration in the pathogenesis of glaucoma. Int J Biol Sci. 2025; 21:211-232.
5. Cui N, Jia J, He Y. Glaucomatous retinal ganglion cells: Death and protection. Int J Ophthalmol. 2025; 18:160-167.
6. Quigley HA. Ganglion cell death in glaucoma: Pathology recapitulates ontogeny. Aust N Z J Ophthalmol. 1995; 23:85-91.
7. Mo X, Yokoyama A, Oshitari T, Negishi H, Dezawa M, Mizota A, Adachi-Usami E. Rescue of axotomized retinal ganglion cells by BDNF gene electroporation in adult rats. Invest Ophthalmol Vis Sci. 2002; 43:2401-2405.
8. Osborne A, Khatib TZ, Songra L, Barber AC, Hall K, Kong GYX, Widdowson PS, Martin KR. Neuroprotection of retinal ganglion cells by a novel gene therapy construct that achieves sustained enhancement of brain-derived neurotrophic factor/tropomyosin-related kinase receptor-B signaling. Cell Death Dis. 2018; 9:1007.
9. Donahue RJ, Fehrman RL, Gustafson JR, Nickells RW. BCLXL gene therapy moderates neuropathology in the DBA/2J mouse model of inherited glaucoma. Cell Death Dis. 2021; 12:781.
10. Li Y, Schlamp CL, Nickells RW. Experimental induction of retinal ganglion cell death in adult mice. Invest Ophthalmol Vis Sci. 1999; 40:1004-1008.
11. Yokoyama A, Oshitari T, Negishi H, Dezawa M, Mizota A, Adachi-Usami E. Protection of retinal ganglion cells from ischemia-reperfusion injury by electrically applied Hsp27. Invest Ophthalmol Vis Sci. 2001; 42:3283-3286.
12. Dezawa M, Takano M, Negishi H, Mo X, Oshitari T, Sawada H. Gene transfer into retinal ganglion cells by *in vivo* electroporation: A new approach. Micron. 2002; 33:1-6.
13. Mey J, Thanos S. Intravitreal injections of neurotrophic factors support the survival of axotomized retinal ganglion cells in adult rats *in vivo*. Brain Res. 1993; 602:304-317.
14. Yu YL, Li HY, Zhang PX, Yin XF, Han N, Kou YH, Jiang BG. Comparison of commonly used retrograde tracers in rat spinal motor neurons. Neural Regen Res. 2015; 10:1700-1705.
15. Makarenko IG. DiI tracing of the hypothalamic projection systems during perinatal development. Front Neuroanat. 2014; 8:144.
16. Paxinos G, Franklin KBJ. Paxinos and Franklin's the Mouse Brain in Stereotaxic Coordinates. Academic Press, 2019.
17. Magharious MM, D'Onofrio PM, Koeberle PD. Optic nerve transection: A model of adult neuron apoptosis in the central nervous system. J Vis Exp. 2011; 51:2241.
18. Cristino L, Pica A, Della Corte F, Bentivoglio M. Co-induction of nitric oxide synthase, bcl-2 and growth-associated protein-43 in spinal motoneurons during axon regeneration in the lizard tail. Neuroscience. 2000; 101:451-458.
19. Korsching S. The neurotrophic factor concept: A reexamination. J Neurosci. 1993; 13:2739-2748.
20. Daadi MM, Saporta S, Willing AE, Zigova T, McGrogan MP, Sanberg PR. *In vitro* induction and *in vivo* expression of bcl-2 in the hNT neurons. Brain Res Bull. 2001; 56:147-

152.
21. Holm KH, Cicchetti F, Bjorklund L, Boonman Z, Tandon P, Costantini LC, Deacon TW, Huang X, Chen DF, Isacson O. Enhanced axonal growth from fetal human *bcl-2* transgenic mouse dopamine neurons transplanted to the adult rat striatum. Neuroscience. 2001; 104:397-405.
22. Goldberg JL, Espinosa JS, Xu Y, Davidson N, Kovacs GTA, Barres BA. Retinal ganglion cells do not extend axons by default: promotion by neurotrophic signaling and electrical activity. Neuron. 2002; 33:689-702.
23. Lambricht L, Lopes A, Kos S, Sersa G, Préat V, Vandermeulen G. Clinical potential of electroporation for gene therapy and DNA vaccine delivery. Expert Opin Drug Deliv. 2016; 13:295-310.

Received September 20, 2025; Revised October 26, 2025; Accepted November 1, 2025.

**Address correspondence to:*
Jiawen Fan, Eye Institute and Department of Ophthalmology, Eye & ENT Hospital, Fudan University, Shanghai, China, 200031.
E-mail: jiawen.fan@fdeent.org

Released online in J-STAGE as advance publication December 13, 2025.

Original Article

DOI: 10.5582/ddt.2025.01106

A phase II investigator-initiated, continuation trial of 5-aminolevulinic acid hydrochloride/sodium ferrous citrate (5-ALA-HCl/SFC) for patients with adult-onset Still's disease (AOSD) refractory to glucocorticoids

Remi Sumiyoshi[1,2], Tomohiro Koga[1,*], Osamu Kamisawa[2], Shimpei Morimoto[2], Naoki Hosogaya[2], Hiroshi Yamamoto[2], Makoto Hori[3], Yosuke Inaba[3], Yoko Hattori[3], Tamiki Hikake[3], Tomoya Kurokawa[3], Hideki Hanaoka[3], Shuzo Sato[4], Kiyoshi Migita[4,5], Noriyoshi Ogawa[6], Motomu Hashimoto[7], Atsushi Kawakami[1]

[1] Department of Immunology and Rheumatology, Division of Advanced Preventive Medical Sciences, Nagasaki University Graduate School of Biomedical Sciences, Nagasaki, Japan;
[2] Clinical Research Center, Nagasaki University Hospital, Nagasaki, Japan;
[3] Clinical Research Center, Chiba University Hospital, Chiba, Japan;
[4] Department of Rheumatology, Fukushima Medical University School of Medicine, Fukushima, Japan;
[5] Department of Rheumatology, St. Francis Hospital, Nagasaki, Japan;
[6] Department of Internal Medicine 3, Division of Immunology and Rheumatology, Hamamatsu University School of Medicine, Hamamatsu, Japan;
[7] Department of Clinical Immunology, Osaka Metropolitan University Graduate School of Medicine, Osaka, Japan.

SUMMARY: The aim of this study is to evaluate the efficacy and safety of 5-aminolevulinic acid hydrochloride/sodium ferrous citrate (5-ALA-HCl/SFC) in patients with adult-onset Still's disease (AOSD) refractory to glucocorticoids during the maintenance treatment period of a phase II investigator-initiated randomized, double-blind, parallel-group clinical trial. This multicenter, open-label, continuous trial was limited to participants from the preceding study, which was planned for 30 enrollees but was stopped early after four enrollees because of slow recruitment. The current trial maintained a 16-week treatment period and remained double-blind until the previous study database was locked and unblinded. Two dose groups were used: 5-ALA-HCl/SFC 100 and 300 mg. Participants previously assigned to placebo were re-randomized 1:1 to either dose group. The dosage and administration were identical to those of the previous protocol. The primary endpoint was the achievement of adapted ACR 30 at week 16. All four participants achieved the primary endpoints. Secondary outcomes, including the adapted ACR 90/100 and the change in serum ferritin levels, showed numerically greater improvement in the participant who received the high-dose compared with the other. Eleven adverse events occurred in three participants, including one serious event and one discontinuation; all were deemed unrelated to the study drug, and no deaths were reported. This study identified potential efficacy signals, particularly in the high-dose group. However, because of premature termination and a very limited sample size, the data were insufficient to establish the efficacy and safety profile of 5-ALA-HCl/SFC in refractory AOSD. Larger studies are required to confirm these findings.

Keywords: Adult-onset Still's disease (AOSD), glucocorticoids, heme oxygenase-1 (HO-1), 5-aminolevulinic acid/sodium ferrous citrate (5-ALA-HCl/ SFC)

1. Introduction

Adult-onset Still's disease (AOSD) is a systemic inflammatory disorder. Autoantibodies, such as antinuclear antibodies, are generally not detected; however, hypercytokinemia involving interleukin (IL)-1β, IL-6, IL-18, and tumor necrosis factor-α (TNF-α) due to abnormal activation of innate immune cells, such as monocytes and macrophages, may be involved in disease pathogenesis (*1*). Although the recent European Alliance of Associations for Rheumatology/Paediatric Rheumatology European Society (EULAR/PReS) guidelines recommend biologics as the first-line treatment (*2*), in Japan, initial therapy often begins with

glucocorticoids (GCs). The prognosis is generally good; however, approximately 60% of patients experience a prolonged disease course. As GCs alone are often insufficient to control the disease, biologic agents targeting IL-6 and IL-1β or immunosuppressants are used in combination. However, these carry the risk of side effects, such as increased susceptibility to infection. Therefore, there is a need to develop new therapeutic drugs with novel mechanisms.

Elevated levels of heme oxygenase-1 (HO-1) have been reported in the sera of patients with AOSD (*3,4*). The dynamics of HO-1 are similar to those of serum ferritin, which is a marker of disease activity in AOSD. The decrease in HO-1 expression with treatment suggests that it may contribute to the pathogenesis of the disease.

5-Aminolevulinic acid (5-ALA) is an amino acid involved in porphyrin metabolism in plants and animals. Within cells, eight molecules of 5-ALA undergo a series of enzymatic reactions to form protoporphyrin IX (PpIX), which is then converted into heme by ferrochelatase through the insertion of ferrous iron. The co-administration of 5-ALA hydrochloride (5-ALA-HCl) with sodium ferrous citrate (SFC) enhances the conversion of PpIX to heme (*5*).

Preclinical studies in Balb/c mice and Sprague-Dawley rats have demonstrated that oral intake of 5-ALA-HCl combined with SFC increases intracellular heme levels, leading to the upregulation of HO-1 expression. HO-1, also known as heat shock protein 32 (HSP32), is a 32-kDa enzyme that degrades heme and exhibits anti-inflammatory properties (*6,7*). It has been shown to be beneficial in conditions such as ischemia-reperfusion injury, cisplatin-induced nephropathy, and various inflammatory disorders (*8, 9*). Importantly, the administration of 5-ALA-HCl alone does not sufficiently induce HO-1 expression or achieve therapeutic benefits in these conditions. Therefore, the combination of 5-ALA-HCl and SFC is considered essential for eliciting a significant anti-inflammatory response (*8-10*).

Based on these findings, we thought that 5-ALA-HCl/SFC could be a potential therapeutic agent for AOSD, we conducted a Phase II study (jRCT2071220040) to confirm its efficacy of 5-ALA-HCl/SFC in patients with AOSD. This study was an extension trial designed to evaluate the efficacy and safety of continuous administration over a 16-week period.

2. Methods

2.1. Study design

This is an investigator-initiated, multicenter, open-label, continuous clinical trial of the efficacy and safety of 5-ALA-HCl/SFC in patients with AOSD who are refractory to GCs. Owing to early termination, this study only presents pilot data from four participants. The small sample size means that the results can only be considered preliminary evidence that requires validation in larger, adequately powered studies.

This study was conducted at 12 centers in Japan and was performed in accordance with the principles of the Declaration of Helsinki (*11*) and Japan Good Clinical Practice. The study was registered in the Japan Registry of Clinical Trials (*https://jrct.mhlw.go.jp*) as jRCT2071220086 and was approved by the Institutional Review Board of Nagasaki University Hospital, Hokkaido University Hospital, Hamamatsu University School of Medicine, University of Tsukuba Hospital, National Hospital Organization Kyushu Medical Center, Osaka Metropolitan University Hospital, Fukushima Medical University Hospital, Okayama Saiseikai Outpatient Center Hospital, Keio University Hospital, Nagoya University Hospital, Yokohama City University Hospital, and Hiroshima University Hospital. Participants were recruited from 25 January 2023 to 1 February 2024. This trial is a continuation of a previous Phase II physician-initiated randomized double-blind parallel group comparative clinical trial (*12*) (jRCT2071220040). The participants were divided into two groups: the 5-ALA-HCl 100 mg/day + SFC 78.4 mg/day (low-dose) group and the 5-ALA-HCl 300 mg/day + SFC 235.2 mg/day (high-dose) group. The rationale for selecting the dosage in this clinical trial was as follows. Previous clinical studies conducted in patients with type 2 diabetes and cisplatin-induced nephropathy demonstrated the efficacy of 5-ALA-HCl at 300 mg/day (150 mg administered twice daily) (trial IDs: NPJ005-DM2-0522 and SPP3C301). The proposed mechanisms of action involve activation of the electron transport chain and induction of HO-1 expression, leading to anti-inflammatory effects in type 2 diabetes and HO-1 induction in cisplatin nephropathy (*8,9,13*). As these mechanisms are thought to overlap with the pathophysiology of AOSD, a dose of 300 mg/day was anticipated to be effective in this indication as well. In addition, because this study was designed as a dose-finding trial, a lower dose group (100 mg/day) was included, resulting in two study arms: 100 mg/day and 300 mg/day.

2.2. Patients

Participants who met all of the following criteria were recruited: (1) patients who had completed the prior study; (2) patients whose free informed consent could be obtained in writing and who were able to comply with the requirements of the study protocol; (3) females of childbearing potential or males who were sexually active with females of childbearing potential who agreed to use an effective contraceptive method (*e.g.*, condom) for the duration of the study and until the day after the last dose of the study drug.

Key exclusion criteria were as follows: (1) females who were lactating, pregnant, or intend to become

pregnant during the study period; (2) patients who have been off study medication for more than 14 consecutive days between the start of the prior study and the start of the continuation study; (3) patients who have been off study medication for more than 7 consecutive days from the week 8 evaluation date of the prior study to the time of enrollment; (4) patients with macrophage activation syndrome (MAS) or disseminated intravascular coagulation syndrome since the start of the prior study; (5) patients who have started a new or increased dose of methotrexate or other disease-modifying anti-rheumatic drugs between the end of the prior study and the time of enrollment; (6) patients with serious complications that make them unsuitable for the study as determined by the investigator or sub-investigator, (7) other patients deemed inappropriate by the investigator or sub-investigator.

2.3. Interventions

This trial was a continuation of a previous Phase II physician-initiated randomized double-blind parallel group clinical trial (*12*) (jRCT2071220040). The study was conducted in two groups: low-dose and high-dose groups. Subjects who were assigned to the placebo group in the previous study were randomly assigned at a 1:1 ratio to either the low-dose or high-dose group at the time of assignment in the previous study. The remaining groups received equivalent dosages and administration as in the previous study. The study drug (5-ALA-HCl/SFC) was provided by KIYAN PHARMA Co., Ltd. It was administered orally twice daily for 16 weeks. The study was conducted under double-blind conditions until the database of the previous study was finalized and unlocked. The target enrollment was 30 participants (10 per group). This calculation was based on the assumption that approximately 550 patients with AOSD would receive outpatient care at the 11 major institutions and their associated facilities that were expected to participate in the trial. According to a national survey of patients with AOSD, 11.6% were deemed by their physicians to have residual disease activity at the final assessment (*14*). Similarly, when the trial was planned, approximately 20% of patients with AOSD at Nagasaki University Hospital were considered to have residual disease activity. In accordance with these figures, it was estimated that around 80 patients (approximately 15% of the total) across the 11 institutions (including affiliated sites) would meet this criterion. In a previous clinical trial (UMIN000028010: randomized, double-blind, parallel-group comparison of tocilizumab for colchicine-resistant familial Mediterranean fever), approximately 40% of the screened patients were successfully enrolled. Based on this experience, it was projected that 30 participants would participate in the present investigator-initiated trial. However, because the study was terminated early, only four patients were enrolled, and their data are presented here as pilot data. Participants who achieved adapted ACR 30 at follow-up visits were eligible for GCs tapering at the physician's discretion. The GCs' tapering regimen was performed in accordance with a predetermined protocol. If an increase or re-increase in oral GCs was considered necessary, the study drug was discontinued. The study drug was also discontinued if the investigator or sub-investigator determined that an adverse event was causally related to the study drug and was serious, medically significant, or unacceptable. This period was limited to a maximum of two consecutive weeks (*i.e.*, 14 days). If no improvement was observed during this period, the study drug was discontinued. Even if the study drug was withdrawn, evaluation and observation were continued as part of the trial.

During the study period, the initiation of the following treatments was prohibited: administration of immunosuppressants, biologics, or Janus kinase inhibitors; intra-articular GC injections at joints; and suppositories.

Participants were discontinued prematurely if they met any of the following criteria: if they asked to leave the trial, if it was determined after registration that they were ineligible for the trial, if an investigator or sub-investigator determined that continuing the trial was difficult due to complications worsening or adverse events, if pregnancy was confirmed, if the entire clinical trial was discontinued, if any other serious violations of the clinical trial protocol were identified, or if the investigator or sub-investigator determined that termination was necessary.

2.4. Study endpoints

The primary endpoint was the achievement of adapted ACR30 (*2,15*) at week 16 following the initiation of 5-ALA-HCl/SFC administration. For participants in the active drug group in the previous study, 5-ALA-HCl/SFC administration was defined as the start date of the previous study. For subjects in the placebo group in the previous study, it was defined as the start date of the current study. Adapted ACR 30 is a composite measure of the disease activity. It was defined as meeting the following criteria: improvement of ≥ 30% in three or more of the following five items 1) to 5) from baseline, with no fever exceeding 38°C in the past week, and no worsening of more than 30% in any of the following five items. 1) Physician-assessed global assessment of disease activity (VAS); 2) Patient-assessed disease activity (VAS); 3) Functional status assessed using the Health Assessment Questionnaire Disability Index (HAQ-DI); 4) Number of active joints (swollen joints and tender joints); 5) Laboratory values of ESR (mm/hr) or CRP (mg/dL).

The secondary endpoints included the following: Adapted ACR 30 at weeks 4, 8, 12, 20, and 24; Adapted ACR 50/ 70/ 90/ 100 at weeks 4, 8, 12, 16, 20, and 24; GCs dose reduction at weeks 4, 8, 12, 16, 20,

and 24; changes in systemic feature scores (SFS) at weeks 4,8, 12, 16, 20,and 24; changes in serum ferritin levels at weeks 8, 16,and 24; and changes in EuroQol 5-dimensions 5-levels (EQ-5D-5L) at weeks 4, 8, 12, 16, 20, and 24. Adverse events were also collected as safety data. For adapted ACR 50/ 70/ 90/ 100, it is defined as meeting the following criteria: three or more of the five items listed in 1) to 5) above have improved by 50%, 70%, 90%, or 100%, there has been no fever exceeding 38°C in the past week, and no more than one item has worsened by more than 30% of the five items listed in 1) to 5) above. The SFS scoring system consists of five clinical and five laboratory assessments and was designed to evaluate systemic disease features (*16*). It has also been used previously as a secondary endpoint in a phase III trial investigating the efficacy of tocilizumab in Japanese patients with AOSD (*17*). Assessments in weeks 20 and 24 were limited to participants who had received the active drug in the prior study.

2.5. Statistical analysis

Although the study initially aimed to enroll 30 participants, it was terminated prematurely, and data from only four participants were available for analysis and were reported as pilot observations. Owing to early discontinuation and the limited sample size, no formal inferential statistical analyses were performed. Instead, descriptive statistics were provided for each patient. Categorical variables are summarized as counts and percentages based on the number of participants analyzed, whereas continuous variables are presented as medians with corresponding minimum and maximum values. All analyses were performed using SAS software version 9.4 (SAS Institute Inc., Cary, NC, USA).

3. Results

3.1. Patient flow and characteristics

The trial was conducted from July 28, 2022, to April 30, 2024. Owing to the impact of the COVID-19 pandemic, the recruitment of clinical trial participants did not proceed as planned. Owing to delays in participant enrollment and funding issues, the trial investigator decided to terminate the trial early. Four participants who completed the previous study were enrolled. Figure 1 shows a flowchart of the study. The details are as follows: one participant who was in the placebo group in the previous study was enrolled in the low-dose group, resulting in one participant in the high-dose group and three participants in the low-dose group. Among the three participants in the low-dose group, two discontinued the study drug during the trial period: one due to a worsening of the underlying disease on day 37, and one due to an adverse event and discontinuation of the study drug for more than 14 days on day 71. However, they completed the remaining observation period of the trial after switching to a different treatment.

Table 1 presents the results of the baseline

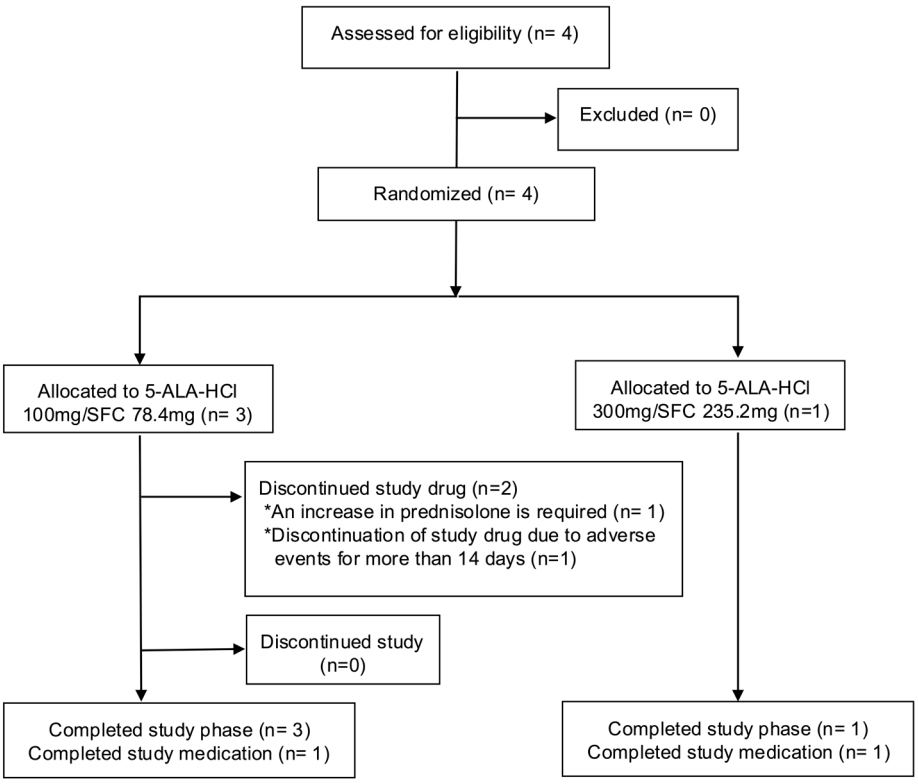

Figure 1. Flowchart of the study.

characteristics of the participants. The median age of the participants was 59.5 years. Two of the four participants were female. The median disease duration was 28.3 months. Of the four participants, three had a history of treatment with drugs other than prednisolone, and one participant (in the low-dose group) had no history of treatment with drugs other than prednisolone. The median dose of concomitant prednisolone was 14 mg/day. The median CRP, ESR, and ferritin levels were 3.23 mg/dL, 37.5 mm/h, and 1819 ng/mL, respectively. The median systemic feature score was 3, and the median EQ-5D-5L score was 0.72.

3.2. Primary endpoint

The primary endpoint, the adapted ACR 30 at week 16 after administration of the study drug, was met by all participants (four participants: one in the high-dose group and three in the low-dose group). However, in two participants in the low-dose group (cases 2 and 4), the study drug was discontinued by week 16 (day 71 and day 37), and week 16 was evaluated under another treatment.

3.3. Secondary endpoints

Table 2 lists the secondary endpoints and the CRP and ESR levels for each case.

3.3.1. Adapted ACR 30 at weeks 4, 8, 12, 20, and 24

The participant in the high-dose group (Case 1) achieved adapted ACR 30 at all time points. One participant in the low-dose group (Case 2) also achieved adapted ACR 30 at all time points; however, the study drug was discontinued on day 71 of this study. Another participant in the low-dose group (Case 3) achieved adapted ACR 30 at week 4 but did not achieve it at weeks 8, 12, 20, or 24. One participant who was in the placebo group in the prior study and enrolled in the low-dose group in this study (Case 4) achieved adapted ACR30 at week 12 only (the study drug was discontinued on day 37 of this study).

3.3.2. Adapted ACR 50/ 70/ 90/ 100 at weeks 4, 8, 12, 16, 20, and 24

One participant in the high-dose group (Case 1) achieved adapted ACR 70 at week 4, adapted ACR 90 at weeks 8, 12, 16, and 24, and adapted ACR 100 at week 20. In the low-dose group, Case 2 achieved adapted ACR 70 at weeks 4, 8, 20, and 24 but did not achieve adapted ACR 50 at week 12 and achieved adapted ACR 50 at week 16 (the study drug was discontinued on day 71). Case 3 achieved adapted ACR 50 at week 4 but did not achieve adapted ACR 50 at any time point after week 8. Case 4 achieved adapted ACR 50 at week 12 but did not achieve adapted ACR 50 at weeks 4, 8, or 16 (the study drug was discontinued on Day 37).

3.3.3. GCs dose reduction

One participant in the high-dose group (Case 1) received a prednisolone dose of 10 mg per day at all time points from baseline to the final observation date. In the low-dose group, Case 2 (baseline dose: 30 mg/day) experienced the changes at weeks 4, 8, 12, 16, 20 and

Table 1. Baseline characteristics of patients with adult onset still's disease treated with study drug (*n* = 4)

Characteristics	Median (min-max) or n (%)	Case 1	Case 2	Case 3	Case 4
Study drug		5-ALA-HCl 300 mg/day + SFC 235.2 mg/day	5-ALA-HCl 100 mg/day + SFC 78.4 mg/day	5-ALA-HCl 100 mg/day + SFC 78.4 mg/day	5-ALA-HCl 100 mg/day + SFC 78.4 mg/day
Age	59.5 (19-77)	77	65	54	19
Sex, female, n (%)	2 (50%)	Female	Male	Male	Female
Body weight, kg	63.4 (44.4-91.4)	44.4	61.8	65	91.4
Disease duration, months	28.3 (7.8-145.2)	48.4	145.2	7.8	8.2
Previous treatment other than prednisolone, n (%)	3 (75%)	Yes	Yes	Yes	No
Tocilizumab, n (%)	1 (25%)		Yes		
Methotrexate, n (%)	1 (25%)		Yes		
Cyclosporine A, n (%)	2 (50%)		Yes	Yes	
Methylprednisolone plus therapy, n (%)	2 (50%)	Yes	Yes		
Dose of concomitant prednisolone, mg	14 (10-30)	10	30	13	15
CRP, mg/dL	3.23 (0.07-7.4)	7.4	2.76	3.69	0.07
ESR, mm/hr	37.5 (9-101)	101	41	34	9
Serum ferritin, ng/mL	1819 (110-4610)	4610	3360	278	110
Systemic feature score	3 (1-5)	5	3	3	1
EQ-5D-5L (score)	0.72 (0.04-0.78)	0.04	0.78	0.68	0.76
EQ-5D-5L (VAS)	62.5 (20-75)	20	50	75	75

CRP: C-reactive protein; EQ-5D-5L: EuroQol 5-dimensions 5-levels; ESR: erythrocyte sedimentation rate; SFC: sodium ferrous citrate; VAS: visual analog scale; 5-ALA: 5-aminolevulinic acid.

Table 2. Primary, secondary endpoints, CRP, and ESR levels

Endpoints	Case 1	Case 2	Case 3	Case 4*
Study drug	5-ALA-HCl 300 mg/day + SFC 235.2 mg/day	5-ALA-HCl 100 mg/day + SFC 78.4 mg/day	5-ALA-HCl 100 mg/day + SFC 78.4 mg/day	5-ALA-HCl 100 mg/day + SFC 78.4 mg/day
At the time of discontinuation of study drug	-	Day 71	-	Day 37
Achieved Adapted ACR values				
Week 4 (Day 29)	70	70	50	Not achieved
Week 8 (Day 57)	90	70	Not achieved	Not achieved
Week 12 (Day 85)	90	30	Not achieved	50
Week 16 (Day 113)	90	50	30	30
Week 20 (Day 141)	100	70	Not achieved	-
Week 24 (Day 169)	90	70	Not achieved	-
Systemic feature score				
Baseline (Day 1)	5	3	3	1
Week 4 (Day 29)	4	3	4	3
Week 8 (Day 57)	2	2	4	2
Week 12 (Day 85)	2	2	3	1
Week 16 (Day 113)	2	2	4	1
Week 20 (Day 141)	2	2	4	-
Week 24 (Day 169)	2	2	4	-
Serum ferritin (ng/mL)				
Baseline (Day 1)	4610	3360	278	110
Week 8 (Day 57)	431	386	431	7863
Week 16 (Day 113)	98	105	431	239
Week 24 (Day 169)	267	188	562	-
EQ-5D-5L scores				
Baseline (Day 1)	0.04	0.78	0.68	0.76
Week 4 (Day 29)	0.89	0.94	0.89	0.71
Week 8 (Day 57)	0.94	0.94	0.76	0.8
Week 12 (Day 85)	0.94	0.94	0.84	0.94
Week 16 (Day 113)	0.94	0.94	0.84	0.88
Week 20 (Day 141)	0.94	0.89	0.84	-
Week 24 (Day 169)	0.82	0.94	0.76	-
EQ-5D-5L (VAS)				
Baseline (Day 1)	20	50	75	75
Week 4 (Day 29)	95	90	90	40
Week 8 (Day 57)	99	90	50	80
Week 12 (Day 85)	99	60	90	85
Week 16 (Day 113)	100	50	70	85
Week 20 (Day 141)	100	60	60	-
Week 24 (Day 169)	80	90	40	-
CRP (mg/dL)				
Baseline (Day 1)	7.4	2.76	3.69	0.07
Week 4 (Day 29)	3.45	0.39	3.88	0.93
Week 8 (Day 57)	1.04	0.31	8.92	0.56
Week 12 (Day 85)	0.27	0.75	1.63	0.009
Week 16 (Day 113)	0.73	1.05	4.67	0.02
Week 20 (Day 141)	0.52	0.009	8.16	-
Week 24 (Day 169)	1.41	0.59	6.55	-
ESR (mm/hr)				
Baseline (Day 1)	101	41	34	9
Week 4 (Day 29)	79	42	31	21
Week 8 (Day 57)	55	47	77	8
Week 12 (Day 85)	41	22	65	2
Week 16 (Day 113)	36	18	69	1
Week 20 (Day 141)	35	12	92	-
Week 24 (Day 169)	77	40	75	-
Prednisolone dose (mg/day)				
Baseline (Day 1)	10	30	13	15
Week 4 (Day 29)	10	25	13	12.5
Week 8 (Day 57)	10	17.5	13	60
Week 12 (Day 85)	10	20	13	50
Week 16 (Day 113)	10	20	13	30
Week 20 (Day 141)	10	30	13	-
Week 24 (Day 169)	10	20	13	-

ACR: American College of Rheumatology; CRP: C-reactive protein; EQ-5D-5L: EuroQol 5-dimensions 5-levels; ESR: erythrocyte sedimentation rate; SFC: sodium ferrous citrate; VAS: visual analog scale; 5-ALA: 5-aminolevulinic acid. *Case 4 is the placebo group of the prior study and only has data up to 16 weeks. All other cases have results up to 24 weeks, using the induction of study drug in the prior study as baseline. The study drug was discontinued for Cases 2 and 4 during the trial, after which the patients were transferred to standard treatment.

24: -5, -12.5, -10, -10, 0 and -10 mg/day. However, the study drug was discontinued on Day 71. Case 3 received a prednisolone dose of 13 mg/day at all time points. Case 4 (baseline dose: 15 mg/day) experienced the changes at weeks 4, 8, 12 and 16: -2.5, +45, +35 and +15 mg/day. However, the study drug was discontinued on Day 37.

3.3.4. Changes in systemic feature scores, serum ferritin, and EQ-5D-5L

Table 2 shows the absolute SFS, absolute serum ferritin levels, absolute EQ-5D-5L index scores and absolute EQ-5D-5L VAS scores for each case at baseline and subsequent visits.

Case 1 (the high dose group) showed SFS changes of -1, -3, -3, -3, -3, -3 at weeks 4, 8, 12, 16, 20, and 24. In the low-dose group, one participant (Case 2) showed SFS changes of 0, -1, -1, -1, -1, -1 at weeks 4, 8, 12, 16, 20, and 24. In another participant (Case 3), the SFS change at weeks 4, 8, 12, 16, 20, and 24 were +1, +1, 0, +1, +1, +1. Case 4 had SFS changes of +2, +1, 0, and 0 at weeks 4, 8, 12, and 16.

We also observed changes in serum ferritin levels. The changes in serum ferritin levels at weeks 8, 16, and 24 in the high-dose group (Case 1) were -4,179, -4,512, and -4,343 ng/mL, respectively. In the low-dose group, Case 2 showed changes in ferritin levels at weeks 8, 16, and 24 of -2,974, -3,255, and -3,172 ng/mL, respectively (the study drug was discontinued on Day 71). In another participant (Case 3) in the low-dose group, the changes at weeks 8, 16, and 24 were +153, +153, and +284 ng/mL, respectively. Case 4, the changes in serum ferritin levels at weeks 8 and 16 were +7,753 and +129 ng/mL, respectively. The study drug was discontinued on Day 37. In the high-dose group, serum ferritin levels improved by week 8, and continued to improve thereafter.

The changes in the EQ-5D-5L scores at weeks 4, 8, 12, 16, 20, and 24 in the high-dose group (Case 1) were +0.85, +0.90, +0.90, +0.90, +0.90, and +0.78, respectively. Case 2 were +0.16, +0.16, +0.16, +0.16, +0.11, and +0.16. Case 3 were +0.21, +0.08, +0.16, +0.16, +0.16, and +0.08, respectively. Case 4, the changes in scores at weeks 4, 8, 12, and 16 were -0.05, +0.04, +0.18, and +0.12, respectively.

In the EQ-5D-5L VAS (where 100 represents the best possible state and 0 represents the worst possible state), the changes in the EQ-5D-5L VAS from baseline to each time point at weeks 4, 8, 12, 16, 20, and 24 in the high-dose group (Case 1) were +75, +79, +79, +80, +80, and +60, respectively. In the low-dose group, one participant (Case 2) showed the EQ-5D-5L VAS changes of +40, +40, +10, 0, +10, and +40, respectively. Another participant (Case 3) showed EQ-5D-5L VAS changes of +15, -25, +15, -5, -15, and -35, respectively. For a fourth participant (Case 4), the EQ-5D-5L VAS changed by -35, +5, +10, and +10 at weeks 4, 8, 12, and 16, respectively.

3.4. Safety

Adverse events (AEs) were observed in three of four participants (one in the high-dose group and two in the low-dose group), with a total of 11 events (four in the high-dose group and seven in the low-dose group). Table 3 lists the AEs. In the low-dose group, one participant (Case 3) experienced no AE during the 24-week period, including the 8-week period of the prior study. All AEs reported in this clinical study were determined to have no causal relationship with the study drug. One case of a serious AE (compression fracture) and one case of an AE leading to discontinuation of the study drug (drug eruption) were each reported in the same participant (Case 2), but both AEs were determined to have no causal relationship with the study drug. However, because the drug eruption was initially suspected to be a side effect of the study drug, administration of the study drug was suspended. As the suspension period exceeded 14 days, administration of the study drug was discontinued on Day 71. No deaths, AEs leading to death, or AEs leading to trial discontinuation were observed.

Table 3. Adverse events

Adverse event (preferred term)	n (%)	Study drug discontinuation	Association with study drug	Serious adverse event
High-dose group (*n* = 1)				
Conjunctival haemorrhage	1 (25%)	No	No	No
Hordeolum	1 (25%)	No	No	No
Influenza	1 (25%)	No	No	No
Purpura senile	1 (25%)	No	No	No
Low-dose group (*n* = 3)				
Conjunctivitis	1 (25%)	No	No	No
Cytomegalovirus infection	1 (25%)	No	No	No
Drug eruption	1 (25%)	Yes	No	No
Oral candidiasis	1 (25%)	No	No	No
Skin erosion	1 (25%)	No	No	No
Compression fracture	1 (25%)	No	No	Yes
White blood cell count decreased	1 (25%)	No	No	No

The data are *n*, %. The terminology is based on the Medical Dictionary for Regulatory Activities version 25.0.

4. Discussion

This study represents the first investigator-initiated Phase II clinical trial in the world to evaluate the efficacy and safety of 5-ALA-HCl/SFC in patients with GC-refractory, disease-active AOSD. Although enrollment was originally planned for 30 patients, recruitment did not progress as expected, and the trial was terminated early after the enrollment of four participants. Therefore, the results of this study should be regarded as pilot data, and definitive conclusions regarding the efficacy and safety of 5-ALA-HCl/SFC in AOSD cannot be drawn. Nevertheless, we believe that the findings provide useful preliminary information that may contribute to the design of future clinical studies.

Regarding efficacy, one participant (Case 1) in the high-dose group demonstrated improvements across multiple endpoints, including adapted ACR achievements, SFS scores, EQ-5D-5L scores, and serum ferritin levels. Among the three participants in the low-dose group, two (Case 2 and Case 4) discontinued study drug administration during the trial and subsequently switched to alternative treatments after week 12 and week 8, respectively. Case 3 continued the study drug through week 24, allowing a straightforward evaluation; however, no apparent improvement was observed in any efficacy indicators. These included composite measures (adapted ACR achievements, SFS scores), laboratory markers (ferritin, CRP, ESR), and patient-reported outcomes (EQ-5D-5L). On the other hand, Case 2 showed improvements in adapted ACR, SFS scores, ferritin, CRP, ESR, and EQ-5D-5L from baseline through week 8 while on the study drug, along with a reduction in prednisolone dose. Although the sample size is extremely small and no firm conclusions can be reached, these observations suggest that 5-ALA-HCl — particularly at a dose of 300 mg (with SFC 235.2 mg) per day — may have therapeutic potential in AOSD.

Elevated HO-1 levels have been reported in AOSD, and a correlation with ferritin levels has been established (*3,4*). HO-1 is a stress-responsive enzyme and a powerful anti-inflammatory and immune regulatory molecule (*18*). It is known to suppress inflammatory cytokines (TNF-α, IL-1β, IL-6, IL-18, *etc.*) and induce anti-inflammatory cytokines such as IL-10 through the production of heme metabolites (CO, bilirubin) (*19*). It has been suggested that induction of HO-1 may mitigate cytokine storms and immune hyperactivity in AOSD. We focused on this point and considered that induction of HO-1 expression through 5-ALA/SFC administration could serve as a therapeutic target for AOSD. In preclinical studies, 5-ALA showed preventive and therapeutic effects in collagen-induced arthritis in DBA/1 mice. In addition, no significant effect on adaptive immune cells was observed, and 5-ALA mainly acted on macrophages and dendritic cells, which was reflected in a significant decrease in serum chemokines IP-10 and MIP-1β (*20*). 5-ALA/SFC suppressed systemic inflammation in a mouse model of AOSD, a systemic disease, and its severe form, macrophage activation syndrome, using C57BL/6N mice repeatedly administered CpG phosphorothioate oligodeoxynucleotides (*20*). Additionally, in patients with AOSD inadequate response to existing treatments (excluding severe cases), supplementation with 5-ALA enabled reduction of prednisolone dosage (*20,21*).

Regarding the treatment of AOSD, aside from GCs, biological agents targeting elevated cytokines such as IL-6 and IL-1β have been the mainstay. However, these agents have issues such as immunosuppression-related infections, the need for intravenous or subcutaneous injections, and high costs. In contrast, 5-ALA-HCl/SFC offers the advantages of being an oral treatment with a simple administration regimen and having fewer concerns regarding immunosuppression compared to GCs or biological agents.

The limitations of this study are as follows: Firstly, the sample size was limited to just four cases. While the primary endpoint was achieved by all participants, this may have been influenced by the small number of cases enrolled. The effect of concomitant GCs should also be considered. However, the participant in the high-dose group received a lower dose of concomitant GCs than the other three participants. Given the small cohort size and the inherent variability in AOSD, these findings should be interpreted with caution. Furthermore, participant background factors were heterogeneous, including age, weight, disease duration, prior medications, comorbidities and laboratory test results. The uneven distribution of cases between the treatment groups (one case in the high-dose group and three cases in the low-dose group) also made it difficult to interpret trends in efficacy, particularly with regard to potential dose-response relationships. Therefore, the results should be considered descriptive and exploratory, and no definitive conclusions can be drawn about the relative efficacy of different doses. Secondly, there is the issue of the validity of the assessment criteria. As there are no established clinical assessment tools for AOSD, the validity of this endpoint is uncertain. Nevertheless, the efficacy evaluation revealed similar trends in adjusted ACR, CRP, ESR and SFS values within the same participants. Furthermore, while 5-ALA-HCl/SFC is thought to exert anti-inflammatory effects by inducing HO-1, this study was unable to measure HO-1 in serum or peripheral blood mononuclear cells due to cost considerations. HO-1 should be included as a key biomarker in future studies. Thirdly, the observation period was limited to 24 weeks. A single serious adverse event, a compression fracture, was deemed to be unrelated to the study drug, and tolerability at 24 weeks was good. Nevertheless, two participants discontinued the study drug during the trial, which makes a longer-term evaluation of efficacy and safety desirable.

Despite early termination, a very small sample

size (n = 4), and a 16-week treatment period with assessments through Week 24, all participants met the primary endpoint (adapted ACR30 at Week 16); the high-dose participant demonstrated the most consistent improvements across secondary outcomes, and no treatment-related safety concerns were identified. These hypothesis-generating findings offer preliminary evidence that 5-ALA-HCl/SFC may provide clinical benefit in refractory AOSD. Larger, adequately powered randomized trials are warranted to confirm efficacy, clarify dose–response relationships, and further characterize safety.

5. Conclusion

This study provides preliminary efficacy signals (all participants achieved ACR30, with more significant improvements in the high-dose group) and safety evidence (no treatment-related adverse events) for 5-ALA-HCl/SFC in the treatment of GC-refractory AOSD. However, due to limitations such as small sample size and uneven group distribution, the efficacy and safety profiles of 5-ALA-HCl/SFC cannot be established. In the future, large-sample, randomized controlled trials are needed to verify the dose-response relationship and long-term efficacy, while incorporating HO-1 detection to improve mechanistic validation.

Acknowledgements

We thank all the patients who participated in this study and their families. We thank Masaru Kato (Hokkaido University Hospital), Hiroto Tsuboi (University of Tsukuba Hospital), Tomoya Miyamura (National Hospital Organization Kyushu Medical Center), Masahiro Yamamura (Okayama Saiseikai Outpatient Center Hospital), Yuko Kaneko (Keio University Hospital), Takeshi Kondo (Nagoya University Hospital), Yohei Kirino (Yokohama City University Hospital), Shintaro Hirata (Hiroshima University Hospital), all of whom are investigators of joint research institutions. We also thank the clinicians, investigators, technicians, and clinical research coordinators who collaborated on this study.

Funding: This study was funded by the Japan Agency for Medical Research and Development (Grant no. JP23ek0109563 to AK). Partial financial support was provided by KIYAN PHARMA Co., Ltd.

Conflict of Interest: The study drug (5-ALA-HCl/SFC) was provided by KIYAN PHARMA Co., Ltd. MH received research grants and/or speaker fee from Asahi Kasei, Astellas, AstraZeneca, Ayumi Pharma, Brystol Meyers, Chugai, Eisai, Eli Lilly, Gilead Sciences Japan, Janssen pharma, Ono Pharma, Taisho Pharma, Tanabe Mitsubishi, UCB Japan. AK has Speaker fees from AbbVie, Actelion, Asahi Kasei, Astellas, AstraZeneca, AYUMI, Boehringer Ingelheim, Bristol, Canon, Celltrion, Chugai, Daiichi Sankyo, Eisai, Eli Lilly, Fushimi, Gilead, GSK, Janssen, Kissei, Mitsubishi Tanabe, KIYAN PHARMA, Nihon Servier, Novartis, ONO, Otsuka, Pfizer, Sanofi, Sumitomo, Taisho, Takeda, and UCB; and grants and research support from AbbVie, Actelion, Asahi Kasei, Astellas, AYUMI, Boehringer Ingelheim, Bristol-Myers Squibb, Celltrion, Chugai, Daiichi Sankyo, Eisai, Eli Lilly, Gilead, Mitsubishi Tanabe, KIYAN PHARMA, Novartis, ONO, Pfizer, Sanofi, Taisho, Takeda, Teijin, and UCB. The other authors have no conflicts of interest to declare.

References

1. Kadavath S, Efthimiou P. Adult-onset Still's disease-pathogenesis, clinical manifestations, and new treatment options. Ann Med. 2015; 47:6-14.
2. Bindoli S, De Matteis A, Mitrovic S, Fautrel B, Carmona L, De Benedetti F. Efficacy and safety of therapies for Still's disease and macrophage activation syndrome (MAS): a systematic review informing the EULAR/PReS guidelines for the management of Still's disease. Ann Rheum Dis. 2024; 83:1731-1747.
3. Kirino Y, Takeno M, Iwasaki M, Ueda A, Ohno S, Shirai A, Kanamori H, Tanaka K, Ishigatsubo Y. Increased serum HO-1 in hemophagocytic syndrome and adult-onset Still's disease: use in the differential diagnosis of hyperferritinemia. Arthritis Res Ther. 2005; 7:R616-624.
4. Kirino Y, Kawaguchi Y, Tada Y, *et al*. Beneficial use of serum ferritin and heme oxygenase-1 as biomarkers in adult-onset Still's disease: A multicenter retrospective study. Mod Rheumatol. 2018; 28:858-864.
5. Nishio Y, Fujino M, Zhao M, Ishii T, Ishizuka M, Ito H, Takahashi K, Abe F, Nakajima M, Tanaka T, Taketani S, Nagahara Y, Li XK. 5-Aminolevulinic acid combined with ferrous iron enhances the expression of heme oxygenase-1. Int Immunopharmacol. 2014; 19:300-307.
6. Morse D, Choi AM. Heme oxygenase-1: the "emerging molecule" has arrived. Am J Respir Cell Mol Biol. 2002; 27:8-16.
7. Fujino M, Nishio Y, Ito H, Tanaka T, Li XK. 5-Aminolevulinic acid regulates the inflammatory response and alloimmune reaction. Int Immunopharmacol. 2016; 37:71-78.
8. Hou J, Cai S, Kitajima Y, Fujino M, Ito H, Takahashi K, Abe F, Tanaka T, Ding Q, Li XK. 5-Aminolevulinic acid combined with ferrous iron induces carbon monoxide generation in mouse kidneys and protects from renal ischemia-reperfusion injury. Am J Physiol Renal Physiol. 2013; 305:F1149-1157.
9. Terada Y, Inoue K, Matsumoto T, *et al.* 5-Aminolevulinic acid protects against cisplatin-induced nephrotoxicity without compromising the anticancer efficiency of cisplatin in rats *in vitro* and *in vivo*. PLoS One. 2013; 8:e80850.
10. Hou J, Zhang Q, Fujino M, Cai S, Ito H, Takahashi K, Abe F, Nakajima M, Tanaka T, Xu J, Zou H, Ding Q, Li XK. 5-Aminolevulinic acid with ferrous iron induces permanent cardiac allograft acceptance in mice *via* induction of regulatory cells. J Heart Lung Transplant. 2015; 34:254-263.

11. World Medical A. World Medical Association Declaration of Helsinki: ethical principles for medical research involving human subjects. JAMA. 2013; 310:2191-2194.
12. Sumiyoshi R, Koga T, Kamisawa O, *et al.* A Phase-II Investigator-Initiated Randomized, Double-Blind, Parallel-Group Clinical Trial of 5-Aminolevulinic Acid Hydrochloride/Sodium Ferrous Citrate (5-ALA-HCl/SFC) for Patients With Adult-Onset Still's Disease (AOSD) Refractory to Corticosteroids. Cureus. 2025; 17:e90354.
13. Hara T, Koda A, Nozawa N, Ota U, Kondo H, Nakagawa H, Kamiya A, Miyashita K, Itoh H, Nakajima M, Tanaka T. Combination of 5-aminolevulinic acid and ferrous ion reduces plasma glucose and hemoglobin A1c levels in Zucker diabetic fatty rats. FEBS Open Bio. 2016; 6:515-528.
14. Asanuma YF, Mimura T, Tsuboi H, Noma H, Miyoshi F, Yamamoto K, Sumida T. Nationwide epidemiological survey of 169 patients with adult Still's disease in Japan. Mod Rheumatol. 2015; 25:393-400.
15. Ruperto N, Brunner HI, Quartier P, *et al.* Two randomized trials of canakinumab in systemic juvenile idiopathic arthritis. N Engl J Med. 2012; 367:2396-2406.
16. Vojinovic J, Damjanov N, D'Urzo C, Furlan A, Susic G, Pasic S, Iagaru N, Stefan M, Dinarello CA. Safety and efficacy of an oral histone deacetylase inhibitor in systemic-onset juvenile idiopathic arthritis. Arthritis Rheum. 2011; 63:1452-1458.
17. Kaneko Y, Kameda H, Ikeda K, Ishii T, Murakami K, Takamatsu H, Tanaka Y, Abe T, Takeuchi T. Tocilizumab in patients with adult-onset still's disease refractory to glucocorticoid treatment: a randomised, double-blind, placebo-controlled phase III trial. Ann Rheum Dis. 2018; 77:1720-1729.
18. Campbell NK, Fitzgerald HK, Dunne A. Regulation of inflammation by the antioxidant haem oxygenase 1. Nat Rev Immunol. 2021; 21:411-425.
19. Ryter SW. Heme Oxgenase-1, a Cardinal Modulator of Regulated Cell Death and Inflammation. Cells. 2021; 10:515.
20. Koga T, Sumiyoshi R, Tsuji Y, Kodama K, Endo Y, Furukawa K, Kawakami A. Efficacy and safety of 5-aminolevulinic acid in adult-onset Still's disease: A preclinical study in mice and a pilot study in humans. Clin Immunol. 2023; 257:109846.
21. Sumiyoshi R, Koga T, Shimizu T, Sato S, Tashiro S, Hosogaya N, Yamamoto H, Kawakami A. Single-arm, open-label pilot intervention study to investigate an effect of oral 5-aminolevulinic acid plus sodium ferrous citrate on glucocorticoid reduction in patients with adult-onset Still disease: Study protocol for clinical trial (SPIRIT compliant). Medicine (Baltimore). 2020; 99:e22708.

Received September 30, 2025; Revised November 20, 2025; Accepted November 25, 2025.

**Address correspondence to:*
Tomohiro Koga, Department of Immunology and Rheumatology, Nagasaki University Graduate School of Biomedical Sciences, 1-7-1 Sakamoto, Nagasaki 852-8501, Japan.
E-mail: tkoga@nagasaki-u.ac.jp

Released online in J-STAGE as advance publication December 11, 2025.

Original Article

DOI: 10.5582/ddt.2025.01105

Comparative study of contrast-enhanced ultrasound and contrast-enhanced computed tomography in the diagnosis of benign and malignant lesions of the gallbladder

Liang Fang[1,§], Zhiying Qiu[1,§], Lingwen Xu[1], Fei Hu[2], Yuchen Tao[1], Shengnan Ding[1], Jing Zhou[3], Ling Wang[4,*], Lin Chen[1,*]

[1] Department of Ultrasonic Diagnosis, Huadong Hospital Affiliated to Fudan University, Shanghai, China;
[2] Department of radiology, Huadong Hospital Affiliated to Fudan University, Shanghai, China;
[3] Department of Obstetrics and Gynecology, Nanfang Hospital, Southern Medical University, Guangzhou, Guangdong, China;
[4] Department of Obstetrics, The First Affiliated Hospital, Guizhou University of Traditional Chinese Medicine, Guiyang, China.

SUMMARY: This study compared the diagnostic value of contrast-enhanced ultrasound (CEUS) and contrast-enhanced computed tomography (CECT) for differentiating benign and malignant gallbladder (GB) lesions. A retrospective analysis was performed on 151 hospitalized patients with GB lesions: 74 underwent CEUS alone, 25 CECT alone, and 52 both examinations preoperatively. Histopathology served as the reference standard. Imaging features of benign/malignant lesions were compared using *t*-test or chi-square (χ^2) test; CEUS quantitative parameters were analyzed *via t*-test. Diagnostic efficacy of the two modalities was compared by χ^2 test. Of 151 patients, 57 (37.7%) had malignant and 94 (62.3%) benign lesions. Statistically significant differences between benign and malignant groups were observed in CEUS/CECT features (vascular enhancement morphology, contrast distribution, GB wall integrity, ill-defined borders with adjacent liver) and CEUS washout time (WT) (all $P < 0.05$). In the entire cohort, no significant differences existed between CEUS and CECT in sensitivity (89.2% *vs.* 85.7%), specificity (78.8% *vs.* 74.3%), accuracy (84.9% *vs.* 80.5%), positive predictive value (PPV) (85.7% *vs.* 80.0%) and negative predictive value (NPV) (83.7% *vs.* 81.2%) (all $P > 0.05$). Similar non-significant differences were noted in the 52-patient subgroup (sensitivity: 65.0% *vs.* 80.0%; specificity: 62.5% *vs.* 80.0%; accuracy: 63.5% *vs.* 76.9%; PPV: 40.6% *vs.* 50.0%; NPV: 51.3% *vs.* 66.7%; all $P > 0.05$). CEUS is effective for differentiating benign and malignant GB lesions, with diagnostic efficacy comparable to CECT.

Keywords: contrast enhanced ultrasound (CEUS), gallbladder cancer (GBC), contrast enhanced CT (CECT)

1. Introduction

Gallbladder cancer (GBC) can originate from multiple sites such as the fundus, body, neck of the gallbladder (GB), or cystic duct, accounting for approximately 80% to 95% of biliary tract malignancies (*1,2*), making it the most common biliary tract malignancy. Due to its insidious onset and highly aggressive nature, most GBC patients are diagnosed at advanced stages, with a 5-year survival rate < 20% in most countries (*3-9*). Therefore, improving the diagnoses and early detection rate of GBC is crucial for the treatment of GBC and has significant implications for enhancing the survival rate of GBC patients.

Contrast-enhanced computed tomography (CECT) enables hepatobiliary scanning during arterial or portal phase within a single breath-hold and allows thin-section (1 mm) scanning of the region of interest, significantly increasing the lesion detection rates. However, CECT has its limitations. Firstly, as a timed scanning technique, it cannot achieve prolonged continuous scanning, potentially missing lesion enhancement at specific time points. Secondly, restricted by planar imaging, it only provides transverse cross-section views. Thirdly, CECT is contraindicated for patients with allergy to the iodine contrast agent, renal insufficiency, or severe hyperthyroidism. Finally, CECT is costly and involves radiation exposure. Thus, exploring for an imaging diagnostic modality that complements CECT is particularly crucial for clinical practice.

Given the excellent contrast between bile within GB and the GB wall, intramural lesions, stones, and adjacent liver tissue, coupled with its superior spatial resolution compared to other tomographic methods, conventional

ultrasound (US) has become a common imaging method for detecting and diagnosing GB lesions (*10,11*). However, conventional US has limitations in visualizing GB wall integrity at the lesion and lesion vascularity (*12*).

Contrast-enhanced ultrasound (CEUS), a technically simple imaging modality utilizing microbubble contrast agents and contrast-specific US modes, has been introduced to overcome the limitations of B-mode and color Doppler US. CEUS has been increasingly used in abdominal diseases, with diagnostic efficacy comparable to CECT and contrast-enhanced magnetic resonance imaging (CEMRI) (*13,14*). Several studies have explored the role of CEUS in GB malignancies (*11,15-18*). However, comparative studies between CEUS and CECT for differentiating benign and malignant GB diseases remain scarce. The objective of this study was to investigate the sensitivity and specificity of CEUS and CECT in GBC by comparing pathological findings.

2. Methods

2.1. Patients

A retrospective analysis was conducted on 151 patients with GB diseases who were admitted to Huadong Hospital Affiliated to Fudan University and underwent surgical treatment between January 2020 and June 2025. All patients had confirmed pathological results. Before surgery, the patients underwent either CEUS, CECT, or both examinations: 126 patients underwent CEUS (CEUS group), which included 74 patients who underwent CEUS alone and 52 patients who underwent both CEUS and CECT; 77 patients underwent CECT (CECT group), which included 25 patients who underwent CECT alone and 52 patients who underwent both examinations. 126 patients (51males and 75 females; age range 29 to 90 years with an average of 64.6 ± 9.3 years; lesion diameter 11 to 136 mm with an average of 43.5 ± 27.4 mm) were examined by CEUS (CEUS group), 77 (32 males and 45 females; age range 37 to 81 years with an average of 63.2 ± 10.9 years; lesion diameter 14 to 58 mm with an average of 31.6 ± 17.2 mm) were examined by CECT (CECT group). In the two groups, 52 patients (21 male and 31 female; age range 32 to 87 years with an average of 63.1 ± 10.3 years; lesion diameter 11 to 42 mm with an average of 22.9 ± 6.8 mm) were examined by both CECT and CEUS (CECT and CEUS group) within one week.

This study was approved by the hospital ethics committee, and written informed consent forms were obtained from all patients and their families.

2.2. Inclusion and exclusion criteria

2.2.1. Inclusion criteria

The inclusion criteria were 1) definitive postoperative pathological diagnosis with complete clinical data, including CEUS and CECT; 2) signed informed consent forms; 3) normal communication and expression abilities.

2.2.2. Exclusion criteria

The exclusion criteria were 1) under 18 years old; 2) pregnant or lactating women; 3) severe hepatic or renal insufficiency; 4) recent acute myocardial infarction, cerebral infarction, and severe pulmonary hypertension; 5) allergy to contrast agents; 6) preoperative percutaneous transhepatic GB drainage; 7) postoperative pathological confirmation of GB sludge; 8) unclear CEUS images.

2.3. CEUS

2.3.1. Equipment and contrast agents

TOSHIBA Aplio 400, TOSHIBA Aplio 500, AcusonSequoia-31, and Mindray Resona 8 color Doppler ultrasound diagnostic systems were used, all equipped with abdominal convex array probes (1.0 to 5.0 MHz), high frequency probes (7.5 to 12.0 MHz), and real-time CEUS imaging software (mechanical index ≤ 0.1). The contrast agent used was sulfur hexafluoride microbubbles (SonoVue, Bracco, Italy).

2.3.2. Procedure

After fasting for 8 hours, patients were placed in a supine position or a left lateral decubitus position at angle of 45 - 90°. Conventional US was performed first. For patients with multiple lesions, the largest lesion visible on US was selected for examination. Location, size, extent, echogenicity, and color Doppler flow features of the lesion were recorded. The optimal view was selected and switched to dual-mode CEUS. The contrast agent (2.4 mL) was diluted with 5 mL of 0.9% normal saline, vigorously shaken, and injected as a bolus *via* the antecubital vein, followed by 5 mL saline flush. CEUS images were observed and recorded for 3 min after injection. A second injection was performed at least 20 min after the first injection if initial enhancement was missed or the target lesion was lost.

2.3.3. Image analysis

Two sonographers (> 10 years' CEUS experience) blind to each other's findings and the final diagnosis, independently analyzed the images, focusing on the following features: 1) enhancement phase: arterial phase (10-30 s post-injection) and venous phase(31-180 s); 2) enhancement level as compared with normal liver parenchyma or GB wall at the same depth: none, hypo-, iso-, or hyper-enhancement; 3) vascular

enhancement morphology: regular or irregular during the arterial phase; 4) enhancement pattern: homogeneous or heterogeneous enhancement within the lesion during the arterial phase. 5) GB wall integrity: continuous (all layers intact) or discontinuous (layer interruption). 6) border with adjacent liver tissue: well-defined or ill-defined. Quantitative parameters were observed *via* time-intensity curves (TICs), including arrival time (AT), arrival time of liver parenchyma (LAT), time to peak enhancement (TTP), rise time (RT), and washout time (WT).

2.4. CECT

2.4.1. Equipment and contrast agent

Siemens Drive and Force whole-body spiral CT machines and non-ionic iodine contrast agent (Omnipaque™ 300) were used.

2.4.2. Procedure

After fasting for 4-6 h, the patient underwent a non-contrast liver scan in a supine position. Contrast (1.5 mL/kg) was injected *via* antecubital vein at 3.5 to 4 mL/s using an automatic pressure injector. The scan was triggered using bolus-tracking technology (cursor at T12 level aorta and threshold at 100 HU). Arterial phase (full liver, breath-hold at 18 s), portal phase (breath-hold at 50 s), and delayed phase (after 100 s) were acquired.

2.4.3. Image analysis

Images were recorded and post-processed using a secondary workstation (Syngo MMWP version 2008C, Siemens Healthcare). Two other experienced radiologists, blind to the final diagnosis, recorded and analyzed changes in tumor morphology, vascularity, enhancement patterns in the arterial and venous phases (homogeneous/heterogeneous, hyper-enhancement/iso-enhancement/hypo-enhancement), local extension, fat planes with surrounding structures, and necrotic lymph nodes.

2.5. Statistical analysis

Statistical analysis was performed using Stata 11.0 software. Continuous variables were presented as mean ± SD, and categorical variables were presented as counts (n) and percentages (%). Histopathological findings served as the gold standard. For the entire cohort, the χ^2 test was used to compare the imaging features of benign and malignant lesions between CEUS and CECT, as well as the diagnostic indices (sensitivity, specificity, accuracy, positive predictive value (PPV), negative predictive value (NPV)) of the two modalities. For the paired subgroup (52 patients in the CEUS and CECT groups), the paired χ^2 test was used to compare the diagnostic efficacy of CEUS and CECT. The significance level was set at $\alpha = 0.05$, and $P < 0.05$ was considered statistically significant.

3. Results

3.1. Histopathological findings

All 151 patients underwent surgical resection with confirmed histopathological results (Table 1). In the CEUS group (n = 126), 74 (58.7%) were histopathologically diagnosed as malignant and 52 (41.3%) as benign. In the CECT group (n = 77), 40 (51.9%) were histopathologically diagnosed as malignant and 37 (48.1%) as benign. In the CEUS and CECT group (n = 52), 20 (38.5%) were histopathologically diagnosed as malignant (Figure 1) and 32 (61.5%) as benign (Figures 2 and 3). Among 17 adenomas according to WHO classification (*19*) in the CEUS and CECT group, 9 were papillary adenomas, including 6 with atypical hyperplasia and 4 with malignant transformation; 6 were tubular adenomas, including 4 with atypical hyperplasia and 2 with malignant transformation; 2 were tubulopapillary adenomas, both with atypical hyperplasia and 1 with malignant transformation. All 7 adenomas with malignant transformation were classified into the malignant adenocarcinoma group, and the remaining 10

Table 1. Histopathological findings of 151 GB lesions

Histopathological type	CECT	CEUS	BOTH
Malignant			
Adenocarcinoma	31 (40.3)	59 (46.8)	17 (32.7)
Squamous cell carcinoma	5 (6.5)	8 (6.3)	1 (1.9)
Adenosquamous carcinoma	3 (3.9)	5 (4.0)	1 (1.9)
Papillary carcinoma	1 (1.3)	2 (1.6)	1 (1.9)
ALL	40 (51.9)	74 (58.7)	20 (38.5)
Benign			
Xanthogranulomatous cholecystitis	7 (9.1)	10 (7.9)	6 (11.5)
Gallbladder adenomyomatosis	6 (7.8)	7 (5.6)	5 (9.6)
Chronic cholecystitis	7 (9.1)	5 (4.0)	4 (7.7)
Adenoma	10 (13.0)	17 (13.5)	10 (19.2)
Cholesterol polyp	7 (9.1)	13 (10.3)	7 (13.5)
ALL	37 (48.1)	52 (41.3)	32 (61.5)
Total	77 (100)	126 (100)	52 (100)

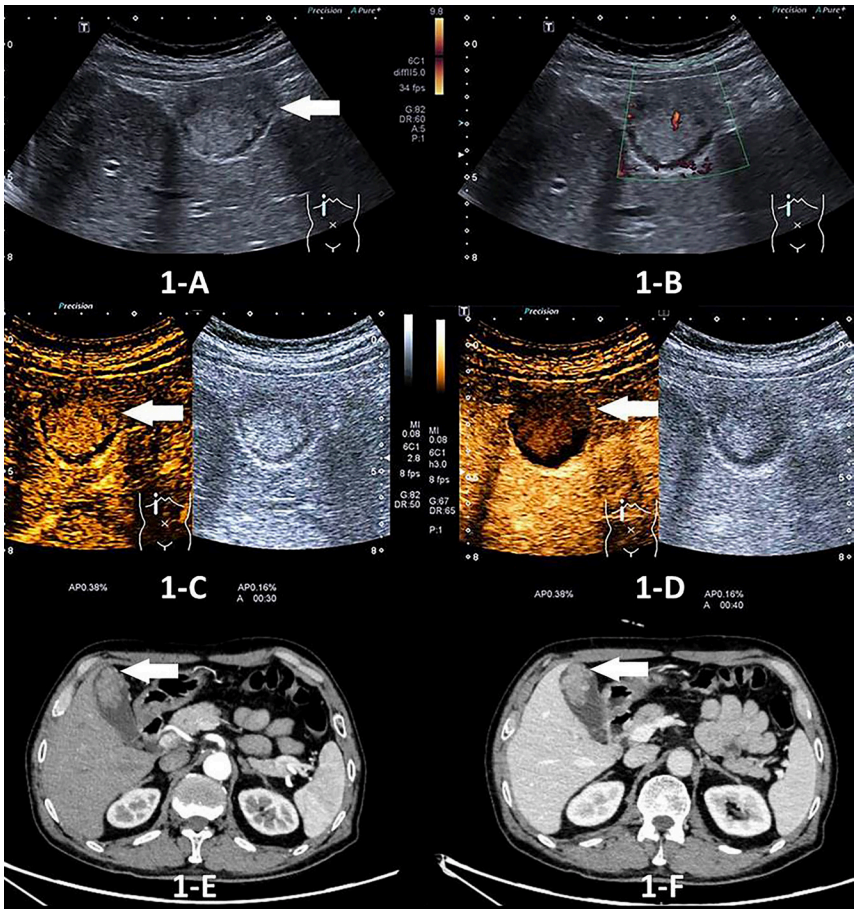

Figure 1. A 67-year-old man with a 26.3 × 16.6 mm GBC was diagnosed using CEUS and CECT. (A-B): A mildly hyperechoic lesion located in the fundus of GB (arrow) and power Doppler showed a few strip-like blood flow signals on conventional ultrasound. **(C-D)**: The tumor was of heterogenous hyper-enhancement in the arterial phase (arrow) and washout at 40 s in the late phase (arrow) on CEUS. **(E-F)**: The lesion was obviously enhanced in the arterial phase (arrow) and hypo-enhancement in the venous phase as compared to liver (arrow) on CECT.

into the benign adenoma group.

3.2. Comparison of US, CEUS and CECT imaging features in 52 cases of benign and malignant GB lesions

On US, color Doppler showed that intralesional vascularity was significantly associated with malignant lesions ($P = 0.012$). On CEUS, irregular tumoral enhancement ($P < 0.001$), heterogeneous internal enhancement ($P = 0.002$), GB wall destruction ($P < 0.001$), and ill-defined border with adjacent liver tissue ($P < 0.001$) were significantly associated with malignant lesions. On CECT, arterial hyper-enhancement ($P < 0.001$), heterogeneous internal enhancement ($P < 0.001$), GB wall destruction ($P < 0.001$), ill-defined border with adjacent liver tissue ($P < 0.001$), necrotic lymph nodes ($P < 0.001$), and distant metastases ($P < 0.001$) were significantly associated with malignant lesions. Comparison of CEUS and CECT imaging features between benign and malignant GB lesions is presented in Table 2.

3.3. Quantitative analysis of CEUS TICs for GB lesion assessment

No significant differences were observed between benign and malignant lesions in AT, LAT, RT, or TTP (Table 3). Malignant lesions exhibited significantly earlier washout than benign lesions (WT: 38.1 ± 13.7 seconds *vs.* 71.4 ± 26.9 seconds, $P < 0.001$). Receiver operating characteristic (ROC) curve analysis determined a WT cutoff value of 46.3 seconds for diagnosing malignant lesions, with a sensitivity of 88.2%, specificity of 84.5%, and area under the curve (AUC) of 0.900.

3.4. Comparison of diagnostic efficiency of CEUS and CECT for GBC

CEUS diagnosed 77 malignant lesions, with 66 accurate diagnoses and 11 misdiagnoses (3 chronic cholecystitis, 3 xanthogranulomatous cholecystitis, 5 adenomas). It diagnosed 49 benign lesions, with 41 accurate diagnoses and 8 misdiagnoses (5 adenocarcinomas, 2 squamous cell carcinomas, 1 adenosquamous carcinoma). CECT diagnosed 45 malignant lesions, with 36 accurate diagnoses and 9 misdiagnoses (3 cholesterol polyps, 1 xanthogranulomatous cholecystitis, 3 adenomas, 2 chronic cholecystitis).

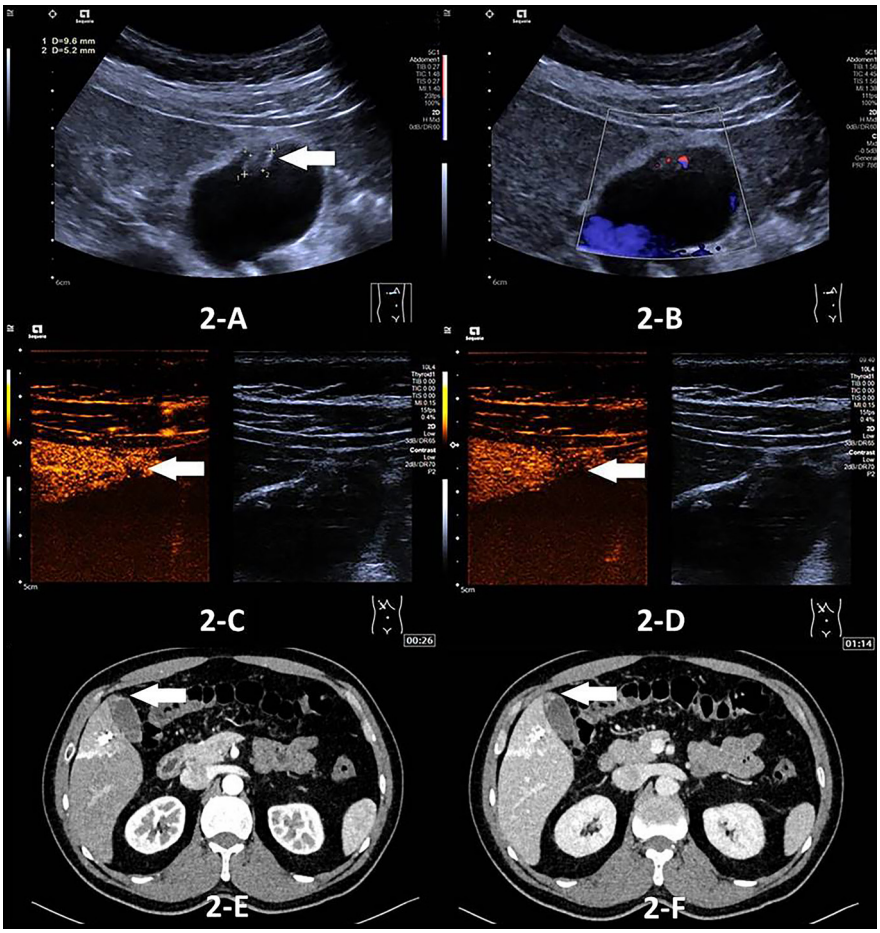

Figure 2. A 44-year-old man with a 9.6 × 5.2 mm xanthogranulomatous cholecystitis diagnosed using CEUS and CECT. (A-B): A mildly hyperechoic lesion fundus of GB (arrow) and Color Doppler blood flow imaging (CDFI) showed a few strip-like flow signals on conventional ultrasound. **(C-D)**: No obvious contrast agent filling was observed throughout, and a small amount of GB wall destruction was visible (arrows) on CEUS. **(E-F)**: The lesion showed homogenous iso-enhancement, similar to the liver (arrow) in the arterial phase and prolonged enhancement (arrow) in the venous phase on CECT.

It diagnosed 32 benign lesions, with 26 accurate diagnoses and 6 misdiagnoses (4 adenocarcinomas, 1 papillary carcinoma, 1 adenosquamous carcinoma). Based on the histopathological gold standard, the diagnostic efficacy of CEUS and CECT was further compared in both the entire cohort and the paired subgroup. The sensitivity (89.2% *vs.* 85.7%), specificity (78.8% *vs.* 74.3%), accuracy (84.9% *vs.* 80.5%), PPV (85.7% *vs.* 80.0%), and NPV (83.7% *vs.* 81.2%) between CEUS and CECT in diagnosing benign and malignant GB lesions were no statistically significant differences ($P > 0.05$ for all) (Table 4). In the paired subgroup of 52 patients of the CEUS and CECT group, CEUS demonstrated a sensitivity of 65.0% (13/20), specificity of 62.5% (20/32), accuracy of 63.5% (33/52), PPV of 40.6% (13/32), and NPV of 51.3% (20/39); whereas CECT showed a sensitivity of 80.0% (16/20), specificity of 80.0% (24/32), accuracy of 76.9% (40/52), PPV of 50.0% (16/32), and NPV of 66.7% (24/36). No statistically significant differences were detected between the two modalities in the paired subgroup (all $P > 0.05$).

4. Discussion

Gallbladder polypoid lesions are categorized into neoplastic and non-neoplastic categories. Neoplastic lesions include gallbladder cancer and gallbladder adenoma, while non-neoplastic lesions include cholesterol polyps, inflammatory polyps, and gallbladder adenomyomatosis. GBC is a malignant tumor that seriously threatens human health, with adenocarcinoma being the most common pathological type. Other types include squamous cell carcinoma, adenosquamous carcinoma, neuroendocrine carcinoma, clear cell carcinoma, and signet ring cell carcinoma (*20*). Early-stage GBC lacks obvious clinical symptoms, with a detection rate of only about 23% (*21*). Most GBC patients are diagnosed at advanced stages, losing surgical opportunities (*22*). In recent years, its incidence and mortality have risen significantly (*23,24*), making early diagnosis and treatment crucial. CEUS and CECT are primary methods for diagnosing gallbladder lesions.

CECT offers high clarity and spatial resolution, providing information on tumor location and size, liver

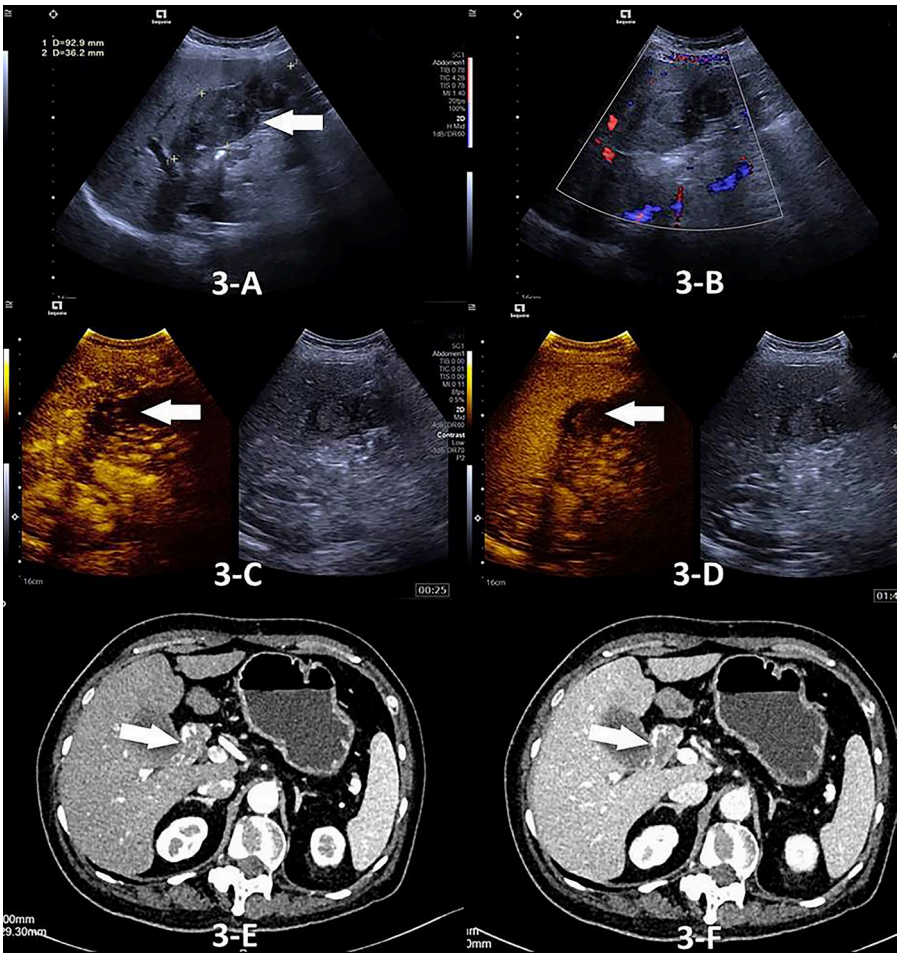

Figure 3. A 68-year-old woman with a 23.5 × 21.4 mm polypoid lesion of GB was diagnosed using CEUS and CECT. (A-B): The GB was filled with heterogeneous hypoechoic and a few stones while CDFI showed no blood flow signals. **(C-D)**: The lesion was heterogeneous hyper-enhancement simultaneously with the GB wall in the arterial phase (arrow) and hypo-enhancement in late phase (arrow) on CEUS. **(E-F)**: The lesion shows heterogeneous hyper-enhancement with calcification at the margin in the arterial phase (arrow) and hyper-enhancement in late phase (arrow).

Table 2. US, CEUS, and CECT features of 52 GB lesions

	Benign (n = 32)	Malignant (n = 20)	P value
Gender (F/M)	12/20	9/11	0.592
Age (years)[a]	53.6 ± 11.2 (32-82)	56.8 ± 15.9 (41-87)	0.614
US			
Size	23.9 ± 9.2 (23-41)	33.7 ± 11.8 (29-46)	0.061
Cholelithiasis	11 (34.4%)	7 (35.0%)	0.963
Echogenicity hyper/iso/hypo/mixed	12/8/6/6	2/5/5/8	0.135
Positive intralesional vascularity on color doppler	11 (34.4%)	14 (70.0%)	0.012*
CEUS			
Arterial phase enhancement hyper/iso (hypo)	25/7	16/4	0.872
Enhancement pattern in the arterial phase: regular and irregular	29/3	2/18	< 0.001*
the homogeneity of enhancement: homogenous/heterogeneous	25/7	7/13	0.002*
Enhancement in the venous phase: hyper (iso) / hypo	6/26	5/15	0.591
Disruption of GB wall	6 (18.8%)	19 (95.0%)	< 0.001*
Border with surrounding liver tissue: clear/unclear	28/4	6/14	< 0.001*
CECT			
Cholelithiasis	7 (21.9%)	5 (25.0%)	0.795
Hyper-enhancement in the arterial phase	9 (28.1%)	17 (85.0%)	< 0.001*
Heterogeneous enhancement in the arterial phase	5 (15.6%)	14 (70.0%)	< 0.001*
Disruption of GB wall	6 (18.9%)	18 (90.0%)	< 0.001*
Border with surrounding liver tissue: clear/unclear	4/28	14/6	< 0.001*
hypo-enhancement in the venous phase	7 (21.9%)	9 (45.0%)	0.079
Necrotic nodes	0	8 (40%)	< 0.001*
distant metastasis	0	4 (20%)	< 0.001*

Table 3. Quantitative time intensity curve analysis of CEUS examinations

Contrast enhancement phase	Benign (n = 32) / s	Malignant (n = 20) / s	P value
AT (s) [a]	17.6 ± 5.7 (6-26)	15.9 ± 5.1 (3-23)	0.595
LAT (s) [a]	20.9 ± 7.1 (8-39)	15.7 ± 5.2 (5-26)	0.123
RT(s) [a]	6.7 ± 1.9 (7-13)	5.3 ± 1.7 (4-11)	0.372
TTP(s) [a]	25.1 ± 6.3 (14-37)	21.1 ± 6.7 (9-31)	0.069
WT(s) [a]	71.4 ± 26.9 (43-139)	38.1 ± 13.7 (21-107)	< 0.001*

Table 4. Comparison of the accuracy between CEUS and CECT in the diagnosis of GBC

Methods	Sensitivity	Specificity	Accuracy	PPV	NPV
CECT	36/42 (85.7%)	26/35 (74.3%)	62/77 (80.5%)	36/45 (80.0%)	26/32 (81.2%)
CEUS	66/74 (89.2%)	41/52 (78.8%)	107/126 (84.9%)	66/77 (85.7%)	41/49 (83.7%)
P value	0.581	0.620	0.415	0.411	0.778

invasion, depth of liver invasion, metastasis, vascular invasion, and involvement of regional lymph nodes and distant organs. It quantifies lesion density by CT values to distinguish the components, *e.g.* fat, water, or calcification, aiding lesion characterization.

SonoVue, a second-generation ultrasound contrast agent, consists of sulfur hexafluoride microbubbles with a phospholipid shell that demonstrates favorable flexibility and stability. The microbubbles resonate at low acoustic pressure and persist long in blood. CEUS, through contrast imaging, overcomes limitations of conventional grayscale ultrasound and color Doppler ultrasound in imaging accuracy. It not only clearly reflects the hemodynamic changes at the lesion site but also provides sufficient time to observe the dynamic changes of tumor enhancement during contrast imaging, significantly aiding tumor differentiation.

In this study, malignancies diagnosed by both CECT and CEUS are predominantly adenocarcinomas (31/40 or 77.5% *vs.* 59/74 or 79.7%), followed by squamous cell carcinomas, adenosquamous carcinomas, and papillary carcinomas, which is consistent with the study by Moeini A *et al.* (*20*). Gallbladder adenomas is a common benign GB tumor, with an incidence of 0.2% to 0.5% (*25*) and a canceration rate of about 30% (*26*). In this study, 7 adenoma cases showed precancerous lesions, with a canceration rate of 41.2%, slightly higher than that reported in the literature (*26*).

Conventional ultrasound in this study revealed no significant differences between benign and malignant groups in lesion size, internal echogenicity, and gallstones. However, color Doppler ultrasound showed significantly higher intralesional vascularity in malignancies than in benign masses, aligning with the results of Hirooka Y *et al.* (*27*). Color Doppler blood flow detection is easily affected by lesion size, intralesional blood flow velocity, and instrument sensitivity. In addition, conventional ultrasound inadequately assesses GB wall integrity and liver involvement.

Previous studies comparing the diagnostic efficacy of US and CEUS for gallbladder diseases found superior sensitivity and specificity of CEUS over US but lacked detailed analysis of CEUS features of gallbladder malignant lesions and quantitative analysis using time-intensity curves (*11,28*). Another study involving 1,044 patients with gallbladder space-occupying lesions reported a sensitivity of 81%, a specificity of 87%, a diagnostic odds ratio of 58.84, and an AUC of 0.93 of CEUS in differentiating gallbladder lesion (*18*). Similarly, this study did not provide specific CEUS features. Bo X *et al.* compared the diagnostic accuracy of various imaging modalities in differentiating gallbladder cancer from xanthogranulomatous cholecystitis and found higher CEUS sensitivity and specificity than CECT (*29*), but did not compare CEUS and CECT for other lesions. In a meta-analysis of 25 studies involving 2,469 patients with focal gallbladder lesions, Zhang L *et al.* found that CEUS and CECT had comparable diagnostic efficacy but omitted feature analysis (*30*).

This current study aimed to investigate the value of CEUS and time-intensity curves in differentiating benign and malignant gallbladder lesions and to compare the diagnostic efficacy of CEUS and CECT. Irregular enhancement (CEUS), heterogeneous enhancement (CEUS), GB wall disruption (CEUS or CECT), ill-defined border with adjacent liver tissue (CEUS or CECT), WT (CEUS), and arterial hyper-enhancement (CECT) were found to be significantly associated with malignancies, suggesting that CEUS has an important role to play in describing abnormal gallbladder features detected by imaging examinations.

Unlike the liver, the GB has single-artery blood supply (cystic artery), resulting in stronger wall enhancement than the liver parenchyma. Arterial hyper-enhancement was observed in 16 GBC cases (16/20, 75.0%) due to GBC growth, invasion, and metastasis as a result of high-density neovascularization. However, 25 (25/32, 78.1%) benign lesions also exhibited arterial hyper-enhancement, probably attributable to inflammation-induced angiogenesis, with no statistical

differences between the benign and malignant groups. Xie XH *et al.* (*16*) studied GBC 33 patients and 47 patients with benign gallbladder diseases and concluded that arterial hyper-enhancement could not differentiate benign and malignant gallbladder space-occupying lesions, which is consistent with our findings. Inoue T *et al.* (*31*) and Numata K *et al.* (32) also noted limited diagnostic value of CEUS vascularity for gallbladder diseases using a coded phase-inversion harmonic US and Levovist.

Tumor neovascularization is of great significance for the occurrence and development of malignancies, and vascular morphology provides diagnostic basis for CEUS. Four main vascular type have been identified in gallbladder lesions, *i.e.* punctate, linear, branched, and irregular. In our cohort, 90.0% (18/20) malignancies presented irregular patterns against 90.6% (29/32) regular patterns (punctate, linear, and branched) in benign lesions, without statistically significant difference ($P < 0.05$). This observation is attributable to rich large and irregular neovessels (twisted and deformed with dense clusters) in malignancies and a tendency to form a large number of arteriovenous shunts, thus often an irregular pattern on CEUS. In contrast, neovascularization in benign gallbladder lesions is slow, with a single flow pattern and fewer branches, which is closer to normal tissue (*33*).

Heterogeneous perfusion was observed in 65.0% (13/20) malignancies, significantly higher than 21.9% (7/32) in benign lesions ($P < 0.05$), consistent with previous studies (*26,34*). The reason lies the disorganized neovascularization in malignant tumors, which can cause uneven vascular distribution. In addition, neovessels within malignant tumors cannot supply sufficient nutrients required for the rapid growth. Consequently, ischemic necrosis occurs within the tumor, manifesting asheterogeneous enhancement on CEUS.

Most benign gallbladder lesions exhibit homogeneous internal echogenicity. However, in some patients with cholecystitis and gallbladder adenomyomatosis, due to acute and chronic inflammation or the formation of Rokitansky-Aschoff sinuses within the gallbladder wall at the lesion area, hypo-enhancement or non-enhanced areas appear, showing heterogeneous perfusion on CEUS.

Gallbladder cancer originates from atypical mucosal hyperplasia and gradually progresses to carcinoma in situ, invasive carcinoma, surrounding tissue invasion, and distant metastasis. Therefore, evaluating the structural integrity of the gallbladder wall is of great significance for the diagnosing GBC (*33*). In this study, 19 cases (19/20, 95.0%) of gallbladder cancer exhibited varying degrees of gallbladder wall destruction, among which 14 showed ill-defined borders with adjacent liver tissue. Kong WT *et al.* (*35*) found that the blurred boundary between the gallbladder wall and the liver was an independent predictor of malignancy in 49 gallbladder lesions. Xie XH *et al.* (*16*) found that gallbladder wall destruction highly predicted malignancy, with a sensitivity of 84.8% and a specificity of 100%. Chen LD *et al.* (*17*) claimed that an interrupted inner layer was an independent predictor of malignancy. US is barely satisfactory in evaluating the thickness, continuity, and internal echogenicity of the gallbladder wall, whereas CEUS can not only clearly display the mucosal and serosal layers of the gallbladder wall but also perform real-time scanning and acquire data (*17,36*). Therefore, CEUS is more effective for diagnosing benign and malignant gallbladder lesions.

Hypo-enhancement in the delayed phase is an important CEUS feature of hepatic malignancies, but it is not applicable to gallbladder lesions because all gallbladder cancers and most benign gallbladder diseases exhibit hypo-enhancement in the delayed phase, as demonstrated in this study. The reason for this phenomenon may be related to the fact that gallbladder blood supply is solely provided by branches of the hepatic artery. Due to the absence of portal vein supply, the persistence of contrast agent in the venous phase shortens, thus potentially being misinterpreted as washout, especially for small lesions. On the other hand, we consider contrast agent WT to be a useful feature for differentiating benign and malignant gallbladder lesions. In this study, with a WT cutoff value of 46.3 s, its sensitivity for diagnosing malignant lesions was 89.4%, specificity was 86.1%, and AUC was 0.900. However, opinions vary regarding the optimal cutoff value for contrast agent washout. Xie XH *et al.* (*16*) proposed 35 s as the critical cutoff value for WT, with a sensitivity of 90.9% and a specificity of 87.2% in malignancy diagnosis. Serra C *et al.* (*37*) and Wang W *et al.* (*38*) suggested 60 s as the optimal cut-off value for defining malignancy with higher diagnostic accuracy.

In our study, 4 adenoma cases s with canceration were misdiagnosed as adenomas due to the small size of the lesions (all smaller than 2 cm) and the presence of benign lesion features on CEUS. Regarding CEUS manifestations of adenoma canceration, some researchers (*39*) believe that gallbladder adenomas after canceration demonstrate "slow enhancement and rapid washout", whereas Hattori M *et al.* (*40*) studied 60 gallbladder space-occupying lesions and concluded that the CEUS manifestations of adenoma canceration are identical to those of gallbladder cancer, both showing "rapid enhancement and rapid washout". However, only two gallbladder adenoma lesions were included in their study, thus the results are not generalizable. The reason for discrepancies in CEUS manifestations of cancerated adenomas may be ascribed to differences in patient populations, such as clinical profiles, disease stages, and age. Thus, accurate diagnosis of early-stage GBC remains a challenge for ultrasound.

In the benign group of this study, four benign cases

were misdiagnosed as malignant tumors due to the displayed interruption of GB wall integrity. Among them, 2 cases had cholecystitis with perforation, and liver inflammatory lesions secondary to perforation were misinterpreted as tumor invasion on CEUS. The other two cases were of xanthogranulomatous cholecystitis and also exhibited incomplete GB walls, possibly due to the release of phospholipase A from the GB mucosal epithelium stimulated by inflammation or bile stasis, which hydrolyzes lecithin in bile into lysophosphatidylcholine. The latter further destroys the integrity of the mucosal epithelial cells and causes irregular morphology of the mucosal layer. The authors consider that ill-defined borders between the gallbladder wall and liver tissue, along with significant wall thickening and loss of normal structure, can be regarded as malignant features, whereas mere continuity interruption requires consideration of possibile benign lesions.

This study included three adenomas misdiagnosed as malignant due to short contrast agent WT. This indicates that using rapid washout as a predictor for malignancy may cause false positives in lesions. Therefore, the role of the optimal cutoff value of WT in differentiating benign and malignant gallbladder lesions still warrants further evaluation.

This study used pathological results as the gold standard, finding that CEUS outperformed CECT in diagnosing gallbladder cancer in the respects of sensitivity (89.2% *vs.* 85.7%), specificity (78.8% *vs.* 74.3%), accuracy (84.9% *vs.* 80.5%), PPV (85.7% *vs.* 80.0%), and NPV (83.7% *vs.* 81.2%), but without statistical significance ($P > 0.05$). CECT showed poor accuracy in diagnosing benign gallbladder lesions. In other words, it more readily tended to misdiagnose them as malignant. The reason might lie in CECT's limitation to cross-sectional scanning. For some benign lesions, the pedicle could not be observed, only displaying broad-based soft tissue shadows protruding into the gallbladder lumen with significant arterial enhancement and thus easily misdiagnosed as malignant lesions. In addition, CECT could only select scanning times empirically and could not visualize real-time enhancement process. This makes it highly susceptible to individual patient differences and operator experience, preventing accurate observation of the enhancement patterns at peak enhancement, particularly for small gallbladder lesions where CT scanning poses difficulties in summarize the enhancement characteristics. In this cohort, 9 benign lesions (3 cholesterol polyps, 1 xanthogranulomatous cholecystitis, 3 adenomas, and 2 chronic cholecystitis) were misdiagnosed as malignant by CECT. However, compared with CEUS, CECT had certain advantages in detecting retroperitoneal lymph node metastasis, distant metastasis, and intrahepatic metastasis within ultrasound blind zones (*4*). Among the 2 CEUS-misdiagnosed gallbladder cancer cases, CECT diagnosed 1 case with gallbladder cancer with necrotic retroperitoneal lymph nodes and 1 case with omental infiltration before surgery. Thus, in displaying gallbladder lesions, CECT offers advantages over CEUS in evaluating the degree and extent of lesion invasion of surrounding tissues and occurrence of lymph node metastasis.

Some limitations are mentionable. This study did not include thick-walled GB lesions which might lead to statistical bias. Second, the number of cases diagnosed by both CEUS and CECT is small; therefore, the diagnostic value of the former should be validated in subsequent studies with larger patient cohorts. Finally, our study was retrospective in nature. In future studies, a prospective, paired design should be employed, where all enrolled patients undergo both CEUS and CECT examinations simultaneously. This will allow for direct, one-to-one comparison using pathology as the gold standard, maximizing statistical power and yielding more reliable conclusions.

CEUS facilitates differentiation between benign and malignant GB lesions and holds high diagnostic value, warranting clinical promotion and application. In our present study, the diagnostic efficacy of CEUS was found comparable to that of CECT. CEUS can serve as an alternative to CECT in patients with iodine contrast anaphylaxis or renal insufficiency. The two modalities can complement each other and provide more valuable information for the differential diagnosis of GB lesions, thereby improving diagnostic accuracy.

Funding: This work was supported by a grant from Shanghai Municipal Health Commission (grant No. 202340140 to ZY Qiu), and the National Natural Science Foundation of China (grant No. 82374243 to L Wang).

Conflict of Interest: The authors have no conflicts of interest to disclose.

References

1. Lazcano-Ponce EC, Miquel JF, Muñoz N, Herrero R, Ferrecio C, Wistuba II, Alonso de Ruiz P, Aristi Urista G, Nervi F. Epidemiology and molecular pathology of gallbladder cancer. CA Cancer J Clin. 2001; 51:349-364.
2. Sharma A, Sharma KL, Gupta A, Yadav A, Kumar A. Gallbladder cancer epidemiology, pathogenesis and molecular genetics: Recent update. World J Gastroenterol. 2017; 23:3978-3998.
3. Mao W, Deng F, Wang D, Gao L, Shi X. Treatment of advanced gallbladder cancer: A SEER-based study. Cancer Med. 2020; 9:141-150.
4. Hundal R, Shaffer EA. Gallbladder cancer: epidemiology and outcome. Clin Epidemiol. 2014; 6:99-109.
5. Yuan B, Zhao X, Wang X, Liu E, Liu C, Zong Y, Jiang Y, Hou M, Chen Y, Chen L, Zhang Y, Wang H, Fu J. Patient-derived organoids for personalized gallbladder cancer modelling and drug screening. Clin Transl Med. 2022; 12:e678.

6. Nie C, Yang T, Liu L, Hong F. Trend analysis and risk of gallbladder cancer mortality in China, 2013-2019. Public Health. 2022; 203:31-35.
7. Torre LA, Siegel RL, Islami F, Bray F, Jemal A. Worldwide Burden of and Trends in Mortality From Gallbladder and Other Biliary Tract Cancers. Clin Gastroenterol Hepatol. 2018; 16:427-437.
8. Feo CF, Ginesu GC, Fancellu A, Perra T, Ninniri C, Deiana G, Scanu AM, Porcu A. Current management of incidental gallbladder cancer: A review. Int J Surg. 2022; 98:106234.
9. Wernberg JA, Lucarelli DD. Gallbladder cancer. Surg Clin North Am. 2014; 94:343-360.
10. Gore RM, Thakrar KH, Newmark GM, Mehta UK, Berlin JW. Gallbladder imaging. Gastroenterol Clin North Am. 2010; 39:265-ix.
11. Zhang HP, Bai M, Gu JY, He YQ, Qiao XH, Du LF. Value of contrast-enhanced ultrasound in the differential diagnosis of gallbladder lesion. World J Gastroenterol. 2018; 24:744-751.
12. Liang X, Jing X. Meta-analysis of contrast-enhanced ultrasound and contrast-enhanced harmonic endoscopic ultrasound for the diagnosis of gallbladder malignancy. BMC Med Inform Decis Mak. 2020; 20:235.
13. Fang L, Bai K, Chen Y, Zhan J, Zhang Y, Qiu ZY, Chen L, Wang L. A comparative study of contrast-enhanced ultrasound and contrast-enhanced CT for the detection and characterization of renal masses. Biosci Trends. 2021; 15:24-32.
14. Fang L, Zhu Z, Huang BJ, Ding H, Mao F, Li C, Zeng M, Zhou J, Wang L, Wang W, Chen Y. A comparative study of contrast enhanced ultrasound and contrast enhanced magnetic resonance imaging for the detection and characterization of hepatic hemangiomas. Biosci Trends. 2015; 9:104-110.
15. Xu JM, Guo LH, Xu HX, Zheng SG, Liu LN, Sun LP, Lu MD, Wang WP, Hu B, Yan K, Hong D, Tang SS, Qian LX, Luo BM. Differential diagnosis of gallbladder wall thickening: the usefulness of contrast-enhanced ultrasound. Ultrasound Med Biol. 2014; 40:2794-2804.
16. Xie XH, Xu HX, Xie XY, Lu MD, Kuang M, Xu ZF, Liu GJ, Wang Z, Liang JY, Chen LD, Lin MX. Differential diagnosis between benign and malignant gallbladder diseases with real-time contrast-enhanced ultrasound. Eur Radiol. 2010; 20:239-248.
17. Chen LD, Huang Y, Xie XH, Chen W, Shan QY, Xu M, Liu JY, Nie ZQ, Xie XY, Lu MD, Shen SL, Wang W. Diagnostic nomogram for gallbladder wall thickening mimicking malignancy: using contrast-enhanced ultrasonography or multi-detector computed tomography. Abdom Radiol (NY). 2017; 42:2436-2446.
18. Cheng Y, Wang M, Ma B, Ma X. Potential role of contrast-enhanced ultrasound for the differentiation of malignant and benign gallbladder lesions in East Asia: A meta-analysis and systematic review. Medicine (Baltimore). 2018; 97:e11808.
19. Wu MC. Liver malignant diseases. In: Huang Jiasi Surgery(Wu JP, Qiu FZ, eds.). People's Medical Publishing House, Beijing, China, 2002; pp. 1223.
20. Moeini A, Haber PK, Sia D. Cell of origin in biliary tract cancers and clinical implications. JHEP Rep. 2021; 3:100226.
21. Pradhan S, Shukla VK, Agrawal S, Dixit VK, Sharma OP. Sonographic and colour doppler morphology in carcinoma gallbladder. Indian J Cancer. 2002; 39:143-148.
22. Li J, Wu XR, Yu TZ. Comparative analysis of contrast-enhanced ultrasound and contrast-enhanced CT in differential diagnosis of benign and malignant space-occupying lesions of gallbladder. Int J Biomed Eng. 2018; 41:261-264+270.
23. Sung H, Ferlay J, Siegel RL, Laversanne M, Soerjomataram I, Jemal A, Bray F. Global Cancer Statistics 2020: GLOBOCAN Estimates of Incidence and Mortality Worldwide for 36 Cancers in 185 Countries. CA Cancer J Clin. 2021; 71:209-249.
24. Xia C, Dong X, Li H, Cao M, Sun D, He S, Yang F, Yan X, Zhang S, Li N, Chen W. Cancer statistics in China and United States, 2022: profiles, trends, and determinants. Chin Med J (Engl). 2022; 135:584-590.
25. Pang L, Zhang Y, Wang Y, Kong J. Pathogenesis of gallbladder adenomyomatosis and its relationship with early-stage gallbladder carcinoma: an overview. Braz J Med Biol Res. 2018; 51:e7411.
26. Sun LP, Guo LH, Xu HX, Liu LN, Xu JM, Zhang YF, Liu C, Bo XW, Xu XH. Value of contrast-enhanced ultrasound in the differential diagnosis between gallbladder adenoma and gallbladder adenoma canceration. Int J Clin Exp Med. 2015; 8:1115-1121.
27. Hirooka Y, Naitoh Y, Goto H, Furukawa T, Ito A, Hayakawa T. Differential diagnosis of gall-bladder masses using colour Doppler ultrasonography. J Gastroenterol Hepatol. 1996; 11:840-846.
28. Xing RW, Mu YH, Li WJ, Li B, Nie HQ, Yin P. Comparative analysis of contrast-enhanced ultrasound and enhanced CT in diagnosis of polypoid lesions of gallbladder. Gan Dan Yi Wai Ke Za Zhi. 2019; 6:356-359. (in Chinese)
29. Bo X, Chen E, Wang J, Nan L, Xin Y, Wang C, Lu Q, Rao S, Pang L, Li M, Lu P, Zhang D, Liu H, Wang Y. Diagnostic accuracy of imaging modalities in differentiating xanthogranulomatous cholecystitis from gallbladder cancer. Ann Transl Med. 2019; 7:627.
30. Zhang L, Tang Y, Gong J, Li Y, Li C, Wen M. Meta-analysis of the diagnostic value of contrast-enhanced CT and contrast-enhanced ultrasound in focal gallbladder lesions. Lin Chuang Fang She Xue Za Zhi. 2018; 2:271-6. (in Chinese)
31. Inoue T, Kitano M, Kudo M, Sakamoto H, Kawasaki T, Yasuda C, Maekawa K. Diagnosis of gallbladder diseases by contrast-enhanced phase-inversion harmonic ultrasonography. Ultrasound Med Biol. 2007; 33:353-361.
32. Numata K, Oka H, Morimoto M, Sugimori K, Kunisaki R, Nihonmatsu H, Matsuo K, Nagano Y, Nozawa A, Tanaka K. Differential diagnosis of gallbladder diseases with contrast-enhanced harmonic gray scale ultrasonography. J Ultrasound Med. 2007; 26:763-774.
33. Fei X, Luo YK. Interpretation and image analysis of gallbladder ultrasonography guideline. Zhonghua Yi Xue Chao Sheng Za Zhi. 2018; 15:5-10. (in Chinese)
34. Miwa H, Numata K, Sugimori K, Sanga K, Hirotani A, Tezuka S, Goda Y, Irie K, Ishii T, Kaneko T, Tanaka K, Maeda S. Differential diagnosis of gallbladder polypoid lesions using contrast-enhanced ultrasound. Abdom Radiol (NY). 2019; 44:1367-1378.
35. Kong WT, Shen HY, Qiu YD, Han H, Wen BJ, Wu M. Application of contrast enhanced ultrasound in gallbladder lesion: is it helpful to improve the diagnostic capabilities? Med Ultrason. 2018; 20:420-426.
36. Tang S, Wang Y, Wang Y. Contrast-enhanced ultrasonography to diagnose gallbladder perforation. Am J

Emerg Med. 2013; 31:1240-1243.
37. Serra C, Felicani C, Mazzotta E, Gabusi V, Grasso V, De Cinque A, Giannitrapani L, Soresi M. CEUS in the differential diagnosis between biliary sludge, benign lesions and malignant lesions. J Ultrasound. 2018; 21:119-126.
38. Wang W, Fei Y, Wang F. Meta-analysis of contrast-enhanced ultrasonography for the detection of gallbladder carcinoma. Med Ultrason. 2016; 18:281-228.
39. Sun LP, Guo LH, Xu HX, Liu LN, Xu JM, Zhang YF, Liu C, Bo XW, Xu XH. Value of contrast-enhanced ultrasound in the differential diagnosis between gallbladder adenoma and gallbladder adenoma canceration. Int J Clin Exp Med. 2015; 8:1115-1121.
40. Hattori M, Inui K, Yoshino J, Miyoshi H, Okushima K, Nakamura Y, Naito T, Imaeda Y, Horibe Y, Hattori T, Nakazawa S. Usefulness of contrast-enhanced ultrasonography in the differential diagnosis of polypoid GB lesions. Nihon Shokakibyo Gakkai Zasshi. 2007; 104:790-798. (in Japanese)

Received September 2, 2025; Revised December 4, 2025; Accepted December 9, 2025.

[§]These authors contributed equally to this work.

**Address correspondence to:*
Lin Chen, Department of Ultrasonic Diagnosis, Huadong Hospital Affiliated to Fudan University, 221 West Yanan Road, Shanghai 200040, China.
E-mail: hdchenlin@fudan.edu.cn

Ling Wang, Department of Obstetrics, The First Affiliated Hospital, Guizhou University of Traditional Chinese Medicine, No. 71 Baoshan North Road, Guiyang 550001, China.
E-mail: dr.wangling@vip.163.com

Released online in J-STAGE as advance publication December 16, 2025.

Brief Report

DOI: 10.5582/ddt.2025.01099

Modulatory effects of ingesting dietary fiber and protein before carbohydrates on postprandial interstitial glucose responses

Yuko Wada Imanaka[1], Sanae Tanaka[2], Chisato Watanabe[1], Ken-ichi Shimokawa[3], Fumiyoshi Ishii[1,*]

[1] Department of Self-medication and Health Care Sciences, Meiji Pharmaceutical University, Tokyo, Japan;
[2] Kraft Co. Ltd., Tokyo, Japan;
[3] Department of Pharmaceutical Sciences, Meiji Pharmaceutical University, Tokyo, Japan.

SUMMARY: Rapid postprandial elevations in interstitial glucose contribute to the progression of type 2 diabetes and associated vascular complications. Nutritional sequencing strategies, such as consuming dietary fiber or protein before carbohydrate intake, have been proposed to attenuate glucose excursions by delaying gastric emptying, stimulating incretin secretion, and enhancing insulin responsiveness. However, observational evidence under real-world conditions remains scarce in both healthy individuals and those with diabetes. We performed an observational study including healthy participants and individuals with type 2 diabetes. All participants were equipped with a continuous glucose monitoring system (FreeStyle Libre™) for 14 days to capture interstitial glucose profiles under daily living conditions. Participants simultaneously recorded dietary intake and meal timing. Postprandial glucose excursions were evaluated by comparing carbohydrate ingestion alone with ingestion preceded by fiber and/or protein. Preceding carbohydrate intake with dietary fiber or protein was associated with significant attenuation of postprandial glucose excursions compared with carbohydrate alone. This effect was particularly evident within the first 120 minutes after eating and was most pronounced when fiber and protein were consumed in combination. Attenuation occurred in both healthy individuals and participants with type 2 diabetes, though the magnitude of suppression varied across groups. Our findings indicate that consuming fiber and protein prior to carbohydrate intake can substantially mitigate rapid postprandial glucose rises. These results support the physiological rationale for macronutrient sequencing and underscore the potential of simple, practical dietary strategies to improve glycemic control in daily life among both healthy individuals and those with diabetes.

Keywords: Continuous glucose monitoring (FreeStyle Libre™), postprandial glucose excursions, macronutrient sequencing, type 2 diabetes mellitus and healthy individuals

1. Introduction

The global prevalence of diabetes has markedly increased in recent decades, mainly driven by the continuous rise in type 2 diabetes mellitus (T2DM). According to the International Diabetes Federation (*1*), more than 537 million adults aged 20–79 years were living with diabetes in 2021, corresponding to a prevalence of 10.5%, and the numbers are projected to continue rising. In 2021, marking the centenary of the discovery of insulin, the World Health Organization launched the Global Diabetes Compact to accelerate efforts to prevent diabetes and ensure universal access to care, underscoring the urgent need for global action (*2*).

Shared risk factors underlying the rise in T2DM include urbanization, population aging, reduced physical activity, and increasing rates of overweight and obesity. These observations indicate that T2DM is, to a significant extent, preventable through lifestyle modification, particularly dietary management.

Postprandial hyperglycemia plays a key role in the development of diabetic vascular complications and thus represents a central target of dietary therapy (*3,4*). The amount and type of dietary carbohydrate are primary determinants of postprandial glycemic responses, with the total carbohydrate intake being the strongest predictor (*5*). Dietary research in diabetes has traditionally focused on nutrient quantity and composition, but recent attention has shifted toward the influence of food order on glycemic excursions. Several studies have demonstrated that consuming vegetables (*6*), fish or meat (*7*), whey protein (*8*), or olive oil (*9*) before carbohydrate intake can attenuate postprandial glycemic excursions in patients with T2DM. However, few studies have

examined the combined effects of vegetables and protein, and comparative investigations involving both healthy individuals and patients with T2DM remain limited.

Therefore, this study aimed to evaluate the effects of pre-meal vegetable consumption, alone or in combination with protein, on postprandial glucose responses in both healthy individuals and patients with T2DM.

2. Methods

2.1. Participants

This study was conducted between 2020 and 2023 at Kraft Co., Ltd. and Meiji Pharmaceutical University. Healthy adults and patients diagnosed with T2DM were recruited. Written informed consent was obtained from all participants prior to enrollment. Exclusion criteria for healthy participants included (I) myocardial infarction or stroke within 6 months; (II) angina, heart failure, or severe arrhythmia; (III) diagnosis of diabetes; (IV) chronic obstructive pulmonary disease; (V) acute joint pain, arthritis, lumbago, or neuralgia; (VI) acute pneumonia or hepatitis; (VII) use of implantable medical devices (contraindicated with FreeStyle Libre™); and (VIII) physician-directed dietary restrictions or difficulty in food intake due to dysphagia or anorexia. A total of 34 healthy participants and 4 patients with T2DM were deemed eligible.

The study protocol was approved by the Ethics Committee of Meiji Pharmaceutical University (Approval No. 202020) and conducted in accordance with the Declaration of Helsinki.

2.2. Glucose Monitoring

The blood glucose level was evaluated by measuring the glucose level in the interstitial fluid using a minimally invasive continuous glucose monitoring system, FreeStyle Libre™ (Abbott Japan, Tokyo Minato-ku) (Figure 1), which does not require blood sampling and has a high correlation with the blood glucose level (*10*).

Attached to the upper arm, the sensor automatically recorded glucose levels every 15 min for up to 14 days without requiring participant or clinician intervention. Considering that glucose readings are less stable during the first 2 days after sensor placement, all experimental sessions were initiated from day 3 onward.

2.3. Experimental procedures

Participants wore the glucose sensor for 14 consecutive days and recorded dietary intake and meal times in a diary. After a fasting period of at least 3 h (water only), participants consumed two rice balls (salmon onigiri, Seven-Eleven Japan, Tokyo Chiyoda-ku). Three test conditions were applied: (I) rice balls alone, (II) rice balls preceded by salad (lettuce mix with Japanese-style dressing), and (III) rice balls preceded by salad with chicken breast (plain "salad chicken"). In condition (III), participants consumed the salad/chicken salad first, followed immediately by the rice ball. The order of interventions was randomized across days. For 3 h postprandially, participants refrained from vigorous exercise and from consuming anything other than water.

All test meals were commercially available products from Seven-Eleven convenience stores, chosen for their wide availability, ensuring standardized access and feasibility for all participants (Table 1).

2.4. Statistical analysis

Data were analyzed using Microsoft® Excel® version 2108 and BellCurve for Excel version 4.09. Friedman test was used to compare mean values, expressed as the mean ± standard error (SE). A P-value < 0.05 was considered significant.

Figure 1. The process of scanning data from a sensor attached to the arm (up) using a reader device (FreeStyle Libre™ system, Abbott Japan) (down).

3. Results and Discussion

3.1. Effects of vegetable- and protein-first intake

A total of 9 healthy men, 25 healthy women, and 4 male patients with T2DM participated in the study. All participants completed all experimental sessions. The effects of consuming salad alone ("vegetable-first") or salad with protein ("vegetable & protein-first") prior to carbohydrate intake on postprandial glucose excursions were evaluated.

At baseline (0 min), interstitial glucose concentrations were significantly higher in the T2DM group (103 ± 26 mg/dL) than in the healthy group (67 ± 8.9 mg/dL) (Figure 2). In both groups, an increase in interstitial glucose was observed following rice ball consumption; however, the peak occurred at 68 ± 38 min in healthy subjects (Figure 2A) and was markedly delayed to 86 ± 38 min in patients with T2DM (Figure 2B). Baseline interstitial glucose concentrations did not significantly differ among the experimental conditions (rice ball-alone, vegetable-first, and vegetable & protein-first) in either group (healthy: 67, 67, and 66 mg/dL; T2DM: 103, 92, and 92 mg/dL).

In healthy subjects, postprandial glucose increases were evident 15 min after ingestion for both the rice

Table 1. Meal composition and nutrient content in the experimental schedule

Days	Experimental diet	Nutrition facts
1-2	Preparation period until the sensor becomes stable	
3-8	Two rice balls	Calories: 173 kcal Protein: 4.6 g Total fats: 1.7 g Total carbohydrate: 33.8 g Dietary fiber: 1.9 g
9-10	Salad → two rice balls	Calories: 234 kcal Protein: 5.8 g Total fats: 5.3 g Total carbohydrate: 38.5 g Dietary fiber: 4.5 g
11-12	Salad with steamed chicken → two rice balls	Calories: 348 kcal Protein: 29.9 g Total fats: 7.3 g Total carbohydrate: 38.5 g Dietary fiber: 4.5 g
13-14	Spare days for retests	

Day 3-14 can be in a different order.

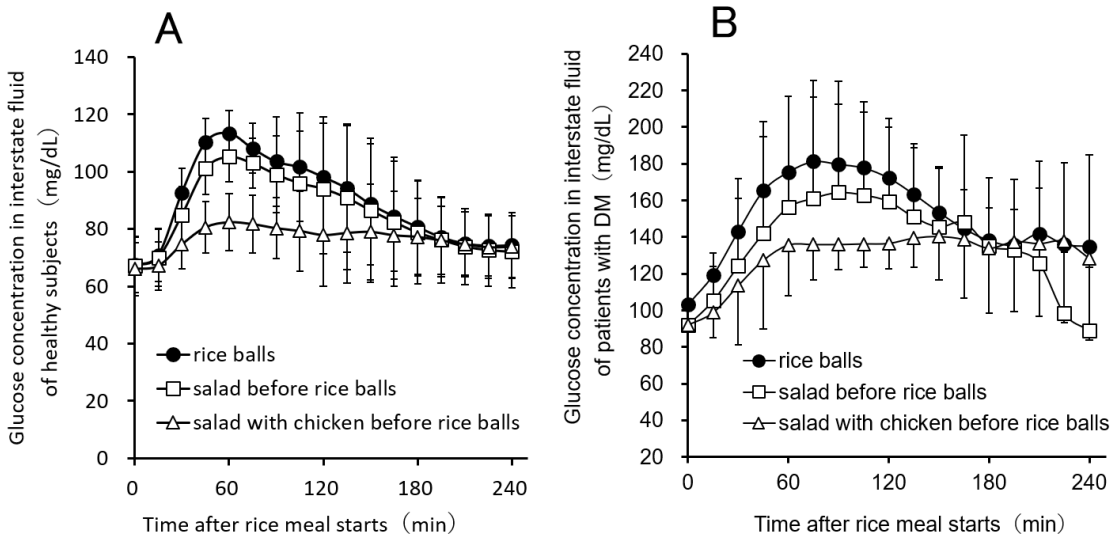

Figure 2. Glucose concentration in the interstitial fluid of healthy subjects (*n* = 34) (A) and patients with T2DM (*n* = 4) (B). A: healthy subjects, B: patients with T2DM. Closed cercle: rise balls, Open square: salad before rise balls, Open triangle: salad with chicken before rice balls.

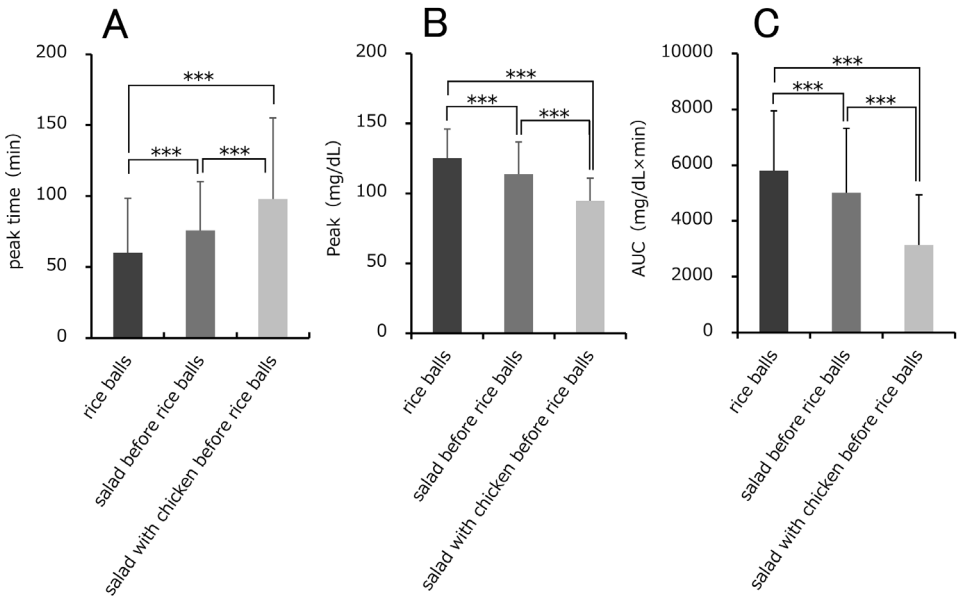

Figure 3. The time of peak (A), the peak glucose concentration in interstate fluid (B) and the AUC (C) of healthy subjects (n = 34). A: Peak time, B: Peak, C: AUC. ***P < 0.001, Friedman-test.

ball-alone and vegetable-first conditions, whereas the increase was delayed to 30 min for the vegetable & protein-first condition (Figure 2A). From 30 to 120 min, glucose concentrations were lower for the vegetable-first condition than for the rice ball-alone condition (P < 0.05), and from 30 to 150 min, they were significantly lower for the vegetable & protein-first condition than for the rice ball-alone condition (P < 0.05) (Figure 2A).

3.2. Effects on peak glucose and Area Under the Curve (AUC)

When vegetables were consumed first (72 ± 34 min), the time to reach the peak glucose level was significantly delayed compared with consuming rice balls alone (68 ± 38 min) (P < 0.001). The delay was even greater when vegetables and protein were consumed first (110 ± 57 min) (P < 0.001) (Figure 3A). Peak glucose concentrations were significantly lower for the vegetable-first condition (114 ± 23 mg/dL) compared with the rice ball-alone condition (125 ± 21 mg/dL) and were further reduced for the vegetable & protein-first condition (95 ± 16 mg/dL) (P < 0.001) (Figure 3B). The area under the glucose concentration–time curve (AUC) was significantly lower for the vegetable-first (5,013 ± 2,302 mg/dL·min) and vegetable & protein-first (3,144 ± 1,791 mg/dL·min) conditions compared with the rice ball-alone condition (5,804 ± 2,136 mg/dL·min) (P < 0.001) (Figure 3C).

In the T2DM group, although no significant differences were observed, glucose concentrations from 15 to 150 min were lower for both the vegetable-first and vegetable & protein-first conditions than for the rice ball-alone condition (Figure 2B). The time to peak glucose concentration was 86 ± 38 min for the rice ball-alone condition, 120 ± 64 min for the vegetable-first condition, and 176 ± 89 min for the vegetable & protein-first condition; the peak was slightly delayed for the vegetable & protein-first condition compared with the rice ball-alone condition, but the difference was not significant (Figure 4A). The peak glucose level tended to be lower in the condition where vegetables were consumed first (174 ± 40 mg/dL) compared with the rice-ball–only condition (193 ± 39 mg/dL), and was even lower when vegetables and protein were consumed first (169 ± 43 mg/dL) (Figure 4B). Similarly, the AUC also tended to be lower in both the vegetable-first condition (8,995 ± 8,306 mg/dL·min) and the vegetable-plus-protein-first condition (7,599 ± 4,732 mg/dL·min) compared with the rice-ball–only condition (11,956 ± 6,176 mg/dL·min) (Figure 4C).

This study demonstrated that pre-ingesting vegetables and protein, using readily available commercial food products, effectively modulated postprandial glucose responses. By employing standardized and easily accessible foods, the intervention was feasible across all participants, including those unable to prepare meals themselves. This practical design highlights the potential for translating dietary strategies into daily life as supportive measures for glycemic management. The underlying mechanisms likely involve the complementary actions of dietary fiber and protein. Fiber slows gastric emptying and delays carbohydrate absorption (*11*), while protein stimulates insulin and incretin secretion and further contributes to delayed gastric emptying. When combined, these actions produced additive effects, resulting in greater suppression of postprandial glycemia compared with fiber alone.

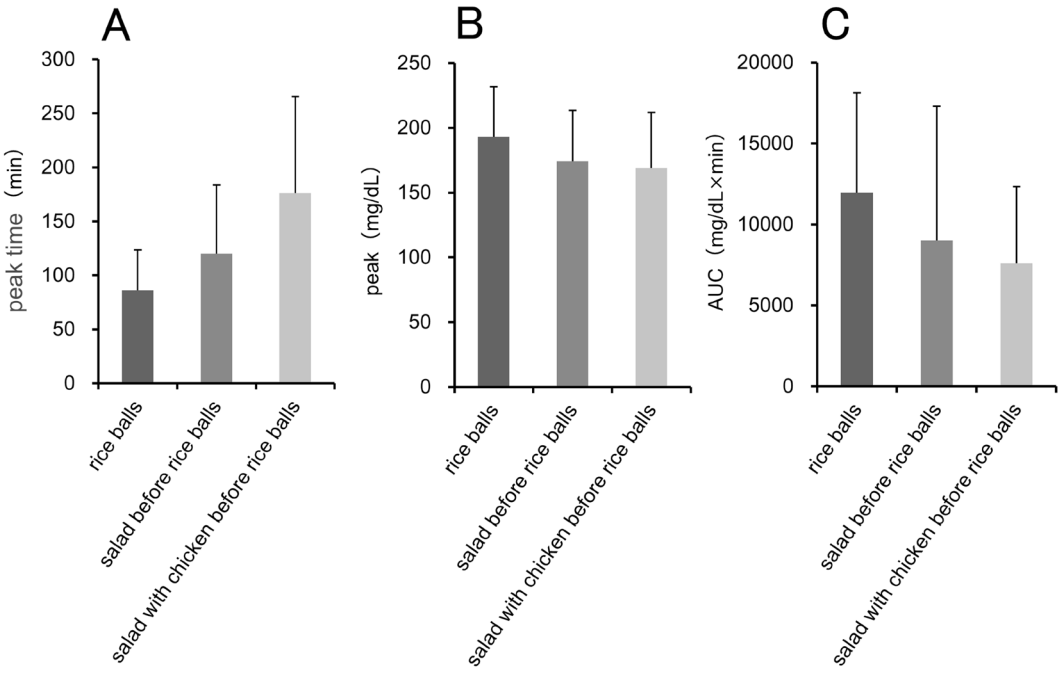

Figure 4. The time of peak (A), the peak glucose concentration in interstate fluid (B) and the AUC (C) of patients with T2DM (*n* = 4). A: Peak time, B: Peak, C: AUC.

Considerable inter-individual variability was also noted. Participants with higher insulin sensitivity exhibited smaller glycemic excursions and correspondingly modest intervention effects, whereas those with greater baseline responses experienced more pronounced benefits. Due to the limited sample size, only a trend toward reduced glucose levels was observed in the T2DM group, and further validation with a larger sample size is warranted. Such heterogeneity has been reported in previous studies (*12*) and underscores the importance of personalized approaches when applying dietary strategies in clinical practice.

Beyond mechanistic insights, this study also highlights the utility of noninvasive interstitial glucose monitoring. The method not only facilitates continuous data collection but also offers practical advantages for patients, including the avoidance of finger-prick sampling, lower cost, and real-time visualization of transient glucose levels using a smartphone. These features suggest its potential role as an educational and self-management tool for guiding dietary behavior.

Several limitations should be considered. Anthropometric and metabolic baseline data were not collected, insulin and incretin levels were not measured, and interventions were conducted at participants' homes, limiting full standardization. Furthermore, interstitial rather than blood glucose was used as the primary endpoint, and the COVID-19 pandemic restricted opportunities for more comprehensive metabolic assessments.

Future studies should involve larger and more diverse cohorts, with integrated assessments of blood glucose, insulin, incretin hormones, and indices of insulin resistance under researcher-supervised conditions. Such investigations are expected to help clarify both the physiological basis and clinical relevance of vegetable- and protein-first strategies, and further define their role as practical adjuncts to pharmacological therapy for optimizing glycemic control.

Funding: None.

Conflict of Interest: The authors have no conflicts of interest to disclose.

References

1. IDF Diabetes Atlas 11th Edition. *https://diabetesatlas.org/atlas/tenth-edition/* (accessed September 16, 2025).
2. New WHO Global Compact to speed up action to tackle diabetes. *https://www.who.int/news/item/14-04-2021-new-who-global-compact-to-speed-up-action-to-tackle-diabetes* (accessed September 16, 2025)
3. Smith-Palmer J, Brandle M, Trevisan R, Orsini Federici M, Liabat S, Valentine W. Assessment of the association between glycemic variability and diabetes-related complications in type 1 and type 2 diabetes. Diabetes Res Clin Pract. 2014; 105:273-284.
4. Leiter LA, Ceriello A, Davidson JA, Hanefeld M, Monnier L, Owens DR, Tajima N, Tuomilehto J. Postprandial glucose regulation: new data and new implications. Clin Ther. 2005; 27 (Suppl B):S42-56.
5. Evert AB, Boucher JL, Cypress M, Dunbar SA, Franz MJ, Mayer-Davis EJ, Neumiller JJ, Nwankwo R, Verdi CL. Urbanski P, Yancy Jr WS. Nutrition therapy recommendations for the management of adults with diabetes. Diabetes Care. 2013; 36:3821-3842.
6. Imai S, Matsuda M, Hasegawa G, Fukui M, Obayashi H, Ozasa N, Kajiyama S. A simple meal plan of 'eating vegetables before carbohydrate' was more effective for

achieving glycemic control than an exchange-based meal plan in Japanese patients with type 2 diabetes. Asia Pac J Clin Nutr. 2011; 20:161-168.
7. Kuwata H, Iwasaki M, Shimizu S, Minami K, Maeda H, Seino S, Nakada K, Nosaka C, Murotani K, Kurose T, Seino Y, Yabe D. Meal sequence and glucose excursion, gastric emptying and incretin secretion in type 2 diabetes: a randomised, controlled crossover, exploratory trial. Diabetologia. 2016; 59:453-461.
8. Ma J, Stevens JE, Cukier K, Maddox AF, Wishart JM, Jones KL, Clifton PM, Horowitz M, Rayner CK. Effects of a protein preload on gastric emptying, glycemia, and gut hormones after a carbohydrate meal in diet-controlled type 2 diabetes. Diabetes Care. 2009; 32:1600-1602.
9. Gentilcore D, Chaikomin R, Jones KL, Russo A, Feinle-Bisset C, Wishart JM, Rayner CK, Horowitz M. Effects of fat on gastric emptying of and the glycemic, insulin, and incretin responses to a carbohydrate meal in type 2 diabetes. J Clin Endocrinol Metab. 2006; 91:2062-2067.
10. Rebrin K, Steil GM. Can interstitial glucose assessment replace blood glucose measurements? Diabetes Technol Ther. 2000; 2:461-472.
11. Lattimer, JM, Haub, MD. Effects of dietary fiber and its components on metabolic health. Nutrients. 2010; 2:1266-1289.
12. Shukla AP, Dickison M, Coughlin N, Karan A, Mauer E, Truong W, Casper A, Emiliano AB, Kumar RB, Saunders KH, Igel LI, Aronne LJ. The impact of food order on postprandial glycemic excursions in prediabetes. Diabetes Obes Metab. 2019; 21:377-381.

Received September 17, 2025; Revised December 4, 2025; Accepted December 7, 2025.

**Address correspondence to:*
Fumiyoshi Ishii, Department of Self-medication and Health Care Sciences, Meiji Pharmaceutical University, 2-522-1, Noshio, Kiyose, Tokyo 204-8588, Japan.
E-mail: fishii@my-pharm.ac.jp

Released online in J-STAGE as advance publication December 11, 2025.

Correspondence

DOI: 10.5582/ddt.2025.01093

Clinical significance of imeglimin in older patients with type 2 diabetes: Analysis of a national database and a long-term case suggesting the potential for sarcopenia prevention

Atsushi Ishimura[1,*], Kaori Hashimoto[2], Hirofumi Ogino[3]

[1] Laboratory of Clinical Pharmacy Assessment, Hoshi University, Tokyo, Japan;
[2] Pharmaceutical Department of Seihikarigaoka Hospital, Chiba, Japan;
[3] Division of Life Science Pharmaceutics, Nihon Pharmaceutical University, Saitama, Japan.

SUMMARY: We aimed to evaluate the clinical significance of imeglimin in older patients with type 2 diabetes. Prescription trends were analyzed using the National Database of Health Insurance Claims and Specific Health Checkups of Japan (2021–2023). Prescriptions for imeglimin increased, with the highest usage among patients in their 70s, followed by those in their 60s, and a clear upward trend in those aged ≥ 80 years. We present the case of an 80-year-old woman with diabetes who repeatedly discontinued treatment. After initiating imeglimin (2000 mg/day), she continued therapy successfully, achieving stable HbA1c levels at approximately 7% over 30 months. Muscle mass indices (creatine kinase, creatinine, and estimated glomerular filtration rate), nutritional status (albumin), and inflammation (C-reactive protein) remained stable, and independent walking and quality of life were preserved. These findings suggest that imeglimin may support glycemic control and may help attenuate frailty and sarcopenia progression in older adults with diabetes.

Keywords: Imeglimin, type 2 diabetes, older adults, frailty, sarcopenia

1. Introduction

Medical care advances have enabled older adults with multiple comorbidities to live independently. However, they are vulnerable to physical, psychological, and social frailty, predisposing them to adverse health outcomes, including disability and mortality. The prevalence of frailty, a pre-disability state, is increasing. Sarcopenia, defined as the age-related loss of muscle mass and strength, is a major underlying cause of frailty. The prevalence of sarcopenia in older adults is approximately 1% in both men and women (*1*). Age-related decline in skeletal muscle is a key contributor to reduced muscle strength, with muscle mass decreasing at an annual rate of 1–2% from the 30s, with 30–40% loss by the 80s compared to that in the 20s. The importance of mitochondrial function in suppressing declines in the number of skeletal muscle stem cells has been highlighted (*2*). Mitochondria, present in nearly all cells except for erythrocytes, possess their own DNA and undergo replication, fusion, and fission. Mitochondrial dysfunction leads to impaired insulin secretion and contributes to the pathogenesis of type 2 diabetes (*3*). Consequently, patients with diabetes are at an increased risk of developing frailty and sarcopenia (*4*). Although multiple recent glucose-lowering agents have improved glycemic control among patients with type 2 diabetes (*5*), frailty and sarcopenia remain significant clinical challenges.

Imeglimin, a novel oral antidiabetic agent, was launched in September 2021 in Japan. While its chemical structure is similar to that of metformin, imeglimin belongs to a distinct class called "glimins" (*6*). Imeglimin enhances glucose-dependent insulin secretion by improving mitochondrial function (*7*). It can exert extrapancreatic effects on skeletal muscle and the liver by reducing oxidative stress (*8-10*). These unique mechanisms raise the possibility of imeglimin attenuating age-related decline in skeletal muscles, thereby contributing to the prevention of frailty in older adults. However, no previous studies have specifically examined the effects of imeglimin on reducing frailty risk. Therefore, in this study, we aimed to (*i*) investigate the real-world use of imeglimin in older adults in Japan using data from the National Database of Health Insurance Claims and Specific Health Checkups of Japan (NDB) and (*ii*) present a long-term case of an older patient with type 2 diabetes who maintained glycemic

control, muscle-related parameters (creatine kinase [CK], creatinine [CRE], estimated glomerular filtration rate [eGFR]), nutritional status (albumin [Alb]) (*11*), and inflammation (C-reactive protein [CRP]) (*12*) during imeglimin therapy.

2. Methods

2.1. Prescription trends of imeglimin by age group

We used open data from the NDB, first released in 2014 by the Ministry of Health, Labor, and Welfare. The NDB provides statistical data that reflect the current status of medical care and health checkups in Japan. In this study, we extracted prescription data for imeglimin from the NDB open data for the fiscal years 2021–2023 (*13*), corresponding to the period after its market launch. Prescription data were obtained from the category "prescription drugs" and included quantities stratified by sex, age group, and drug class, across outpatient (in-hospital and out-of-hospital) and inpatient settings. The proportion of prescriptions in each age group was calculated.

2.2. Case report

The patient was an octogenarian. In 2005, she was diagnosed with type 2 diabetes with an HbA1c level of 8.5%; dietary therapy was initiated. Pharmacotherapy was started in 2006 with voglibose (0.9 mg/day) and glimepiride (2 mg/day), resulting in an HbA1c improvement of 6.3%; however, treatment was discontinued by the patient in the same year. In 2009, during a municipal health checkup, her HbA1c level was 9.5%, and voglibose was restarted, but she discontinued treatment. In 2011, another health checkup revealed diabetes (HbA1c: 8.6%), leading to voglibose re-initiation; however, poor adherence prompted a switch to sitagliptin (50 mg/day), which reduced HbA1c to 6.9%. Subsequent weight gain necessitated the addition of metformin (500 mg/day) and pioglitazone (15 mg/day) in 2013. HbA1c levels stabilized in the 6% range until 2017, when the treatment was discontinued. In 2019, HbA1c increased to 11.4%, and treatment with dulaglutide (0.75 mg/week) and dapagliflozin (5 mg/day) was initiated, improving HbA1c to 7%. However, glycemic control worsened to 8%, and imeglimin (2000 mg/day) was introduced in 2022. Since then, no changes have been made to the regimen, and treatment has been continued. Informed consent was obtained from the patient in accordance with institutional and ethical guidelines.

3. Results and Discussion

Table 1 shows the proportion of imeglimin prescriptions by age group from 2021 to 2023. The total number of tablets dispensed increased from 58.15 million in 2022 to 143.31 million in 2023. In both years, patients in their 70s accounted for approximately 30% of all prescriptions, representing the largest proportion, followed by those in their 60s. The proportion of patients aged ≥ 80 years increased from 2022 to 2023.

Table 2 summarizes the clinical course after the initiation of imeglimin treatment. HbA1c levels were consistently maintained within the 7% range and improved to 7.1% after 30 months of therapy. CK and creatinine levels remained stable. Renal function assessed using CRE and eGFR showed no evidence of deterioration. Nutritional status (Alb) and inflammation (CRP) were stable throughout the observation period. Clinically, the patient maintained independent walking

Table 1. Proportion of imeglimin prescriptions by age group from 2021 to 2023

	under 10 years old	10s	20s	30s	40s	50s	60s	70s	80 years and older
FY2021	0	0	0	0	0	0	0	0	0
FY2022	0	0.0	0.6	2.5	9.4	20.2	22.7	29.0	15.6
FY2023	0	0.1	0.4	2.2	8.3	19.7	22.6	30.0	16.7

Table 2. Clinical course of the patient after initiation of imeglimin

	6 months before the start	at the start of treatment	6 months post-initiation	12 months post-initiation	18 months post-initiation	24 months post-initiation	30 months post-initiation
HbA1c (%)	8	8.4	7.5	7.2	7.6	7.5	7.1
CK (U/L)	49	52	40	48	51	45	51
CRE (mg/dL)	0.67	0.7	0.69	0.6	0.64	0.69	0.69
eGFR (mL/min/1.73 m^2)	63	60	61	61	66	61	61
Alb (g/dL)	4.5	4.4	4.6	4.6	4.6	4.4	4.4
CRP (mg/L)	0.06	0.13	0.22	0.11	0.06	0.04	0.03

HbA1c, hemoglobin A1c; CK, creatine kinase; CRE, creatinine; eGFR, estimated glomerular filtration rate; Alb, albumin; CRP, C-reactive protein.

ability and preserved quality of life.

This study combines an analysis of prescription trends using the NDB with a long-term case report to evaluate the clinical significance of imeglimin in older adults with type 2 diabetes. Our analysis demonstrated that imeglimin prescriptions increased substantially within a few years of its launch, specifically among patients in their 70s, with increasing use observed in those aged ≥80 years. These findings suggest that imeglimin is widely adopted in clinical practice for older patients, likely reflecting its favorable profile of low hypoglycemia risk and suitability in the context of preserved renal function. In Japan, recent trends in diabetes pharmacotherapy among older adults show an increasing use of agents associated with a lower risk of hypoglycemia, such as DPP-4 inhibitors and SGLT2 inhibitors (*14,15*), indicating a shift toward safer treatment options in this population. This shift is particularly relevant in the context of frailty and multimorbidity, which make older adults more susceptible to adverse drug events, including hypoglycemia.

In the patient, despite a history of repeated treatment discontinuation, imeglimin enabled sustained therapy with stable HbA1c control of approximately 7%. Importantly, no decline was observed in muscle-related parameters or renal function, with stable nutritional and inflammatory marker levels. The preservation of independent ambulation suggests that imeglimin may help maintain physical function and may attenuate the progression of frailty and sarcopenia, although further confirmation is needed. Diabetes increases the risk of frailty and sarcopenia (*16*), with mechanisms involving impaired insulin secretion and resistance, chronic inflammation (*17,18*), and oxidative stress-induced skeletal muscle damage (*19*). Imeglimin, by improving mitochondrial function and reducing oxidative stress (*8-10*), may mitigate these pathophysiological processes, thereby supporting muscle and systemic homeostasis. Notably, although imeglimin shares structural similarities with metformin, it exhibits distinct pharmacological properties. Metformin may not always be advantageous for sarcopenia, partly because of risks such as vitamin B12 deficiency and potential mitochondrial effects (*16*). By contrast, the mitochondrial protective action of imeglimin may help maintain skeletal muscle integrity. The present case provides clinical evidence supporting this hypothesis.

Nevertheless, this study has some limitations. First, as a single case report, the findings are limited, and causality between imeglimin therapy and the observed stability in clinical parameters cannot be established. Second, skeletal muscle mass and strength were assessed only indirectly *via* serum markers and renal function, without standardized assessments such as dual-energy X-ray absorptiometry, bioimpedance analysis, or handgrip strength. The lack of direct measurements was primarily due to constraints in the outpatient clinical setting, and therefore the present findings should be interpreted as merely suggestive. Third, lifestyle factors such as diet, physical activity, and nutritional status were not fully controlled during the 30-month observation period, and the potential positive influence of these factors on the outcomes cannot be ruled out. Moreover, because this study used aggregated data from the NDB Open Data, detailed patient-level information such as baseline characteristics, concomitant medications, and comorbidities could not be obtained. Although detailed individual-level analyses were not feasible in the present study, we acknowledge the importance of these characteristics and will consider incorporating such analyses in future investigations using datasets that allow linkage at the individual level. In addition, although our analysis demonstrated a substantial increase in imeglimin prescriptions after its launch, this trend only reflects growing clinical utilization and acceptance and does not indicate that imeglimin has superior efficacy or safety compared with other antidiabetic medications. Although the observation period of 30 months was relatively long, further follow-up with advanced age and analysis of multiple cases is required.

Our results suggest that imeglimin contributes to stable glycemic control in older adults with type 2 diabetes and may help attenuate the progression of frailty and sarcopenia. Future prospective studies with larger cohorts are needed to comprehensively evaluate the effects of imeglimin on muscle mass, muscle strength, physical function, and frailty-related outcomes, using standardized assessment tools and incorporating indicators of nutritional status and chronic inflammation. In addition, more rigorous study designs such as prospective cohort studies targeting older adults at high risk of frailty or sarcopenia, or randomized controlled trials with active comparators are essential to clarify the potential role of imeglimin as a therapeutic option for frailty prevention in older patients with diabetes.

Acknowledgements

This study was conducted with the support of the Japan Society for the Promotion of Science (JSPS) KAKENHI Grant-in-Aid for Young Scientists (Grant Number: 25K21084). The authors express their gratitude for this support.

Funding: None.

Conflict of Interest: The authors have no conflicts of interest to disclose.

References

1. Shafiee G, Keshtkar A, Soltani A, Ahadi Z, Larijani B, Heshmat R. Prevalence of sarcopenia in the world: a systematic review and meta-analysis of general population

studies. J Diabetes Metab Disord. 2017; 16:21.
2. Motohashi N, Minegishi K, Aoki Y. Inherited myogenic abilities in muscle precursor cells defined by the mitochondrial complex I-encoding protein. Cell Death Dis. 2023; 14:689.
3. Kabra UD, Jastroch M. Mitochondrial dynamics and insulin secretion. Int J Mol Sci. 2023; 24:13782.
4. Anagnostis P, Gkekas NK, Achilla C, Pananastasiou G, Taouxidou P, Mitsiou M, Kenanidis E, Potoupnis M, Tsiridis E, Goulis DG. Type 2 diabetes mellitus is associated with increased risk of sarcopenia: A systematic review and meta-analysis. Calcif Tissue Int. 2020; 107:453-463.
5. Yokoyama H, Araki S, Yamazaki K, Kawai K, Shirabe SI, Oishi M, Kanatsuka A, Yagi N, Kabata D, Shintani A, Maegawa H. Trends in glycemic control in patients with insulin therapy compared with non-insulin or no drugs in type 2 diabetes in Japan: a long-term view of real-world treatment between 2002 and 2018 (JDDM 66). BMJ Open Diabetes Res Care. 2022; 10:e002727.
6. Theurey P, Vial G, Fontaine E, Monternier PA, Fouqueray P, Bolze S, Moller DE, Hallakou-Bozec S. Reduced lactic acidosis risk with imeglimin: Comparison with metformin. Physiol Rep. 2022; 10:e15151.
7. Hallakou-Bozec S, Vial G, Kergoat M, Fouqueray P, Bolze S, Borel AL, Fontaine E, Moller DE. Mechanism of action of imeglimin: A novel therapeutic agent for type 2 diabetes. Diabetes Obes Metab. 2021; 23:664-673.
8. Vial G, Lamarche F, Cottet-Rousselle C, Hallakou-Bozec S, Borel AL, Fontaine E. The mechanism by which imeglimin inhibits gluconeogenesis in rat liver cells. Endocrinol Diabetes Metab. 2021; 4:e00211.
9. Vial G, Chauvin MA, Bendridi N, Durand A, Meugnier E, Madec AM, Bernoud-Hubac N, Pais de Barros JP, Fontaine É, Acquaviva C, Hallakou-Bozec S, Bolze S, Vidal H, Rieusset J. Imeglimin normalizes glucose tolerance and insulin sensitivity and improves mitochondrial function in liver of a high-fat, high-sucrose diet mice model. Diabetes 2015; 64:2254-2264.
10. Fouqueray P, Leverve X, Fontaine E, Baquié M, Wollheim C, Lebovitz H, Bozec S. Imeglimin-a new oral antidiabetic that targets the three key defects of type 2 diabetes. J Diabetes Metab. 2011; 2:126.
11. Yanagita I, Fujihara Y, Iwaya C, *et al*. Low serum albumin, aspartate aminotransferase, and body mass are risk factors for frailty in elderly people with diabetes-a cross-sectional study. BMC Geriatr. 2020; 20:200.
12. Velissaris D, Pantzaris N, Koniari I, Koutsogiannis N, Karamouzos V, Kotroni I, Skroumpelou A, Ellul J. C-reactive protein and frailty in the elderly: A literature review. J Clin Med Res. 2017; 9:461-465.
13. Ministry of Health, Labour and Welfare. National Database of Health Insurance Claims and Specific Health Checkups of Japan (NDB) Open Data. Available from: *https://www.mhlw.go.jp/stf/seisakunitsuite/bunya/0000177182.html* (accessed 2025-8-20).
14. Niida Y, NishiokaY, Myojin T, Noda T, Takahashi Y, Imamura T. Trends in Diabetic Medication Use and Hypoglycemia Incidence Among Older Adults in Japan: A Retrospective Observational Study and a 10-Year Analysis Based on Level of Care Need Using Linked Medical and Long-Term Care Data. Cureus. 2025; 17:e87486.
15. Aoyama K, Okada A, Kaneko H, Azegami T, Suzuki Y, Meguro S, Fujiu K, Takeda N, Morita H, Node K, Yamauchi T, Nangaku M, Takeda N, Yasunaga H, Hayashi K. Evolving trends of antidiabetic agents stratified by age, kidney function and body mass index: Insights from a nationwide claims database. Diabetes Obes Metab. 2025; 28:701-710.
16. Morley JE, Malmstrom TK, Rodriguez-Mañas L, Sinclair AJ. Frailty, sarcopenia, and diabetes. J Am Med Dir Assoc. 2014; 15:853-859.
17. Barzilay JI, Blaum C, Moore T, Xue QL, Hirsch CH, Walston JD, Fried LP. Insulin resistance and inflammation as precursors of frailty: the Cardiovascular Health Study. Arch Intern Med. 2007; 167:635-641.
18. Akbaraly TN, Hamer M, Ferrie JE, Lowe G, Batty GD, Hagger-Johnson G, Singh-Manoux A, Shipley MJ, Kivimäki M. Chronic inflammation as a determinant of future aging phenotypes. CMAJ. 2013; 185:E763-E770.
19. Meng SJ, Yu LJ. Oxidative stress, molecular inflammation and sarcopenia. Int J Mol Sci. 2010; 11:1509-1526.

Received September 8, 2025; Revised December 1, 2025; Accepted December 10, 2025.

**Address correspondence to:*
Atsushi Ishimura, Laboratory of Clinical Pharmacy Assessment, Hoshi University, 2-4-41 Ebara, Shinagawa-ku, Tokyo 142-8501, Japan.
E-mail: ishimura.atsushi@hoshi.ac.jp

Released online in J-STAGE as advance publication December 13, 2025.

Correspondence

DOI: 10.5582/ddt.2025.01111

Elamipretide: The first cardiolipin-directed mitochondrial therapeutic for Barth syndrome approved under accelerated approval

Chenru Zhao[1], Xuemei Zhuang[1], Jianjun Gao[2,*]

[1] Department of Pharmacy, Qingdao Central Hospital, University of Health and Rehabilitation Sciences, Qingdao, Shandong, China;
[2] Department of Pharmacology, School of Pharmacy, Qingdao Medical College, Qingdao University, Qingdao, Shandong, China.

SUMMARY: Barth syndrome (BTHS) is a rare X-linked mitochondrial disorder caused by *tafazzin* mutations that impair cardiolipin remodeling, leading to mitochondrial dysfunction and symptoms such as cardiomyopathy, myopathy, and neutropenia. On September 19, 2025, the U.S. Food and Drug Administration (FDA) granted accelerated approval to elamipretide, the first therapy directly targeting the mitochondrial etiology of BTHS. Elamipretide binds to cardiolipin on the inner mitochondrial membrane, stabilizing respiratory chain supercomplexes, enhancing electron transport efficiency, and reducing reactive oxygen species production. In a randomized, double-blind, placebo-controlled, crossover trial, elamipretide resulted in no significant improvement in the 6-minute walk test or fatigue scores; however, sustained benefits were observed during a 168-week open-label extension. The most common adverse events were mild injection-site reactions. As a condition of accelerated approval, a confirmatory trial is required. Elamipretide represents a promising therapy addressing an unmet medical need in BTHS and provides a foundation for future mitochondria-targeted treatments.

Keywords: Barth syndrome, elamipretide, X-linked mitochondrial disorder, mitochondria-targeted therapeutic drugs

Barth syndrome (BTHS) is an X-linked recessive genetic mitochondrial disorder caused by mutations in the *tafazzin* gene located at region q28 of the X chromosome (*1*). The estimated incidence of BTHS is approximately 1 in 300,000 to 400,000 individuals, making it as a rare disease (*2,3*). Dysfunction of tafazzin impairs the synthesis of cardiolipin, a principle phospholipid component of the inner mitochondrial membrane, resulting in reduced stability of the mitochondrial structure and the electron transport chain, abnormal mitochondrial energy metabolism, and the onset of symptoms such as cardiomyopathy, skeletal myopathy, growth delay, neutropenia and increased urinary excretion of 3-methylglutaconic acid (3-MGCA) (*4*). The management of BTHS requires a multidisciplinary approach aimed at providing symptomatic support and preventing complications, including pharmacological management of dilated cardiomyopathy, cardiac transplantation, antibiotic prophylaxis, and granulocyte colony-stimulating factor (G-CSF) therapy. Currently, no targeted therapies address the underlying etiology of the disease.

On September 19, 2025, the U.S. Food and Drug Administration (FDA) granted accelerated approval to elamipretide for the treatment of BTHS, marking the first approval of a therapeutic agent directly targeting the mitochondrial etiology of disease (*5*). Elamipretide has a pharmacological effect by specifically binding to cardiolipin on the inner mitochondrial membrane, which promotes and stabilizes the assembly of respiratory chain supercomplexes, thereby enhancing electron transport efficiency and overall mitochondrial function (6). This mechanism significantly reduces electron leakage and excessive generation of reactive oxygen species (ROS), while simultaneously improving adenosine triphosphate (ATP) synthesis (*6*). In addition, elamipretide suppresses cardiolipin peroxidation and prevents cytochrome c release, effectively blocking the mitochondria-mediated apoptotic pathway and restoring normal mitochondrial cristae morphology (*6*). Collectively, these pleiotropic actions correct the fundamental biochemical abnormalities characteristic of BTHS, including a disrupted mitochondrial structure and impaired energy metabolism.

The efficacy and safety of elamipretide were assessed in a randomized, double-blind, placebo-controlled,

crossover trial followed by an open-label, single-arm extension study (*7*). The randomized phase enrolled 12 patients genetically confirmed to have BTHS. Participants were randomly assigned to receive either elamipretide 40 mg or a placebo administered once daily by subcutaneous injection for 12 weeks, followed by a 4-week washout period before crossing over to the alternate treatment. The primary endpoints were changes in the 6-minute walk test (6MWT) distance and the Barth Syndrome Symptom Assessment (BTHS-SA) total fatigue score. Compared to a placebo, elamipretide did not result in statistically significant improvements in the 6MWT distance or BTHS-SA fatigue scores during the randomized phase (*7*). However, during the open-label extension (OLE) period, in which ten of the twelve participants were enrolled and eight completed the 168-week treatment, sustained improvements from the OLE baseline were observed at all time points in both the 6MWT distance and mean BTHS-SA total fatigue scores (*8*). Moreover, although increases in knee extensor muscle strength — a secondary endpoint — were not detected during the randomized phase, they became apparent during the extension period (*9*). The most frequently reported adverse events were injection-site reactions, including erythema, pain, induration, pruritus, bruising, and urticaria (*8,9*).

As a condition of the accelerated approval, the FDA requires a randomized, double-blind, placebo-controlled trial to confirm the efficacy and safety of elamipretide. Nevertheless, elamipretide represents a promising therapeutic option that may address the current unmet medical need in BTHS and offers hope for improving patients' quality of life. Moreover, its innovative mechanism — specifically targeting mitochondrial cardiolipin — provides valuable insights and inspiration for the development of novel targeted therapies for other mitochondrial disorders.

Funding: None.

Conflict of Interest: The authors have no conflicts of interest to disclose.

References

1. Gonzalez IL. Barth syndrome: TAZ gene mutations, mRNAs, and evolution. Am J Med Genet A. 2005; 134:409-414.
2. Miller PC, Ren M, Schlame M, Toth MJ, Phoon CKL. A Bayesian analysis to determine the prevalence of Barth syndrome in the pediatric population. J Pediatr. 2020; 217:139-144.
3. Jefferies JL. Barth syndrome. Am J Med Genet C Semin Med Genet. 2013; 163C:198-205.
4. Clarke SL, Bowron A, Gonzalez IL, *et al*. Barth syndrome. Orphanet J Rare Dis. 2013; 8:23.
5. U.S. Food and Drug Administration. FDA Grants Accelerated Approval to First Treatment for Barth Syndrome. *https://www.fda.gov/news-events/press-announcements/fda-grants-accelerated-approval-first-treatment-barth-syndrome* (Accessed October 5, 2025).
6. Tung C, Varzideh F, Farroni E, Mone P, Kansakar U, Jankauskas SS, Santulli G. Elamipretide: A review of its structure, mechanism of action, and therapeutic potential. Int J Mol Sci. 2025; 26:944.
7. Reid Thompson W, Hornby B, Manuel R, Bradley E, Laux J, Carr J, Vernon HJ. A phase 2/3 randomized clinical trial followed by an open-label extension to evaluate the effectiveness of elamipretide in Barth syndrome, a genetic disorder of mitochondrial cardiolipin metabolism. Genet Med. 2021; 23:471-478.
8. Thompson WR, Manuel R, Abbruscato A, Carr J, Campbell J, Hornby B, Vaz FM, Vernon HJ. Long-term efficacy and safety of elamipretide in patients with Barth syndrome: 168-week open-label extension results of TAZPOWER. Genet Med. 2024; 26:101138.
9. FORZINITY (elamipretide) injection, for subcutaneous use. *https://www.accessdata.fda.gov/drugsatfda_docs/label/2025/215244s000lbl.pdf* (accessed October 5, 2025).

Received October 7, 2025; Revised November 9, 2025; Accepted November 17, 2025.

**Address correspondence to:*
Jianjun Gao, Department of Pharmacology, School of Pharmacy, Qingdao Medical College, Qingdao University, Qingdao, Shandong, China.
E-mail: gaojj@qdu.edu.cn

Released online in J-STAGE as advance publication November 20, 2025.

News

DOI: 10.5582/ddt.2025.01118

New diagnostic code "5B72 Undernutrition in Adults" approved for inclusion in the 11th Revision of the International Classification of Diseases (ICD-11)

Machiko Uenishi[1], Peipei Song[1,2,*]

[1] Center for Clinical Sciences, Japan Institute for Health Security, Tokyo, Japan;
[2] National College of Nursing, Japan Institute for Health Security, Tokyo, Japan.

SUMMARY: The World Health Organization (WHO) has approved a new diagnostic code, "5B72 Undernutrition in Adults", in the 11th Revision of the International Classification of Diseases (ICD-11). Prior to this update, undernutrition in adults was represented only by the code "5B54 Underweight in Adults". However, the increasing diversity of causes of undernutrition in adults and the accompanying rise in associated diseases have been recognized as global health challenges in recent years. The approval of the "5B72 Undernutrition in Adults" category signifies its formal recognition as a distinct disease entity and is expected to improve data collection and research, enhance clinical diagnosis and interventions, and support policy development and nutritional education.

Keywords: undernutrition, malnutrition, ICD-11, GLIM

1. Introduction

On October 23, 2025, the European Society for Clinical Nutrition and Metabolism (ESPEN) announced through its social media accounts that the WHO and the International Classification of Diseases 11th Revision (ICD-11) team in Geneva had approved the new diagnostic code "5B72 Undernutrition in Adults" for ICD-11, describing this approval as a "milestone for clinical nutrition (*1*)".

According to information released on November 3, 2025 by the American Society for Parenteral and Enteral Nutrition (ASPEN), the code includes three subcategories: *i*) 5B72.0 Undernutrition in adults related to disease with moderate to severe inflammation; *ii*) 5B72.1 Undernutrition in adults related to disease with non-discernible inflammation; and *iii*) 5B72.2 Undernutrition in adults related to starvation (*2*). And according to the news released on November 4, 2025 by the European Geriatric Medicine Society (EuGMS), this new "5B72 Undernutrition in Adults" category was developed in close alignment with the Global Leadership Initiative on Malnutrition (GLIM) framework (*3*). The new codes are scheduled to come into effect in 2027.

An editorial published in 2022 by Cederholm *et al*. noted that since 2020, over 40 international societies of clinical nutrition including ESPEN – which made the aforementioned announcement – had collaborated with the Swedish National Board of Health and Welfare to propose a diagnostic code for "Malnutrition in Adults" (*4*). The revisions to ICD-11 regarding undernutrition, which previously only covered infants through adolescence, reflect recommendations from these academic societies (*5*).

The same editorial pointed out that the current ICD-11 includes only two diagnostic codes for adult undernutrition, with "5B54 Underweight in Adults" having previously served as the primary indicator of undernutrition in adults. This was influenced by experiences from famines in poorer parts of the world during the 1960s and 1970s. The editorial noted that droughts, floods, poverty, and war-related malnutrition still exist, but today's manifestations of malnutrition have evolved and become more complicated, causing increasing concern even among individuals living in developed nations, who are often older and exposed to catabolic diseases.

According to sources including a review on malnutrition in older adults by the Lancet (*6-9*), undernutrition in adults encompasses various outcomes: metabolic abnormalities (*e.g*., hypothermia, impaired glucose tolerance, dyslipidemia, and low T3 syndrome); body composition abnormalities (*e.g*., underweight, sarcopenia/frailty, and associated falls); health complications resulting from vitamin and micronutrient deficiencies (*e.g*., anemia, delayed wound healing, increased pressure ulcers, impaired immune system,

Table 1. Clinical outcomes resulting from undernutrition in adults*

Category	Representative clinical consequences
Metabolic abnormalities	Hypothermia, impaired glucose tolerance, dyslipidemia, low T3 syndrome
Body composition abnormalities	Underweight, sarcopenia/frailty, and associated falls
Health complications due to vitamin and micronutrient deficiencies	Anemia, delayed wound healing, increased pressure ulcers, impaired immune system, taste disorders, osteoporosis
Hormonal imbalances in premenopausal women	Menstrual irregularities, ovulation disorders, increased risk of infertility or pregnancy complications
Higher hospitalization rates and prolonged recovery periods after acute illness	
Premature mortality	

**Source: Ref. (6-9).*

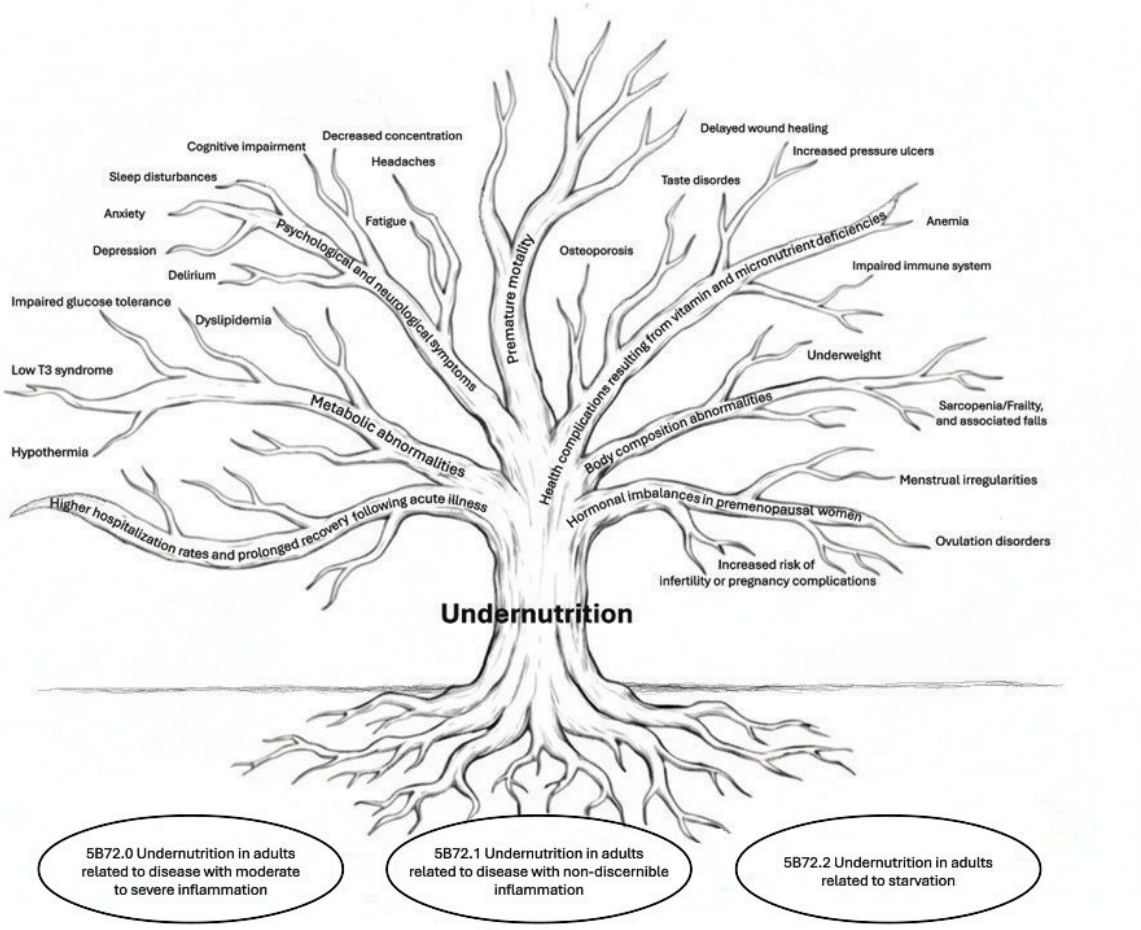

Figure 1. A tree image of undernutrition in adults: Its causes and resulting clinical outcomes. *Source: Ref. (2,6-9).*

taste disorders, and osteoporosis); psychological and neurological symptoms (*e.g.*, delirium, fatigue, sleep disturbances, headaches, depression, anxiety, decreased concentration, and cognitive impairment); hormonal imbalances in premenopausal women (*e.g.*, menstrual irregularities, ovulation disorders, and increased risk of infertility or pregnancy complications); higher hospitalization rates and prolonged recovery periods following acute illness; and premature mortality (Table 1 and Figure 1). These factors collectively pose significant public health concerns.

The approval of the new diagnostic codes has significant implications from multiple perspectives: *i*) Academically, classifying undernutrition in adults as a distinct disease entity will facilitate the refinement of disease concepts and the global standardization of the GLIM criteria; *ii*) Clinically, these new diagnostic codes are expected to enhance diagnostic accuracy in clinical practice and improve alignment with health insurance systems and healthcare benefits; *iii*) Policy-wise, the approval will support the development and implementation of nutritional interventions and aging-related policies globally, while serving as an opportunity to reaffirm the importance of nutritional management

and education across all life stages; and *iv*) Data-wise, improved data precision for the Global Burden of Disease (GBD) study and national nutrition monitoring are expected, enhancing the reliability of epidemiological research and international comparisons.

Funding: None.

Conflict of Interest: The authors have no conflicts of interest to disclose.

References

1. The European Society for Clinical Nutrition and Metabolism. Milestone for clinical nutrition. *https://www.instagram.com/p/DQJA9edjAIh/* (accessed October 25, 2025).
2. ASPEN. ICD-11 will change coding of adult malnutrition. *https://nutritioncare.org/news/icd11/* (accessed November 4, 2025).
3. EuGMS. New ICD-11 code for undernutrition in adults accepted by WHO. *https://www.eugms.org/news/new-icd-11-code-undernutrition-adults-accepted-who* (accessed November 5, 2025).
4. Cederholm T, Rothenberg E, Barazzoni R. Editorial: A clinically relevant diagnosis code for "malnutrition in adults" is needed in ICD-11. J Nutr Health Aging. 2022; 26:314-315.
5. WHO. International Classification of Diseases 11th Revision. *https://icd.who.int/en/* (accessed October 28, 2025).
6. Dent E, Wright ORL, Woo J, Hoogendijk EO. Malnutrition in older adults. Lancet. 2023; 401:951-966.
7. Volkert D, Beck AM, Cederholm T, Cruz-Jentoft A, Goisser S, Hooper L, Kiesswetter E, Maggio M, Raynaud-Simon A, Sieber CC, Sobotka L, van Asselt D, Wirth R, Bischoff SC. ESPEN guideline on clinical nutrition and hydration in geriatrics. Clin Nutr. 2019; 38:10-47.
8. Japan Society for the Study of Obesity. Statement on female underweight/undernutrition syndrome (FUS). *https://www.jasso.or.jp/data/Introduction/pdf/academic-information_statement_20250416.pdf* (accessed October 28, 2025). (in Japanese)
9. Deng Y, Hu X, Hirano Y, Liao R, Takashima S, Zhang K, Nagafusa T, Zhu J, Yamauchi K. Risk factors for and a prediction nomogram of physical frailty in older patients hospitalized with acute calculous cholecystitis. Glob Health Med. 2025; 7:294-305.

Received October 28, 2025; Revised November 10, 2025; Accepted November 12, 2025.

**Address correspondence to:*
Peipei Song, Center for Clinical Sciences, Japan Institute for Health Security, 1-21-1 Toyama, Shinjuku, Tokyo 162-8655, Japan.
E-mail: psong@jihs.go.jp

Released online in J-STAGE as advance publication November 14, 2025.

DD&T
Drug Discoveries & Therapeutics

Guide for Authors

1. Scope of Articles

Drug Discoveries & Therapeutics (Print ISSN 1881-7831, Online ISSN 1881-784X) welcomes contributions in all fields of pharmaceutical and therapeutic research such as medicinal chemistry, pharmacology, pharmaceutical analysis, pharmaceutics, pharmaceutical administration, and experimental and clinical studies of effects, mechanisms, or uses of various treatments. Studies in drug-related fields such as biology, biochemistry, physiology, microbiology, and immunology are also within the scope of this journal.

2. Submission Types

Original Articles should be well-documented, novel, and significant to the field as a whole. An Original Article should be arranged into the following sections: Title page, Abstract, Introduction, Materials and Methods, Results, Discussion, Acknowledgments, and References. Original articles should not exceed 5,000 words in length (excluding references) and should be limited to a maximum of 50 references. Articles may contain a maximum of 10 figures and/or tables. Supplementary Data are permitted but should be limited to information that is not essential to the general understanding of the research presented in the main text, such as unaltered blots and source data as well as other file types.

Brief Reports definitively documenting either experimental results or informative clinical observations will be considered for publication in this category. Brief Reports are not intended for publication of incomplete or preliminary findings. Brief Reports should not exceed 3,000 words in length (excluding references) and should be limited to a maximum of 4 figures and/or tables and 30 references. A Brief Report contains the same sections as an Original Article, but the Results and Discussion sections should be combined.

Reviews should present a full and up-to-date account of recent developments within an area of research. Normally, reviews should not exceed 8,000 words in length (excluding references) and should be limited to a maximum of 10 figures and/or tables and 100 references. Mini reviews are also accepted, which should not exceed 4,000 words in length (excluding references) and should be limited to a maximum of 5 figures and/or tables and 50 references.

Policy Forum articles discuss research and policy issues in areas related to life science such as public health, the medical care system, and social science and may address governmental issues at district, national, and international levels of discourse. Policy Forum articles should not exceed 3,000 words in length (excluding references) and should be limited to a maximum of 5 figures and/or tables and 30 references.

Case Reports should be detailed reports of the symptoms, signs, diagnosis, treatment, and follow-up of an individual patient. Case reports may contain a demographic profile of the patient but usually describe an unusual or novel occurrence. Unreported or unusual side effects or adverse interactions involving medications will also be considered. Case Reports should not exceed 3,000 words in length (excluding references).

Communications are short, timely pieces that spotlight new research findings or policy issues of interest to the field of global health and medical practice that are of immediate importance. Depending on their content, Communications will be published as "Comments" or "Correspondence". Communications should not exceed 1,500 words in length (excluding references) and should be limited to a maximum of 2 figures and/or tables and 20 references.

Editorials are short, invited opinion pieces that discuss an issue of immediate importance to the fields of global health, medical practice, and basic science oriented for clinical application. Editorials should not exceed 1,000 words in length (excluding references) and should be limited to a maximum of 10 references. Editorials may contain one figure or table.

News articles should report the latest events in health sciences and medical research from around the world. News should not exceed 500 words in length.

Letters should present considered opinions in response to articles published in *Drug Discoveries & Therapeutics* in the last 6 months or issues of general interest. Letters should not exceed 800 words in length and may contain a maximum of 10 references. Letters may contain one figure or table.

3. Editorial Policies

For publishing and ethical standards, *Drug Discoveries & Therapeutics* follows the Recommendations for the Conduct, Reporting, Editing, and Publication of Scholarly Work in Medical Journals issued by the International Committee of Medical Journal Editors (ICMJE, *https://icmje.org/recommendations*), and the Principles of Transparency and Best Practice in Scholarly Publishing jointly issued by the Committee on Publication Ethics (COPE, *https://publicationethics.org/resources/guidelines-new/principles-transparency-and-best-practice-scholarly-publishing*), the Directory of Open Access Journals (DOAJ, *https://doaj.org/apply/transparency*), the Open Access Scholarly Publishers Association (OASPA, *https://oaspa.org/principles-of-transparency-and-best-practice-in-scholarly-publishing-4*), and the World Association of Medical Editors (WAME, *https://wame.org/principles-of-transparency-and-best-practice-in-scholarly-publishing*).

Drug Discoveries & Therapeutics will perform an especially prompt review to encourage innovative work. All original research will be subjected to a rigorous standard of peer review and will be edited by experienced copy editors to the highest standards.

Ethical Approval of Studies and Informed Consent: For all manuscripts reporting data from studies involving human participants or animals, formal review and approval, or formal review and waiver, by an appropriate institutional review board or ethics committee is required and should be described in the Methods section. When your manuscript contains any case details, personal information and/or images of patients or other individuals, authors must obtain appropriate written consent, permission and release in order to comply with all applicable laws and regulations concerning privacy and/or security of personal information. The consent form needs to comply with the relevant legal requirements of your particular jurisdiction, and please do not send signed consent form to *Drug Discoveries & Therapeutics* to respect your patient's and any other individual's privacy. Please instead describe the information clearly in the Methods (patient consent) section of your manuscript while retaining copies of the signed forms in the event they should be needed. Authors should also state that the study conformed to the provisions of the Declaration of Helsinki (as revised in 2013, *https://wma.net/what-we-do/medical-ethics/declaration-of-helsinki*). When reporting experiments on animals, authors should indicate whether the institutional and national guide for the care and use of laboratory animals was followed.

Reporting Clinical Trials: The ICMJE (*https:// icmje.org/recommendations/browse/publishing-and-editorial-issues/clinical-trial-registration.html*) defines a clinical trial as any research project that prospectively assigns people or a group of people to an intervention, with or without concurrent comparison or control groups, to study the relationship between a health-related intervention and a health outcome. Registration of clinical trials in a public trial registry

at or before the time of first patient enrollment is a condition of consideration for publication in *Drug Discoveries & Therapeutics*, and the trial registration number will be published at the end of the Abstract. The registry must be independent of for-profit interest and publicly accessible. Reports of trials must conform to CONSORT 2010 guidelines (*https://consort-statement.org/consort-2010*). Articles reporting the results of randomized trials must include the CONSORT flow diagram showing the progress of patients throughout the trial.

Conflict of Interest: All authors are required to disclose any actual or potential conflict of interest including financial interests or relationships with other people or organizations that might raise questions of bias in the work reported. If no conflict of interest exists for each author, please state "There is no conflict of interest to disclose".

Submission Declaration: When a manuscript is considered for submission to *Drug Discoveries & Therapeutics*, the authors should confirm that 1) no part of this manuscript is currently under consideration for publication elsewhere; 2) this manuscript does not contain the same information in whole or in part as manuscripts that have been published, accepted, or are under review elsewhere, except in the form of an abstract, a letter to the editor, or part of a published lecture or academic thesis; 3) authorization for publication has been obtained from the authors' employer or institution; and 4) all contributing authors have agreed to submit this manuscript.

Initial Editorial Check: Immediately after submission, the journal's managing editor will perform an initial check of the manuscript. A suitable academic editor will be notified of the submission and invited to check the manuscript and recommend reviewers. Academic editors will check for plagiarism and duplicate publication at this stage. The journal has a formal recusal process in place to help manage potential conflicts of interest of editors. In the event that an editor has a conflict of interest with a submitted manuscript or with the authors, the manuscript, review, and editorial decisions are managed by another designated editor without a conflict of interest related to the manuscript.

Peer Review: *Drug Discoveries & Therapeutics* operates a single-anonymized review process, which means that reviewers know the names of the authors, but the authors do not know who reviewed their manuscript. All articles are evaluated objectively based on academic content. External peer review of research articles is performed by at least two reviewers, and sometimes the opinions of more reviewers are sought. Peer reviewers are selected based on their expertise and ability to provide quality, constructive, and fair reviews. For research manuscripts, the editors may, in addition, seek the opinion of a statistical reviewer. Every reviewer is expected to evaluate the manuscript in a timely, transparent, and ethical manner, following the COPE guidelines (*https://publicationethics.org/files/cope-ethical-guidelines-peer-reviewers-v2_0.pdf*). We ask authors for sufficient revisions (with a second round of peer review, when necessary) before a final decision is made. Consideration for publication is based on the article's originality, novelty, and scientific soundness, and the appropriateness of its analysis.

Suggested Reviewers: A list of up to 3 reviewers who are qualified to assess the scientific merit of the study is welcomed. Reviewer information including names, affiliations, addresses, and e-mail should be provided at the same time the manuscript is submitted online. Please do not suggest reviewers with known conflicts of interest, including participants or anyone with a stake in the proposed research; anyone from the same institution; former students, advisors, or research collaborators (within the last three years); or close personal contacts. Please note that the Editor-in-Chief may accept one or more of the proposed reviewers or may request a review by other qualified persons.

Language Editing: Manuscripts prepared by authors whose native language is not English should have their work proofread by a native English speaker before submission. If not, this might delay the publication of your manuscript in *Drug Discoveries & Therapeutics*.

The Editing Support Organization can provide English proofreading, Japanese-English translation, and Chinese-English translation services to authors who want to publish in *Drug Discoveries & Therapeutics* and need assistance before submitting a manuscript. Authors can visit this organization directly at *https://www.iacmhr.com/iac-eso/support.php?lang=en. IAC-ESO* was established to facilitate manuscript preparation by researchers whose native language is not English and to help edit works intended for international academic journals.

Copyright and Reuse: Before a manuscript is accepted for publication in *Drug Discoveries & Therapeutics*, authors will be asked to sign a transfer of copyright agreement, which recognizes the common interest that both the journal and author(s) have in the protection of copyright. We accept that some authors (*e.g.*, government employees in some countries) are unable to transfer copyright. A JOURNAL PUBLISHING AGREEMENT (JPA) form will be e-mailed to the authors by the Editorial Office and must be returned by the authors by mail, fax, or as a scan. Only forms with a hand-written signature from the corresponding author are accepted. This copyright will ensure the widest possible dissemination of information. Please note that the manuscript will not proceed to the next step in publication until the JPA Form is received. In addition, if excerpts from other copyrighted works are included, the author(s) must obtain written permission from the copyright owners and credit the source(s) in the article.

4. Cover Letter

The manuscript must be accompanied by a cover letter prepared by the corresponding author on behalf of all authors. The letter should indicate the basic findings of the work and their significance. The letter should also include a statement affirming that all authors concur with the submission and that the material submitted for publication has not been published previously or is not under consideration for publication elsewhere. The cover letter should be submitted in PDF format. For an example of Cover Letter, please visit: Download Centre (*https://www.ddtjournal.com/downcentre)*.

5. Submission Checklist

The Submission Checklist should be submitted when submitting a manuscript through the Online Submission System. Please visit Download Centre (*https://www.ddtjournal.com/downcentre)* and download the Submission Checklist file. We recommend that authors use this checklist when preparing your manuscript to check that all the necessary information is included in your article (if applicable), especially with regard to Ethics Statements.

6. Manuscript Preparation

Manuscripts are suggested to be prepared in accordance with the "Recommendations for the Conduct, Reporting, Editing, and Publication of Scholarly Work in Medical Journals", as presented at *http://www.ICMJE.org*.

Manuscripts should be written in clear, grammatically correct English and submitted as a Microsoft Word file in a single-column format. Manuscripts must be paginated and typed in 12-point Times New Roman font with 24-point line spacing. Please do not embed figures in the text. Abbreviations should be used as little as possible and should be explained at first mention unless the term is a well-known abbreviation (*e.g.* DNA). Single words should not be abbreviated.

Title page: The title page must include 1) the title of the paper (Please note the title should be short, informative, and contain the major key words); 2) full name(s) and affiliation(s) of the author(s), 3) abbreviated names of the author(s), 4) full name, mailing address, telephone/fax numbers, and e-mail address of the corresponding author; 5) author contribution statements to specify the individual contributions of all authors to this manuscript, and 6) conflicts of interest (if you have an actual or potential conflict of interest to disclose, it must be included as a footnote on the title page of the manuscript; if no conflict of interest

exists for each author, please state "There is no conflict of interest to disclose").

Abstract: The abstract should briefly state the purpose of the study, methods, main findings, and conclusions. For article types including Original Article, Brief Report, Review, Policy Forum, and Case Report, a one-paragraph abstract consisting of no more than 250 words must be included in the manuscript. For Communications, Editorials, News, or Letters, a brief summary of main content in 150 words or fewer should be included in the manuscript. For articles reporting clinical trials, the trial registration number should be stated at the end of the Abstract. Abbreviations must be kept to a minimum and non-standard abbreviations explained in brackets at first mention. References should be avoided in the abstract. Three to six key words or phrases that do not occur in the title should be included in the Abstract page.

Introduction: The introduction should provide sufficient background information to make the article intelligible to readers in other disciplines and sufficient context clarifying the significance of the experimental findings.

Materials/Patients and Methods: The description should be brief but with sufficient detail to enable others to reproduce the experiments. Procedures that have been published previously should not be described in detail but appropriate references should simply be cited. Only new and significant modifications of previously published procedures require complete description. Names of products and manufacturers with their locations (city and state/country) should be given and sources of animals and cell lines should always be indicated. All clinical investigations must have been conducted in accordance with the Declaration of Helsinki (as revised in 2013, *https://wma.net/what-we-do/medical-ethics/declaration-of-helsinki*). All human and animal studies must have been approved by the appropriate institutional review board(s) and a specific declaration of approval must be made within this section.

Results: The description of the experimental results should be succinct but in sufficient detail to allow the experiments to be analyzed and interpreted by an independent reader. If necessary, subheadings may be used for an orderly presentation. All Figures and Tables should be referred to in the text in order, including those in the Supplementary Data.

Discussion: The data should be interpreted concisely without repeating material already presented in the Results section. Speculation is permissible, but it must be well-founded, and discussion of the wider implications of the findings is encouraged. Conclusions derived from the study should be included in this section.

Acknowledgments: All funding sources (including grant identification) should be credited in the Acknowledgments section. Authors should also describe the role of the study sponsor(s), if any, in study design; in the collection, analysis, and interpretation of data; in the writing of the report; and in the decision to submit the paper for publication. If the funding source had no such involvement, the authors should so state.

In addition, people who contributed to the work but who do not meet the criteria for authors should be listed along with their contributions.

References: References should be numbered in the order in which they appear in the text. Citing of unpublished results, personal communications, conference abstracts, and theses in the reference list is not recommended but these sources may be mentioned in the text. In the reference list, cite the names of all authors when there are fifteen or fewer authors; if there are sixteen or more authors, list the first three followed by *et al*. Names of journals should be abbreviated in the style used in PubMed. Authors are responsible for the accuracy of the references. The EndNote Style of *Drug Discoveries & Therapeutics* could be downloaded at **EndNote** (*https://www.ddtjournal.com/examples/Drug_Discoveries_Therapeutics.ens*).

Examples are given below:

Example 1 (Sample journal reference):

Nakata M, Tang W. Japan-China Joint Medical Workshop on Drug Discoveries and Therapeutics 2008: The need of Asian pharmaceutical researchers' cooperation. Drug Discov Ther. 2008; 2:262-263.

Example 2 (Sample journal reference with more than 15 authors):

Darby S, Hill D, Auvinen A, *et al*. Radon in homes and risk of lung cancer: Collaborative analysis of individual data from 13 European case-control studies. BMJ. 2005; 330:223.

Example 3 (Sample book reference):

Shalev AY. Post-traumatic stress disorder: Diagnosis, history and life course. In: Post-traumatic Stress Disorder, Diagnosis, Management and Treatment (Nutt DJ, Davidson JR, Zohar J, eds.). Martin Dunitz, London, UK, 2000; pp. 1-15.

Example 4 (Sample web page reference):

World Health Organization. The World Health Report 2008 – primary health care: Now more than ever. *https://apps.who.int/iris/handle/10665/43949* (accessed September 23, 2022).

Tables: All tables should be prepared in Microsoft Word or Excel and should be arranged at the end of the manuscript after the References section. Please note that tables should not in image format. All tables should have a concise title and should be numbered consecutively with Arabic numerals. If necessary, additional information should be given below the table.

Figure Legend: The figure legend should be typed on a separate page of the main manuscript and should include a short title and explanation. The legend should be concise but comprehensive and should be understood without referring to the text. Symbols used in figures must be explained. Any individually labeled figure parts or panels (A, B, *etc*.) should be specifically described by part name within the legend.

Figure Preparation: All figures should be clear and cited in numerical order in the text. Figures must fit a one- or two-column format on the journal page: 8.3 cm (3.3 in.) wide for a single column, 17.3 cm (6.8 in.) wide for a double column; maximum height: 24.0 cm (9.5 in.). Please make sure that artwork files are in an acceptable format (TIFF or JPEG) at minimum resolution (600 dpi for illustrations, graphs, and annotated artwork, and 300 dpi for micrographs and photographs). Please provide all figures as separate files. Please note that low-resolution images are one of the leading causes of article resubmission and schedule delays.

Units and Symbols: Units and symbols conforming to the International System of Units (SI) should be used for physicochemical quantities. Solidus notation (*e.g*. mg/kg, mg/mL, mol/mm^2/min) should be used. Please refer to the SI Guide *www.bipm.org/en/si/* for standard units.

Supplemental data: Supplemental data might be useful for supporting and enhancing your scientific research and *Drug Discoveries & Therapeutics* accepts the submission of these materials which will be only published online alongside the electronic version of your article. Supplemental files (figures, tables, and other text materials) should be prepared according to the above guidelines, numbered in Arabic numerals (*e.g*., Figure S1, Figure S2, and Table S1, Table S2) and referred to in the text. All figures and tables should have titles and legends. All figure legends, tables and supplemental text materials should be placed at the end of the paper. Please note all of these supplemental data should be provided at the time of initial submission and note that the editors reserve the right to limit the size

and length of Supplemental Data.

7. Online Submission

Manuscripts should be submitted to *Drug Discoveries & Therapeutics* online at *https://www.ddtjournal.com/login*. Receipt of your manuscripts submitted online will be acknowledged by an e-mail from Editorial Office containing a reference number, which should be used in all future communications. If for any reason you are unable to submit a file online, please contact the Editorial Office by e-mail at *office@ddtjournal.com*

8. Accepted Manuscripts

Page Charge: Page charges will be levied on all manuscripts accepted for publication in *Drug Discoveries & Therapeutics* (Original Articles / Brief Reports / Reviews / Policy Forum / Communications: $140 per page for black white pages, $340 per page for color pages; News / Letters: a total cost of $600). Under exceptional circumstances, the author(s) may apply to the editorial office for a waiver of the publication charges by stating the reason in the Cover Letter when the manuscript online.

Misconduct: *Drug Discoveries & Therapeutics* takes seriously all allegations of potential misconduct and adhere to the ICMJE Guideline (*https://icmje.org/recommendations*) and COPE Guideline (*https://publicationethics.org/files/Code_of_conduct_for_journal_editors.pdf*). In cases of suspected research or publication misconduct, it may be necessary for the Editor or Publisher to contact and share submission details with third parties including authors' institutions and ethics committees. The corrections, retractions, or editorial expressions of concern will be performed in line with above guidelines.

(As of December 2022)

Drug Discoveries & Therapeutics
Editorial and Head Office
Pearl City Koishikawa 603,
2-4-5 Kasuga, Bunkyo-ku,
Tokyo 112-0003, Japan.
E-mail: office@ddtjournal.com